Kinetic Analysis of Leaching Reactions in Multi-component Mineral Systems

by

Thomas Close

Submitted to the Department of Chemical Engineering
in partial fulfillment of the requirements for the degree of

Doctor of Philosophy in Chemical Engineering

at the

MASSACHUSETTS INSTITUTE OF TECHNOLOGY

February 2021

Author .....
Department of Chemical Engineering
January 14, 2021

Certified by .....
Antoine Allanore
Associate Professor
Department of Materials Science and Engineering
Thesis Supervisor

Certified by .....
T. Alan Hatton
Ralph Landau Professor
Department of Chemical Engineering
Thesis Supervisor

Accepted by .....
Patrick S. Doyle
Robert T. Haslam Professor of Chemical Engineering
Chairman, Committee on Graduate Students

Kinetic Analysis of Leaching Reactions in Multi-component Mineral Systems

by

Thomas Close

Submitted to the Department of Chemical Engineering
on January 14, 2021, in partial fulfillment of the
requirements for the degree of
Doctor of Philosophy in Chemical Engineering

Abstract

The rational design of reactive systems requires the use of kinetic models of system behavior. However, the development of such models for multicomponent systems is complicated by conditions of mutual interference in determining reaction rates. Addressing this shortcoming for mineral systems requires developing methods to solve the fundamental problem of identity and resolve the partitioning of system behavior between components. In this work a complete description of the problem of simultaneous rate determination under conditions of mutual interference is developed and progress towards solving this problem in microfluidic and bulk systems is presented. Results show that there are unique challenges posed in microfluidic systems that hinder the ability to accurately partition the behavior of the total system between its constituents. In contrast, the bulk system permits a practical experimental solution based on particle size and shape for certain classes of solid mixtures.

Thesis Supervisor: Antoine Allanore
Title: Associate Professor
Department of Materials Science and Engineering

Thesis Supervisor: T. Alan Hatton
Title: Ralph Landau Professor
Department of Chemical Engineering

Acknowledgments

It is impossible to acknowledge all of the individuals who enriched this work and made it possible. I am fortunate to have too many people to thank to fit on this page.

I would like to give special recognition to Professor Antoine Allanore, my research advisor, who guided this project through thin times and thinner times. Your support and mentorship was invaluable, even as the project turned into areas neither of us were familiar with. Your patience responding to the many roadblocks encountered in this work far exceeded my own and I will always be thankful for the opportunity to study under such a steadfast leader.

I would also like to thank my co-advisor, Professor T. Alan Hatton, who both allowed this project to begin and contributed immensely in committee meetings and our individual sessions. You helped to keep the project grounded in a chemical engineering approach, and provided a valuable perspective removed from the daily grind of research. Thank you for welcoming me into your group.

To final member of my thesis committee, Professor Klavs Jensen, I must thank you for your insightful and challenging questions. You helped to enforce rigor throughout this project, and it is stronger for your efforts.

I must also thank the former post-docs, Dr. Davide Ciceri and Dr. Dennis Chen, who worked with me in the early stages of the project. Your support and friendship was invaluable in the success of this project.

I would like to thank the members of the Allanore group. Your friendship, assistance, and willingness to debate just about any topic has both deeply enriched this work and likely delayed its completion by several months. I hope only that I have helped any one of you a fraction as much as you all have helped me.

I want to acknowledge our collaborators, Professors David Manning and Allen Barker, for their invaluable assistance in performing plant growth trials for our fertilizer material.

This work was funded in part by the Abdul Latif Jameel World Water and Food Security Lab (J-WAFS). Thank you for making this research possible.

Finally, I would like to thank the family and friends without whom I could not have succeeded.

Contents

List of Figures

List of Tables

Chapter 1

Introduction

The pursuit of pure systems comprises the vast majority of processing in the chemical industry. Each step in the value chain following the primary extraction of raw materials has the goal of removing undesired material and potentially upgrading a desired material to a more useful and valuable state. An emblematic case is that of petroleum. Crude oil exits the well as a thick mixture of hydrocarbons, sand, dissolved gases, and sulfur[57]. As it moves through processing, the sand and gases and removed, the sulfur is discarded or used for sulfuric acid production, and the hydrocarbon mixture is fractionated by boiling point[60]. Further down the value chain, these hydrocarbons will be used as feedstocks for any number of products, ranging from pharmaceuticals to pesticides to simple lubricants. The design and engineering of the processes to handle these chemical transformations requires broad knowledge of the kinetic and thermodynamic behavior of the system, and a deep understanding of what factors influence this behavior, and in what ways.

Detailed models of chemical processes provide this necessary understanding, but require experimental data to formulate and validate. The parameters of these models are generally unobservable quantities; their values must be calculated or inferred from experimental results. While performing this task is straightforward in the case of a single relevant reaction, particularly if clever choices of experimental conditions can simplify the calculation of certain parameters, the introduction of interfering reactions substantially increases the complexity of the problem. Under conditions of

interference, information gained from experiments offers insight only on the convolution of the parameters of different mechanisms, and the relationship between directly measurable quantities and any single unobservable parameter becomes weaker.

The key problem is not in obtaining accurate measurements of the effects of interfering reactions, but in determining the identity of the participants and quantifying their contributions. This increase in problem complexity is fundamental to the case of mixtures, regardless of the sophistication and reliability of the techniques to measure reaction products. Difficulties in multicomponent systems leads to a stifling of model development for natural systems which are difficult or undesirable to purify, such as soils. The development of methods to close this knowledge gap is the subject of this work.

1.1 Kinetic Models

Kinetic models of chemical reactions provide the quantitative capability necessary for the rational design of reactive systems. These models condense the information gathered by exhaustive kinetic studies to the values of one or more model parameters, and their relationship to the relevant physical conditions (concentrations, pressure, etc.) of the system. Such studies generally proceed by measuring the effect of the reaction on one or more observable concentrations or pressures[74]. Past research has focused on expanding the range and sensitivity of available measurement techniques, and the creation of mechanistic models to describe broad classes of reactions. While some progress has been made in predicting kinetic information from molecule structures and energetics[131], the study of reaction kinetics still remains largely an empirical endeavor.

Leaching reactions, involving the removal of one or more mobile species from a less reactive framework, are an important class of reactions to understand for minerals processing and agriculture. Heap leaching, a process where reactive solutions are used to concentrate desired species, generally metals, from large volumes of ore following primary extraction[103, 44], is one such example where a strong understanding of

the underlying reaction mechanisms and could improve efficiency and reduce waste. Agricultural productivity similarly depends on the rates nutrients become available from the soil for plant growth[124]. Both ores and soils are generally complex mixtures of many solid constituents, often of widely varying sizes and physical and chemical properties[72, 31].

Collecting the data necessary to specify and validate a kinetic model is often a non-trivial problem. For each unique parameter in a model, a minimum of one additional, independent, experimental reaction rate measurement is needed to specify its value. In order to avoid over-fitting to data subject to experimental error, the number of independent data should, in the general case, much more numerous than the number of free parameters[59]. In cases with a large number of simultaneous reactions, it often becomes necessary to reduce the complexity of the problem through clever assumptions and study conditions in order to maintain tractability[66].

In many real systems, simultaneous reactions proceed in parallel and series; forming directed graphs with tree-like structures and varying degrees of connectivity between branches[126]. Such instances complicate the determination of kinetic parameters for any single reaction by coupling the concentration change of a tracker species to multiple reactions. Thorough enumeration of the possible reaction pathways, i.e. constructing a reaction tree, followed by a reduction in dimensionality by removing the slowest reactions (trimming the tree) is used to manage such cases[26]. Leaching reactions of heterogeneous mixtures with chemically similar compositions pose a similar problem to that of coupled homogeneous reactions - interference.

The concept of interference in the context of kinetic analysis requires strict definition. For this work, a kinetic measurement is said to made under conditions of mutual interference if any mixture component exhibits a non-zero leaching rates of one or more species for which any other mixture component has a non-zero leaching rate of the same species, or a closely related species. A closely related species is one whose presence affects the measurement of the concentration of the other and is therefore dependent on the method chosen to measure concentration. For common mass-spectroscopy techniques, metal ions of different oxidation states are closely

related species. The interference is said to be mutual, as the presence interference effects the ability to make quantitative statements about any of the components; each phase interferes with the measurement of all phases. This concept is fundamental mixed systems and forms the key challenge which must be addressed in their quantitative study. The partitioning of the overall observable chemical behavior of a system among its various components is fundamentally a task of quantifying identity and is referred to as the identity problem throughout this work.

1.2 The Identity Problem

The identity problem in kinetic analysis refers to the challenge of separating the effects of multiple simultaneous reactions of unknown rates on the observable concentration of a single species. If the reactions are independent, a linear combination of their rates determines the ultimate behavior of the observable quantity, but the inverse problem - calculation of the rates from knowledge of the observable quantity - is underspecified. An analogous problem is encountered in the field of signal processing, and is codified in the famous "Cocktail Party Problem"[18].

The problem is thus: At a cocktail party with many guests speaking over each other, how does one distinguish the voices of each guest from the voices of all the others? This has deep importance for neuroscience[92, 53, 85], as well as practical applications in the design of hearing aids and other assistive devices[80, 133]. The simplest solution one can imagine is to pin a microphone to the lapel of each guest, however this is generally considered outside the bounds of party etiquette and is therefore impossible. If same number of microphones, one for each guest, are instead be placed inconspicuously around the room recording the din of the party, a familiar math problem is encountered. The waveforms of each guest's voice are combined in the recording captured by each microphone, however the ratio of each voice is different between the recordings, due to sound fading over distance. Both the original voices and the mixing weights are unknown, and as such the system is under-specified and cannot be directly solved using standard techniques for linear systems. A common

method of solution is independent component analysis (ICA)[11], which is generally very successful at recovering the original signals if given data equal in size to the number of desired signals.

The parallels to the problem of performing kinetic measurements with interference are striking. The voices are the desired rates, the microphones are our concentration measurements, the inability to record the guest individually is the inability to separate the mixture, and the mixing functions are the experimental conditions which affect the prevalence of the different mixture components. Unfortunately, the parallels do not extend to solution techniques and ICA is not suitable for the quantitative determination of individual leaching rates. This is because the sources found by ICA may differ by a scaling factor and permutation. That is, the signs and magnitudes of the rates may not be correct, and it would not be possible to tell which rate belongs to which phase. For audio signals, these drawbacks are not fatal, as the order of the guest voices is not important, and their volume (the scaling factor) can be adjusted until the recording is understandable. For rate determinations, however, a more deterministic technique is desired.

Developing such a technique requires formulating a rigorous solution to the identity problem. This amounts to determining the mixing function values before seeking a solution to separating the voices and requires extra information. For the case of the cocktail party, if the distance from each guest to each microphone was known, then a proxy of the mixing function would be available, and the modified system is a fully-specified linear system of equations. This search for information specific to a single system component, a single voice in this instance, will be a common theme throughout this work. Finding a proxy for the mixing function in the chemical case should also collapse the problem to a linear system, however it is less clear how this proxy can be determined. Developing an effective method to determine these mixing values, solving the identity problem, effectively provides the solution to the unknown rates as well, given the large number of robust techniques for the solution of linear systems. For this reason, while the goal of this project was the development of a method to quantify the chemical behavior of mixtures, a large portion of the follow-

ing text is devoted to procedures to gather and process identifying information on the mixture constituents. Developing solutions to this problem is the key to enable the rational design of complex mixtures, including a new generation of fertilizers.

1.3 Non-traditional fertilizers

1.3.1 An urgent problem

The United Nations projects that by 2050, in approximately 30 years at time of writing, the population of the Earth will have increased by approximately 2 billion people[98]. Fully half of this growth is expected to occur on the continent of Africa, with the vast majority south of the Sahara. Struggles with food security have long plagued many regions in Sub-Saharan African[24, 113] (SSA), and the addition of one billion more people will stress the food supply even further. As Africa overall is already a net-importer of food[20], increasing domestic food production is one solution to current and future food scarcity, and this requires analyzing why domestic food production has remained insufficient for decades.

The agricultural productivity of the average African farmer is substantially lower than the average farmer worldwide[6, 2]. There are many possible explanations for this; some critics point to the small size of the average farm in SSA (>1 Ha)[2] compared to the developed world (1000 Ha (US))[79] and the word (2.6 Ha)[35], others to the low adoption of irrigation technologies (4%)[13, 40], and others to the much lower application rates of fertilizer in SSA compared to the rest of the world[37]. It is this third point that will be discussed here, as it is the one with the most direct connection to the chemistry of a complex system.

Low adoption rates of fertilizer in SSA have been identified as a potential cause of overall low agricultural productivity for decades[90]. High fertilizer costs - SSA is among the most expensive markets for fertilizer in the world in real terms - is often identified as the largest barrier to increasing fertilizer adoption rates[77, 141]. Smallholders farmers make up the majority of African food production, and the cap-

ital these farmers have is limited. The high costs of fertilizer necessitate that the agronomic benefit, the increase in yield, is likewise large. However traditional fertilizers, generally soluble compounds of nitrogen, phosphorus, and potassium (N,P, and K), have been shown to have reduced effectiveness in tropical soils[61, 130] - which comprise a large portion of the soils of SSA[5]. These dual barriers, high cost and lessened agronomic benefit, create a strong economic disincentive to increasing fertilizer use, even as increasing food production remains an crucial development goal. This multifaceted problem does not have a simple solution, but it does have simple constraints.

For a fertilizer to succeed in driving adoption in SSA, it must be effective, affordable, and available. In engineering terms, these constraints require that the mechanism of action of the fertilizer is compatible with the tropical soils present across much of the continent, that the total cost of production is low, and that the raw materials are not exotic. Satisfying the first requirement necessitates developing a fertilizer which does not release nutrients in the form of readily soluble cations. Tropical soils tend to have poor cation exchange capacity[30] (CEC) and this property causes cationic species, most notably K, to be unable to be held in the soil for long enough to be available for uptake by plants. A fertilizer which avoids this pitfall must make cationic nutrients available at a slower rate, so that they are not simply lost with the first rain. The second requirement places constraints on the processing technologies available. Simple,single-stage, processing techniques, such as roasting, milling, and hydrothermal treatment, are preferred to more complex processing which bears higher costs. The final requirement is a function of the unique context of SSA. In contrast to much of the developed world, where shipping costs are rarely significant, transportation to and within the continent remains very expensive[78, 10]. To satisfy requirement of affordability, fertilizer production must be collocated to a great degree with fertilizer consumption and, given that African agriculture is extensive, satisfying the requirement of availability dictates that fertilizer production be widespread. The only solution to these dual conditions is if the raw materials for production are widely distributed and inexpensive. One material in particular has shown promise in

all three areas, potassium feldspar[121, 4, 76, 107, 127].

1.3.2 Minerals as fertilizers

Potassium Feldspar

Potassium feldspar ($KAlSi_3O_8$) is an incredibly common mineral, with feldspars as a class comprising an estimated 40% of the Earth's crust[109]. As a potassium ore, K-feldspar is very high-grade, containing 14 wt% if pure. It is used in industrial quantities to produce ceramics, and is generally priced less than $80/ton ($600/ton K)[93]. In comparison, a traditional potassium fertilizer, potassium chloride (KCl), has in the recent past sold for $1100/ton K in Kenya[36]. This difference makes available a relatively large processing budget ($500/ton) to produce an effective fertilizer. The ubiquity and affordability of K-feldspar as a feedstock has attracted research interest towards producing a better fertilizer for Africa, and multiple processing technologies have been investigated[120, 127, 121]. One such technology, hydrothermal treatment with calcium oxide, has shown promise as a potassium fertilizer compatible with tropical soils[120]. The material obtained after processing, herein called the hydrothermal material, is a complex mixture of remnant feldspar, calcium-silicate-hydrate (CSH), and calcium-aluminum-silicate-hydrate (CASH) phases. An example micrograph of the material is provide in Figure 1-1.

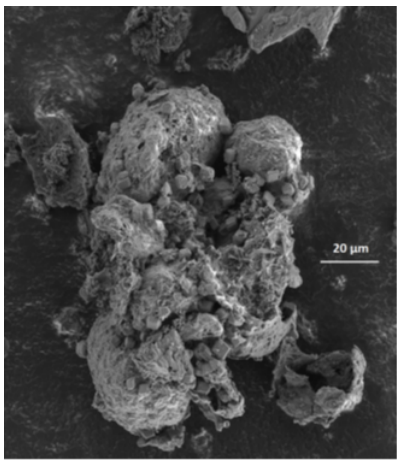

Figure 1-1: An example micrograph of the hydrothermal material. The gel-like shell of CASH phases is clearly seen coating the remnant feldspar.

Optimizing the fertilizing properties of the material requires optimizing its composition. The material composition is tuned through processing, and, while optimizing the processing conditions is beyond the scope of this work, such optimization requires that an optimal product exists. There must be a known target towards which to optimize. It is not feasible to brute-force the study of the fertilizer properties of the material, at all conditions of interest, for all possible permutations of the processing conditions. Mechanistic knowledge of the kinetics of nutrient release for each phase present in the material would allow the identification of an optimal composition for a given chemical (soil) environment. Validating a kinetic model for each phase, and obtaining estimates for the kinetic parameters, requires knowledge of the reaction rates in different chemical environments. Traditionally, this would be done by separating the material and measuring the components individually, but the hydrothermal material has proven very difficult to effectively separate. Knowledge of the aluminum, potassium, and calcium leaching rates is most important, agronomically, as the first is phytotoxic[144, 95, 48], and the others are agricultural valuable. Each of these species is present in multiple phases of the material, and can therefore leach from multiple phases. Without the ability to study these phases independently, this problem is, exactly, the determination of kinetic parameters under conditions of mutual interference.

Other Minerals

Beyond feldspar, a wide range of so-called 'agrominerals' have been investigated for use as fertilizers[130, 22]. As the majority of minerals are formed of a silicate or alumino-silicate framework, it is likely that the processing of many of these agrominerals will produce a complex mixture of secondary silicate and/or alumino-silicate minerals. Determining the properties of these phases is crucial to predicting the fertilizing ability of these materials and developing optimal processing pathways and conditions for various soil chemistries. Once again, it is kinetic models which enable these predictions and optimizations.

Beyond the pressing challenge of securing Africa's food supply, there exist gen-

eral opportunities for novel fertilizer materials to solve widespread challenges with fertilizer use outside tropical soils. Eutrophication, the poisoning of water bodies by nutrient runoff, is a common occurrence in developed nations and a major ecological concern[52, 140, 65]. In contrast to the poor CEC seen in tropical soils, non-tropical soils often have poor anion exchange capacity (AEC) and therefore cannot hold anionic nutrients, nitrate and phosphate in particular, for long periods of time. This reduces the effectiveness of these nutrients for increasing crop yield.

Fundamentally, this problem arises due to a mismatch in rates. The maximum rate of nutrient uptake by a plant is less than the dissolution rate of the rapidly soluble compounds (e.g. ammonium nitrate, mono- and di-ammonium phosphate) widely used as fertilizers. As the plants cannot use the nturients at the rate they are made available, and they cannot be held by the soil, the potential of the excess nutrients is wasted. Materials with a slower nutrient release rate may help address this problem by reducing this rate imbalance. The complex chemistry of mineral fertilizers offers an avenue towards creating these slow-release materials[130].

1.4 Prior Art

Questions on the efficacy of fertilizers and leaching rates of minerals are not new. The fields of agronomy, soil science, and geology have been studying the complex chemical interactions of multicomponent mineral systems since their inception. The experimental methods used in these fields are well-suited to the study of the overall behavior of complex systems, but make no attempt to solve the identity problem and are therefore limited to qualitative statements about the behavior of individual system components. The most relevant techniques in common practice for soil and mineral analysis are batch leaching and flow column leaching[100]. These are often performed in concert with separation techniques, in order to ascribe different behaviors to different soil fractions. There is a noted lack of methods to study separate mixture components without the ability to effectively separate them.

1.4.1 Batch leaching

Soil testing is often aimed towards quantifying soil fertility. This is done by measuring the amount of nutrients released by the soil when subjected to certain chemical conditions, with the final number generally normalized by the mass of soil tested. These numbers are then compared to benchmarks for nutrient content, and fertilizer recommendations are made depending on which nutrients are found to be deficient[25]. The test procedure is very straightforward, a known mass of soil is added to a known volume of leachant solution and allowed to equilibrate[100]. Common leachants are dilute aqueous solutions of organic acids, simple salts, and mineral acids[]. Different results will be obtained for leachants of different strengths, and these different numbers are sometimes ascribed into categories, such as soluble, exchangeable, and non-exchangeable nutrients, according to the strength of leachant required to promote its release into the solution[81, 106]. This procedure is often performed on soil fractions and qualitative statements are made as to the source of the various categories of nutrient release. Ultimately, however, batch leaching is not a technique for kinetic analysis, but a method for determining the equilibrium concentration of these species above the surface of the minerals.

While there is value in determining these equilibrium concentrations, it does not offer direct information on the kinetics of leaching for each phase. The results can be approximated as the average concentration of some species in the water of the soil pores, but says very little about the total rate of availability of this species from the soil sample. For the application of novel fertilizer analysis, it is these rates that are desired and therefore traditional batch leaching is an insufficient source of information.

1.4.2 Flow column leaching

A soil column can be considered a tubular packed-bed reactor with a heterogeneous packing material[100]. The soil in question is a discrete entity through which the leachant solution is driven, generally at very low flowrates($10^{-}7L/s$)[63]. Key insights are offered by these experiments into the transport of species, particularly pollutants,

through soils[32, 63]. The impact of fertilizer and organic matter additions to the nutrient leaching behavior of soil have also been investigated[87, 145]. As flow is an inherent property of these systems, there is a fundamental difference between soil columns and batch leaching experiments. The solution surrounding each soil particle is refreshed with some frequency, which, if often enough, shifts the mechanism controlling the species concentration in solution from equilibrium behavior to kinetic behavior. Flowrates in common use rarely exceed hundreds of nanoliters per second, as the experimental target is generally to study the mobility of certain species through soil under relatively stable moisture conditions. This is intrinsically different goal than the quantification of leaching rates from a multicomponent system, and no attempt to do so using soil columns is noted in the literature.

As in the batch leaching case, no attempt is made to solve the identity problem. The experimental design is such that the independent variable is the addition of a pollutant, or fertilizer, or the composition of the leachant solution, and this leaves no pathway for quantifying the contribution of each phase to the observed overall behavior without physical separation of the mixture.

1.4.3 Segregation techniques

Each of the above techniques is commonly employed on fractions of the total soil mixture, which are generated through one of several common techniques. Physical separations based on component density or size are the most common, and the mechanics of soil sedimentation often pre-sort the soil to some degree according to depth from the surface[39, 86, 12]. Fractionation by size, generally performed by sieving[100], is facile at larger particle sizes, but electrostatics often precludes dry separation of particles smaller than approximately 30 microns[82], and aggregation of particles can cause incomplete separation of phases by size. Wet sieving can be performed to help mitigate size aggregation and size restrictions[112], but can also promote the formation of aggregates, subject to the surface chemistry of the system. Pure fractions of only a single component are rarely obtainable through size separation alone, and therefore the size fractions of a soil mixture are mixtures themselves,

and subject to interference during kinetic measurements. More aggressive techniques involve selective dissolution of certain phases, using interrogative procedures designed to preserve certain classes of minerals while removing others[100]. Such techniques are known to be unreliable, in the sense that the range of soil chemistries is so broad, that completely removing one phase without altering another is a very difficult problem. These techniques, then, are reserved for systems with chemically very dissimilar constituents. Again the obtained mixture fractions are likely to be impure and interference will be present during kinetic measurements.

1.5 Summary

Kinetic models are the starting point for effective process engineering. Technological progress has made creating and validating these models simpler than ever for single-component systems, but these advances have not extended to general mixtures. The problem of identity, of partitioning one measurable value among multiple independent causes, is a core part of the underlying structure of these situations. A solution to the identity problem is both the lock and key to enabling the extension of a host quantitative kinetic analysis procedures to multicomponent systems. Such a solution is a necessary component of permitting the rational design of novel fertilizer materials from natural mineral feedstocks. These new materials may, in turn, provide a solution to challenges with fertilizer effectiveness in tropical soils and help to address long-standing struggles with food security in Africa.

Chapter 2

Hypothesis

2.1 Limitations of Existing Techniques

Direct measurement of the rate of leaching for a single component of a solid mixture is limited to cases where the component of interest is not subject to significant interference, such as when it leaches a unique species. In such cases, inferences must be made as to how leaching rates of species subject to interference relate to the measurable rate, as stoichiometric (congruent) leaching cannot be guaranteed[119]. Further, the determination of the kinetic parameters of a reaction rate model requires multiple measurements of the rate of reaction under different chemical conditions. Reliance on the measurement of a single species concentration to describe the entirety of a solid's multispecies leaching kinetics is, fundamentally, extrapolation and increases the uncertainty of each derived value.

In the case of m solid components leaching n distinct species, there are a total of $m * n$ unknown leaching rates. If congruent leaching cannot be assumed, then each non-zero rate for each solid is independent, and information gathered about one does not reduce uncertainty in the value of another. This implies that mn pieces of information must be known in order to specify the rates. With modern techniques, such as mass spectroscopy, it is generally possible to reliably measure the concentration of individual species in a complex solution. This allows each individual experiment to provide n pieces of information. These results together would see the system closed

with m experiments, however, in practice, this is not the case.

Simply repeating an experiment a number of times offers no original information. Independent experiments, where the manipulated variables in each experiment are linearly independent from all other experiments, are required to gather the necessary information. For the case of solid mixtures, there is no adjustable parameter which may be used to design independent experiments without introducing additional variables.

Heterogeneous reaction rates are commonly described as the product of an intrinsic kinetic rate, r and the active surface area of the solid, A [123]. In any leaching experiment, there will be mn unknown r values and m unknown A values *a priori*. This construction fixes the number of static unknowns to the mn intrinsic rates, and provides m adjustable parameters with which independent experiments may be designed. Measuring the solid surface areas, as well as the leachate concentrations, provides $m+n$ pieces of information with each experiment, but due to the introduction of surface area as a new variable, only n of these help to specify the problem of interest. As before, m independent experiments are needed to solve the system.

Each set of m experiments allows one independent estimate of the rates. If there is no error in the experimentally measured areas and concentrations, then any nominally independent set of experiments will allow an accurate determination of the reaction rates. Under conditions of uncertainty, however, the experimental design becomes critically important. Without defining a model, the problem to solve is of the form $RA = D$, where R is the matrix of rates, A is the concatenation of the column vectors of component areas, and D is some transformation of the experimental measurement dependent on the type of experiment performed. If A is invertible, R can be found via simple matrix inversion. In this case, the uncertainty in the determined rates is dependent both on the experimental error in D, which is likely to be low, and the condition number of A, which is a function of experimental test matrix. An ill-conditioned matrix will drastically increase the variance of the estimates of R and, in turn, necessitate a larger number of experimental sets to produce reliable confidence intervals for the average values of the rates. Given the number of experiments in each

set can also be large, if the number of solid phases is large, practical concerns dictate a careful design of experiments approach to this problem.

The design of independent experiments involves the manipulation of the active surface areas of the mixture constituents. In the case of total control over mixture composition, the problem to be solved is trivial; each mixture component could be measured separately. Therefore, this work focuses on cases, such as naturally-occurring mineral mixtures or products of mineral processing, where the composition of the mixture may be controlled within some range that does not generally include reduction to individual components. Physical separation based on size (sieving), density (flotation)[116], or magnetic properties (magnetic separation)[96] are well-developed industrial processes that may be employed to create independent mixture fractions that can then be used in independent leaching experiments.

Measurement of the surface areas of each component of an arbitrary solid mixture is an unsolved problem in the general case. This is subject to the coastline paradox[50], the quantity measured depends on the length scale of measurement and increases without bound as the measurement length decreases. Several bulk techniques, such as gas absorption[91], gas permeability[14], and laser diffraction[8] exist which may be used to estimate the specific or total surface area of an entire mixture, but, on their own, these techniques provide no information on the area of each constituent. Microscopy may be used to gather phase-specific information on particle sizes and areas[34], but the restrictions of small sample sizes and long analysis times create barriers to its use as the sole solution to the measurement problem. Recent interest has been shown in the development of microfluidic techniques to study mineral leaching [19, 139]. While these techniques are powerful, they are currently limited to studying pure systems as no frameworks exists to extend the technique to multicomponent leaching.

2.2 Scientific Gap

There exists no single technique, or combination of techniques, in current practice with which to study the kinetics of leaching of individual components of solid mixtures under conditions of mutual interference. This hampers the study of systems for which component separation are not possible, and the identification of new materials with desirable properties. Closing this gap by providing a practicable technique with which to study solid mixtures will aid in the identification of candidate materials for new fertilizers, assist in the study of complex solid-liquid systems such as concrete, and provide insight towards the solution of similar problems in other fields.

The core problem is one of identity. Mixing physically averages many identifying properties of the mixture constituents and while techniques exist to measure the relevant quantities (e.g. specific surface area), past investigations have produced no general method to partition these overall measurements into phasal contributions. As such, the calculation of phasal contributions to overall leaching rates remains an unsolved problem.

2.3 Hypothesis Statement

Quantitative determination of heterogeneous reaction kinetics under conditions of mutual interference requires the development of techniques to quantitatively identify phasal contributions to mixture surface areas. It is hypothesized that image analysis of two-dimensional sample sections within a microfluidic channel can provide the necessary information to accurately calculate individual leaching rates under conditions of mutual interference. It is further hypothesized that, under certain conditions, the deconvolution of mixture particle size distributions will allow these same calculations for bulk powder samples.

2.4 Procedure to Test Hypothesis

It is first necessary to demonstrate the capability to accurately estimate surface areas for single component systems in the microfluidic and bulk cases. Then, a procedure to identify contributions from individual mixture components is necessary. In the microfluidic case, this will be performed by image analysis of micrographs, with features discrimination achieved through high-dimensional filtering, cluster analysis, and machine learning. In the bulk case, surface areas will be estimated through the deconvolution of the mixture particle size distribution into the PSDs of each phase. From here, a family of identity distributions will be created, specifying the phase prevalance at each size range. The application of a phase-specific shapefactor function to each size range and modulated by the identity distribution will enable the calculation of phase-specific surface areas. Lastly, continuum models for the leaching experiments in both cases are necessary to relate measured concentrations to reaction rates. Leachate concentrations will be determined by inductively coupled plasma mass spectroscopy (ICP-MS) in nitric acid solution. A full statistical treatment of the propagation of error from the surface area estimations to calculated rates and kinetic parameters will be performed in concert with a rigorous examination of the information flow between the experimental results and the parameter values, in order to minimize both the number of experiments needed and the uncertainty in the derived parameters.

2.5 Assumptions

In order to make the problem of mutually interfering reactions mathematically tractable, the following assumptions will be enforced for both the bulk and microfluidic cases:

1. The leaching rates of each solid phase are independent. This enables the use of a wider range of solution techniques to solve for the rates after collecting sufficient data. It is likely to hold if the enumerated solid phases are present only as distinct particles, and are sufficiently dilute in a fluid suspension. Particles

of mixed identity, solid solutions of minerals for example, will likely violate this assumption.

2. Steady or pseudosteady leaching behavior is achieved for each solid constituent.

3. Each solid phase has a single identifiable average rate for each chemical species that it leaches. It is necessary that the leaching experiments are probing the same rates. If these rates change between experiments, this effectively introduces more variables and hinders or prevents the ability to gather enough information to solve the system. In the context of statistical analysis of the leaching rates, we are constraining the probability density of each rate to be non-uniform, unimodal, and of finite variance.

4. The geometric surface area is a strong proxy for the chemically active surface area of leaching. This neglects the effects of porosity, which can be difficult to measure, and the mechanistic effects of micro- and atomic- scale surface features (grain boundaries, egdes, dislocations, etc.) which may have outsized influence on leaching behavior[143]. Such effects, being highly specific to a single surface, are not ammenable to study in a mixture. If the prevalence of porosity and important features are roughly constant along the surface of each phase, then the error in the leaching rate determination introduced by this assumption is only a constant factor, which may be corrected later in a more focused study.

5. No homogeneous reactions affecting the measured concentration of species are present. This assumption is less restrictive than it may appear. The only homogeneous reactions that cannot occur are those which would affect the measurement of the concentration of a leached species. Transformations such as $Al(OH)_{4aq}^{-} + 4H_{aq}^{+} \rightarrow Al_{aq}^{3+} + 4H_2O_l$ which would not affect the measured concentration of the leached species (Al, in this example), are permitted. Precipitation reactions are strongly prohibited. The use of this assumption necessitates experimental conditions that uphold it, notably that concentrations of leached species during experiment be kept low to minimize any potential for such homo-

geneous interference. Such conditions are also required to prevent equilibrium effects from interfering with assumption 2.

2.5.1 Microfluidic Case

Additional assumptions are enforced for the microfluidic case only:

1. The organic medium surrounding the mounted samples is impermeable to the leachant solution.

2. Chemical interaction with the channel walls is identical in all experiments.

2.5.2 Bulk Case

Additional assumptions are enforced for the bulk case only:

1. Mixtures are comprised of particles of distinct identities and size distributions.

2. The leaching of mixtures does not create particles

2.6 Summary

Determination of the intrinsic rates of leaching reactions in solid mixtures may be performed via the measurement and manipulation of mixture component surface areas. Microfluidics offers a key opportunity to study distinct surfaces and surface features under leaching conditions. Bulk powder experiments offer greater laboratory accessibility with minimal sample preparation. Prior work has identified the suitability of microfluidics for the study of relatively pure systems, however, a framework describing how the technique may be rigorously applied to multicomponent systems is lacking in the literature. It is hypothesized that such an extension can be performed through estimation of solid phase surface areas via image analysis, and a further extension to bulk powder leaching is possible under conditions of particle conservation. Validating the hypothesis requires (1) demonstrating the suitability of image analysis and PSD

deconvolution as surface area estimation techniques, (2) developing a mathematical description of the information flow in these systems to inform a design of experiments approach, and (3) experimental investigation of solid mixtures under leaching conditions and the calculation of the intrinsic leaching rates. Successful validation of the proposed work would allow the quantitative investigation of the leaching behavior of important and prevalent solid mixtures, such as soils. Following these determinations, greater predictive ability for the behavior of complex solid mixtures be available.

Chapter 3

Framework for Multicomponent Microfluidic Leaching Rate Determination

The use of microfluidics to investigate mineral systems dominated by a single component has seen increased interest in recent years[19, 139]. Due to the small scale, microfluidics offers the potential for greater control of the leaching conditions and the ability to operate far from equilibrium with manageable fluid flowrates. An extension of the previously developed single component microfluidics techniques to mixtures is the focus of this chapter.

3.1 Experimental Method

The microfluidic leaching procedure considered herein requires a channel for fluid flow, which is able to be securely mounted above a two-dimensional sample surface. An inlet port brings fresh leachant solution into the channel and an outlet port removes the leachate. The leachate is collected, in batches of equal volume, for analysis of the concentration of leached species. Small channel volumes and relatively high flow rates are used to keep the residence time in the channel low (τ<1 minute) in order to allow a rapid approach to pseudosteady behavior. A schematic of the experimental setup

is shown in Figure 3-1 to serve as a visual aide during discussion of the continuum model; photographs of the device used in this work are presented with experimental results in Chapter 4.

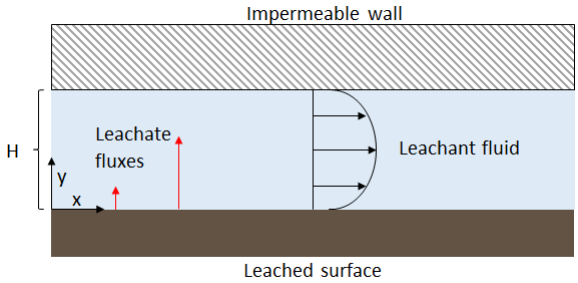

Figure 3-1: Schematic of the microfluidic leaching process

3.2 Continuum Model

Defining a control volume of the fluid in the schematic of Figure 3-1, containing the fluid between the mineral surface and top of the microfluidic channel, the following general balance on the species leached from the surface can be written:

$$\frac{\partial \mathbf{u}}{\partial t} = \nabla \cdot (\mathbf{D}\nabla \mathbf{u}) - \nabla \cdot (\vec{v}\mathbf{u}) + \mathbf{f}(\mathbf{u}) \tag{3.1}$$

Where $\mathbf{u}$ is the vector of species concentrations, $\mathbf{D}$ is the corresponding vector of species diffusivities, $\vec{v}$ is the flow velocity vector, $\mathbf{f}$ is a function describing homogeneous reactions, and t is time.

Several assumptions are helpful for reducing the model to a more practical form, in addition to those stated in 2.5

1. Pseudosteady behavior

2. Incompressible, uni-directional flow

3. Diffusivities are constant for each species

Under these assumptions, the model reduces to:

$$0 = \mathbf{D}\left(\frac{\partial^2 \mathbf{u}}{\partial x^2} + \frac{\partial^2 \mathbf{u}}{\partial y^2} + \frac{\partial^2 \mathbf{u}}{\partial z^2}\right) - v\frac{\partial \mathbf{u}}{\partial x} \tag{3.2}$$

Where x is the principal flow direction, y is the direction perpendicular to the mineral surface, and z is perpendicular to x and parallel to the mineral surface.

The channel has a square cross-section of side length H and length L, and the fluid has an average velocity V; scaling the equation with these values yields:

$$0 = \frac{\mathbf{D}L}{V}\left(\frac{1}{L^2}\frac{\partial^2 \mathbf{u}}{\partial \eta_x^2} + \frac{1}{H^2}\frac{\partial^2 \mathbf{u}}{\partial \eta_y^2} + \frac{1}{H^2}\frac{\partial^2 \mathbf{u}}{\partial \eta_z^2}\right) - \bar{v}\frac{\partial \mathbf{u}}{\partial \eta_x} \tag{3.3}$$

Comparing the magnitudes of the coefficients of the second derivatives, diffusion in the x-direction is negligible as the ratio of the diffusive term in x-direction to those in the y- and z-directions is expected to be the square of the reciprocal of the channel aspect ratio, (10^-5). The Péclet number is expected to be large (10^4), which also supports neglecting axial difusfusion. Diffusion in y and z is the only transport mechanism in these directions and cannot be neglected on the basis of scaling. Rewriting the equation given these simplifications:

$$0 = \frac{\mathbf{D}L}{V}\left(\frac{1}{H^2}\frac{\partial^2 \mathbf{u}}{\partial \eta_y^2} + \frac{1}{H^2}\frac{\partial^2 \mathbf{u}}{\partial \eta_z^2}\right) - \bar{v}\frac{\partial \mathbf{u}}{\partial \eta_x} \tag{3.4}$$

Boundary conditions for 3.4 are:

$$\mathbf{u}(0, \eta_y, \eta_z) = 0 \tag{3.5}$$

$$-\mathbf{D}\frac{\partial \mathbf{u}}{\partial \eta_y}|_{\eta_y=0} = \begin{cases} \mathbf{r} \\ 0 \end{cases} \tag{3.6}$$

$$-\mathbf{D}\frac{\partial \mathbf{u}}{\partial \eta_y}|_{\eta_y=1} = 0 \tag{3.7}$$

$$-\mathbf{D}\frac{\partial \mathbf{u}}{\partial \eta_z}|_{\eta_z z=0,1} = 0 \tag{3.8}$$

That is, the fluid enters the channel free of any species, species leach into the fluid from the mineral surface at a rate determined by their leaching kinetics, and the channel walls are impermeable to the diffusing species. Multiple cases are present in 3.6, as multiple surfaces are present at the interface between the sample and fluid. These surfaces may leach at different rates, or not leach at all, mandating multiple boundary conditions at $y = 0$. This complication all but necessitates the use of numerical techniques to solve 3.4, if the full concentration profiles of the species are desired along the length of the channel.

A further simplification is possible if only the flow-averaged concentration (mixing cup average) at the outlet of the channel is desired. Each term in the equation can be averaged by integrating over the cross-sectional area of the channel, and dividing by the integral of the velocity over the cross section. For clarity, the scaled dimensions will be returned to their unscaled state:

$$0 = \frac{\mathbf{D}}{\int_0^H v \,\mathrm{d}y \,\mathrm{d}z} \left(\iint_0^H \frac{\partial^2 \mathbf{u}}{\partial y^2} \,\mathrm{d}y \,\mathrm{d}z + \iint_0^H \frac{\partial^2 \mathbf{u}}{\partial z^2} \,\mathrm{d}z \,\mathrm{d}y \right) - \frac{\int_0^H v \frac{\partial \mathbf{u}}{\partial x} \,\mathrm{d}y \,\mathrm{d}z}{\int_0^H v \,\mathrm{d}y \,\mathrm{d}z} \tag{3.9}$$

The denominator of the $\mathbf{D}$ term can be replaced by the volumetric flowrate $\dot{q}$. Proceeding with the first integration of the diffusive terms and moving the x-derivative outside the integral:

$$0 = \frac{\mathbf{D}}{\dot{q}} \left(\int_0^H \frac{\partial \mathbf{u}}{\partial y}\Big|_0^H \,\mathrm{d}z + \int_0^H \frac{\partial \mathbf{u}}{\partial z}\Big|_0^H \,\mathrm{d}y \right) - \frac{\partial}{\partial x} \frac{\int_0^H v\mathbf{u} \,\mathrm{d}y \,\mathrm{d}z}{\int_0^H v \,\mathrm{d}y \,\mathrm{d}z} \tag{3.10}$$

The term on the far-right is now recognizable as the definition of the flow-averaged (or mixing-cup average) concentration, u_A. Working to the left, the integral of the z-derivative vanishes due to the no-flux boundary conditions in z. The integral of the y-derivative vanishes at H, but takes on multiple, constant, values at 0.

$$0 = \frac{\mathbf{D}}{\dot{q}} \left(\frac{\{\mathbf{r}, 0\} H_z}{D} \right) - \frac{\mathrm{d}\mathbf{u}_A}{\mathrm{d}x} \tag{3.11}$$

The first term vanishes everywhere on bottom of the channel except where an

active surface exists, in which case the leaching flux of that surface diffuses into the fluid. Completing the integration:

$$\mathbf{u}_A = \frac{1}{\dot{q}}\mathbf{r}\mathbf{a}(x) + \mathbf{u}_0 \tag{3.12}$$

where u_0 is the flow averaged concentration at the channel inlet, $\dot{q}$ is the volumetric flowrate in the channel, and $\mathbf{a}(x)$ is a vector containing the total active surface area of each relevant phase from the channel entrance to coordinate x.

At the end of the channel, and assuming no leached species are present at the channel inlet, the model becomes:

$$\mathbf{u}_A = \frac{1}{\dot{q}}\mathbf{r}\mathbf{a}_T \tag{3.13}$$

where $\mathbf{a}_T$ is a vector of the total surface area of each relevant phase in the channel.

Eq. 3.13 is a much simpler model than that of Eq. 3.4, yet captures all of the relevant physics to enable the determination of the leaching rates. Simulations of the full solution, shown in Figure B-1 comparing the cross-section-averaged concentration to the flow-averaged concentration, show the difference disappears rapidly once the leaching reactions are no longer present. Within roughly one millimeter from the end of the reactive zone of the channel, the fluid is fully homogeneous. This suggests that the full solution is necessary only in cases where it is desired to measure the concentration at an intermediate point in the channel close to the reaction zone. In the case of measurement occurring after the fluid leaves the channel, Eq. 3.13 provides the link between the quantities which must be experimentally measured, $\mathbf{u}_A$ and $\mathbf{a}_T$, and the desired unknowns, $\mathbf{r}$.

3.3 Design of Experiments

For microfluidic leaching systems, the test matrix is the set of desired mixture surface areas present in each trial. It is necessary that this matrix have rank at least equal to the number of mixture constituents; that is, that the number of independent

experiments is at least equal to the number of rates to be calculated. In excess of this requirement, it is desirable for the condition number of this matrix to be low, representing a large divergence from linearity between experiments, in order to reduce the uncertainty in the derived rates. As the surface areas of individual mixture components is not, generally, a freely variable parameter, there are constraints on the conditions which are experimentally accessible.

The small sample size utilized by microfluidic techniques increases the probability that separate trials will have different starting compositions. This small sample effect, essentially an exploitation of the greater sampling bias in small samples, can be used to directly produce independent experiments in separate microfluidic channels, without pre-treatment of the mixture. Control of sample composition using this technique is limited, however it can be employed on any kind of sample. If a pre-treatment method is available to enrich a mixture in one or more components (e.g. sieving, flotation, magnetic separation, etc.), then sampling from multiple mixture fractions can further increase the differences between samples, and therefore their experimental value. A detailed analysis of the experimental design considerations of size-based separation for the bulk powder case is presented in Chapter 6;

3.4 Surface Area Determination

Microscopic investigation of the surface exposed to the fluid in the microfluidic is a convenient method to effect surface area measurement. The problem of separating distinct image objects from a suitably uniform background is effectively solved [51], likewise, utilities to measure the size of these objects is incorporated into many software packages. Therefore, obtaining the total exposed mineral surface area in a microfluidic sample is, relatively, straightforward. The hard part of the problem of quantifying the phase-resolved areas is identifying each object and grouping the like-objects together. In contrast with the problem of image segmentation, classifying image objects into pre-determined categories is still an area of active research[42, 108, 43]. The ability to accurately perform such classification is an essential component of the extension

of microfluidic leaching techniques to multicomponent systems. The various classification methods used in this work are briefly presented below, and results are given in 5.

3.4.1 Image Analysis

To aid the segmentation of images of microfluidic samples, An automated routine was created in the MATLAB scripting language. This routine separates the image background from the present objects - mineral features - and collects measurements of the areas, and other shape features, of the objects. This data can then be used to effect classification of the objects themselves. All microscopy techniques offer access to the shape of the observed objects, which motivates the use of shape factors in addressing object classification. In addition, electron microscopes can offer information about the chemical composition of objects, which can also serve as a useful tool for classification. The differing interaction of polarized light with crystalline features is commonly used in petrology for mineral study[16], and could also offer another avenue through which to identify mineral features.

Shape Factor Classification

Simple shape factors, such as aspect ratio and circularity, are commonly used in other fields [114, 94, 137] to classify image objects. Their application to mineral powder samples seems a straightforward extension, and some higher-dimensional shape factors are found in the literature for this purpose [105]. Given the need to classify the images into an *a priori* unknown number of categories, a general method of grouping similar values is required. In this work, cluster analysis using two algorithsm: Density Based Spatial Clustering of Applications with Noise (DBSCAN)[33] and Ordering Points To Identify the Clustering Structure (OPTICS)[3] is employed to analyze the plots of object shape factors and filter image noise from physical objects.

Chemical Classification

In addition to shape data, the information provided by elemental analysis of image objects has strong discriminatory potential, so long as the phases are chemically distinct. This has the drawbacks of limiting the observation technique to an electron microscope equipped with an energy dispersive spectroscopy (EDS) system and drastically increasing the time required to generate sample images compared to optical microscopy. The size of objects which can be reliably studied via EDS has a strict lower bound, due to the finite interaction volume of the electron beam with the sample [45]. This is highly sample-specific, but is generally on the order of several microns[132].

3.4.2 Classification through Machine Learning

Image classification is one of the original use cases for machine learning (ML), and still an active area of research[62, 58]. The ML technique leveraged in this work is classification via a Convolution Neural Network (CNN). An overview of the basic machinery of CNNs is presented in Section 5.4. Before being used for classification the network must be trained using a set of images with labeled objects. These training images must be created manually, if they can be automatically generated, the classification problem is already solved, and represent a significant hurdle to the implementation of ML to this classification task. The number of training images needed is a function both of the desired classification accuracy and the number of possible categories, but is generally of the order of thousands of images per category [29]. As generating such a large number of training images was not feasible for this work, a transfer learning approach was adopted. A CNN that was previously trained to classify images of general objects (animals, household objects, etc.) was retrained to classify minerals using a small number of manually labeled images of minerals in microfluidic channels.

3.5 Rate Calculation

Calculation of the intrinsic leaching rates follows directly from the continuum model of Eq. 3.13 and efforts to quantify surface areas. In the absence of experimental uncertainty, rates can be directly calculated through matrix inversion. Note that this requires a number of independent experiments equal to the number of mixture components.

$$\mathbf{r} = \dot{q}\mathbf{U}_A\mathbf{A}_T^{-1} \tag{3.14}$$

where $\mathbf{U}_A$ and $\mathbf{A}_T$ are matrices whose columns are the $\mathbf{u}_A$ and $\mathbf{a}_T$ vectors of independent experiments, respectively.

This construction has several advantages: is fast to solve, requires the smallest amount of experimental data of any solution technique, and, if $\mathbf{A}_T$ is invertible, is guaranteed to have a unique solution. However, experimental uncertainty in $\mathbf{U}_A$ and/or A may cause the unique solution for $\mathbf{r}$ to be unrealistic. The condition number of A determines how the uncertainty in A ultimately affects the confidence intervals of the values in $\mathbf{r}$. Strong experimental design is the key to ensuring a small condition number, and therefore reliable rate estimates. The more different the sample surface is between experiments, the more independent the columns of A, and the smaller the condition number. As the number of mixture components increases, so too does the number of independent experiments required to calculate $\mathbf{r}$, which poses another, subtler, challenge to calculating rates. As discussed previously, the individual component surface areas are not generally free to vary. The experimental design space is constrained, with constraints dependent on the techniques available for separating the mixture and their efficiency. As more experiments are required over this finite design space, the degree of linear relation between conditions must increase, which, in turn, leads to widening confidence intervals for $\mathbf{r}$. The realities of experimental error and a constrained experimental design space prohibit direct inversion from being a reliable solution method in the general case. Instead, parameter estimation techniques will be used to smooth noisy data and mitigate limited linear dependence.

The rate calculation can be re-cast as a linear model problem:

$$U_i \circ q_t = A^T r_i + \epsilon \tag{3.15}$$

where U_i is a vector of measured concentrations of species i across different trials, q_t is the vector of flowrates in those trials, $\circ$ is the Hadamard (elementwise) product, A^T is the transpose of the matrix of phase surface areas, r_i is the unknown vector of leaching rates of species i from the mixture phases, ϵ is an error term, generally assumed to be normally distributed with zero mean and constant variance.

In this construction, the entries of r_i are coefficients of the independent variables in A. The abandonment of an exact solution technique due to collinearity in the variables A, also promotes the abandonment simple linear regression techniques. Instead, parameter estimation techniques developed using information theory, notably the method of generalized maximum entropy (GME)[47] will be used to estimate r_i. This technique mitigates the effects of significant collinearity in the independent variables and is described in greater detail in Appendix A.2.

Like all parameter estimation techniques, the values of the parameter estimates will becomes more reliable the more data is used in their calculation. At least one experiment is required to calculate any estimates, though the accuracy of any estimates calculated from a number of experiments less than the number of estimates is likely to be poor. In practice, a number of experiments which is equal to the number of parameters to estimate is the absolute minimum, and three-to-five times this number is necessary to begin to perform descriptive statistics on the values of the parameters. For the leaching rates, this translates to a minimum of one experiment per mixture constituent, with three-to-five times this number being more realistic.

3.6 Post-experimental Validation

The key advantage of microfludic leaching, that the surface features are not anonymous, enables the use of relatively simple methods to validate rates calculated from experimental data. Comparison of the elemental content of features pre- and post-

leaching, and the relative changes of each element, can provide an additional line of evidence, although indirectly, for the leaching rate values. Care must be taken to ensure that such measurements are representative; for instance, composition measurements via EDS should be distributed broadly among features along the channel, rather than clustered. EDS, while among the most convenient methods for a qualitative comparison such as this, can be sensitive to surface roughness[118] and as such the quality of surface preparation pre-experiment, and the condition it maintains post-experiment, are key to achieving accurate results.

A further qualitative factor is the presence or absence of phases after experiment. If a large leaching rate is calculated for a certain phase, the effects of that chemical change may be visible when comparing images of the phase before and after experiment. If a near-zero rate is estimated, then there should be essentially no change across leaching. These qualitative descriptors help to physically bound the otherwise purely mathematical exercise of rate estimation.

3.7 Selection of Relevant Phases

As described in Section 3.5, the number of experiments needed is dependent on the number of phases in the studied mixture. The absolute value of this number for any real mixture is a matter of philosophical concern, particularly with minerals. Many minerals exhibit wide ranges of solid solution behavior, even within singular nominal particles[56, 83]. While defining this number is difficult, it also has great consequences on the practicality of acquiring enough experimental data to calculate reliable rate estimates and therefore requires careful consideration.

In any mixture, it is likely that a subset of phases will dominate the overall leaching behavior and, in such cases, it is desirable that the number of required experiments does not greatly exceed the number of dominant phases. That is, when one desires to know only a subset of the leaching rates, then it is desirable to only perform a number of experiments commensurate with the number of important phases. The most straightforward path to this end would be to simply neglect all phases believed

to be unimportant to the mixture leaching behavior by not including surface area measurements for these phases in the A matrix. However, this simplistic approach introduces non-random error to the linear model described in Eq. 3.15. This effectively introduces a problem with *latent* variables and this can cause difficulty when estimating parameters using standard regression techniques, which assume the parameters contain all of the information needed to map the dependent variables to the independent variables.

A more suitable method is to create a mixed-effects model, where the undesired, minor, rates are represented as non-random, linear, error terms.

$$U_i \circ q_t = A^T r_i + B^T w_i + \epsilon \tag{3.16}$$

Where B^T is a matrix of the surface areas of the minor mixture components and w_i is an unknown vector of the rates associated with these components and species i.

This classic mixed-effect formulation can be made more suitable for the application of rate estimations by collapsing B^T to a single value per experiment: the total surface area of all minor mixture components. The weighting terms, w_i, then become the average rate over all minor components, a value of little utility. Under this formulation, the B^T and w_i terms can be subsumed into the A^T and r_i terms, respectively, yielding a final form:

$$\begin{bmatrix} u_{i,t_1} \\ u_{i,t_2} \\ \vdots \\ u_{i,t_n} \end{bmatrix} \circ \begin{bmatrix} q_{t_1} \\ \vdots \\ q_{t_n} \end{bmatrix} = \begin{bmatrix} a_{1,t_1} & a_{2,t_1} & \dots & a_{m,t_1} & b_{t_1} \\ \vdots & \ddots & \ddots & \ddots & \vdots \\ a_{1,t_n} & a_{2,t_n} & \dots & \dots & b_{t_n} \end{bmatrix} \begin{bmatrix} r_{i,1} \\ r_{i,2} \\ \vdots \\ r_{i,m} \\ w_i \end{bmatrix} + \epsilon \tag{3.17}$$

where u_{i,t_1} denotes the measured concentration of species i in trial 1, a_{1,t_1} is the estimated surface area of major phase 1 in trial 1, b_{t_1} is the total surface area of the minor phases in trial 1, and $r_{i,1}$ is the leaching rate of species i from phase 1.

This formulation shifts the burden of accounting for the systemic error, introduced

by intentionally neglecting the leaching contribution of minor phases, away from the desired parameter values,r_i, to the non-random error parameter, w_i enabling a more accurate estimate to be acquired. Data requirements are reduced from a minimum of one per phase, regardless of importance, to a minimum of one per relevant phase plus one additional experiments, regardless of the number of minor phases. As expected, this approximation is most applicable when the total contribution of the minor phases is small, generally less than 10% of the total rate for any species.

Chapter 4

Microfluidic Leaching of Hydrothermally Altered Potassium Feldspar

Hydrothermally altered potassium feldspar (herein: hydrothermal material) is a multi-phase material which possesses a complex geometry and exhibits complex leaching behavior in aqueous solution[21]. The hydrothermal material shows promise as a potassium fertilizer, however this complexity has thus far prevented the quantitative study of the kinetic contribution of each constituent phase to the fertilizer properties of the overall product. This difficulty hinders any attempt to optimize the material processing pathway and conditions, as the target composition at the end of processing is unknown. To remedy this, two models are needed: one describing the material transformation during processing, and the second describing the leaching kinetics of each phase in the material. As the hydrothermal material is difficult to effectively separate, determining the kinetics of each phase must be done through experiments on the complete material. Separating the contributions of each phase from the total leaching behavior of a complex mixture is the greater focus of this work, and the development of experimental methods to obtain concentration measurements necessary for determining these leaching rates is the subject of this chapter.

4.1 Experimental Design and Procedure

The model given in Eq. 3.15 informs the design of successful experimental apparatus for the gathering of data from multicomponent systems. Of key importance is that homogeneous reactions are suppressed as much as possible, so that the species concentration at the outlet is the product of only the leaching reactions. This requires that the contact time between the leachant fluid and leached surface be minimized, subject to the constraint that species concentrations much be sufficiently large as to be measurable above unavoidable contamination and measurement noise. In addition, the contact between the surface and fluid must be planar in order to allow for a simpler accounting of the surface areas of interaction of each phase with the fluid.

The initial technique employed in this work was adapted from Ciceri and Allanore[19]. A microchannel and fluid inlet and outlet ports were formed in a polydimethylsiloxane (PDMS) cast using a laser cutter. This polymer device was then joined to a thin-section of the desired sample through the use of a corona discharger or plasma cleaner (bonding was identical between techniques) , forming a complete apparatus for the microfluidic leaching of the sample. A schematic and photograph of an example of one such device is given in Figure 4-1.

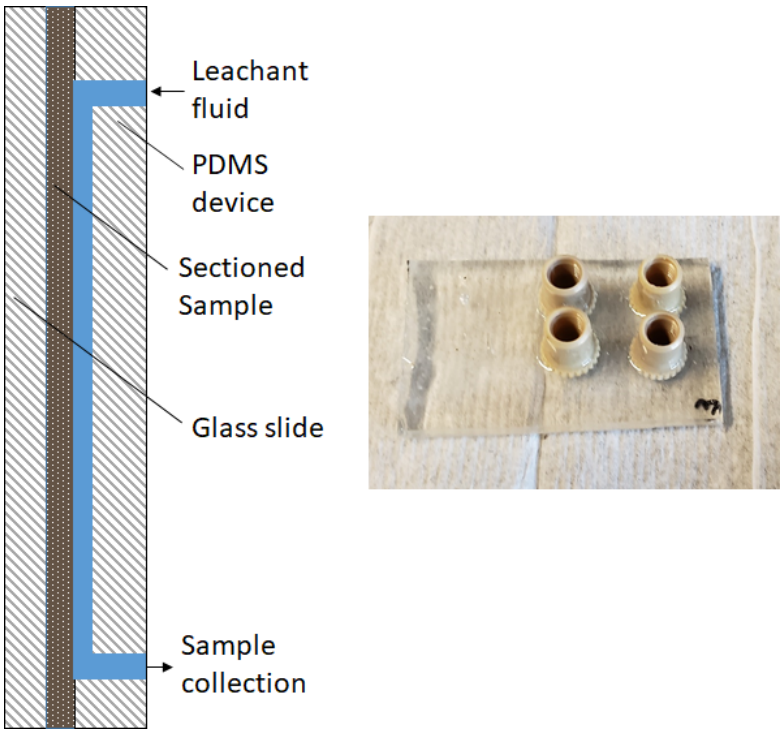

Figure 4-1: Left: Schematic representation of a thin-section microfluidic device. Right: Photograph of example device

In adapting this procedure for multicomponent systems, it was necessary to increase the reliability of the technique substantially. Substantial pressure was required to bond the PDMS to the thin section in order to ensure the bonding was sufficiently strong so as to withstand the pressure of the leaching fluid. This pressure would occasionally crack the glass of the thin section, preventing its use in flow experiments. It was also common for the bonding process to fail to pair the pieces with sufficient strength, which manifested as leaks from the sides of the channels or the formation of bubbles of fluid underneath the PDMS during experiment. Finally, misalignment between the fluid channel and its desired path was ubiquitous and generally of several channel-widths in magnitude. The accumulated errors of the mapping the locations of features of interest, translating that plan to a cutting path at the laser cutter, and finally bonding the device with thin section were simply too great to ensure accurate placement of a 100 micron-wide fluid channel. These physical difficulties, as well as reproducibility issues covered in Section 4.2.1, motivated the creation of a dedi-

cated platform to ensure alignment and reduce failures from bonding strength and the fragility of the glass.

A 304 stainless steel device consisting of two separate plates was created. A schematic and photograph are given in Figure 4-2. The bottom plate contains 8 channels 150 microns wide and deep, and 3 cm long. These channels are packed with the sample powder, and then filled with epoxy. After grinding away the excess epoxy, the plate is polished to prepare the sample surface for imaging and chemical analysis. The top plate contains 8 channels of identical dimensions connected to threaded holes for fluid handling. The channels are isolated by a recessed area which fits a silicone gasket to prevent leaks. Alignment is ensured by guide pins on the top plate, and mating is achieved with 16 screws in the center and around the perimeter of the device. However, as the steel is opaque, transmitted-light microscopy is not possible for analyze sample surfaces in the channel. This precludes the use of polarized light, which is commonly used in thin-section to distinguish classes of minerals[16].

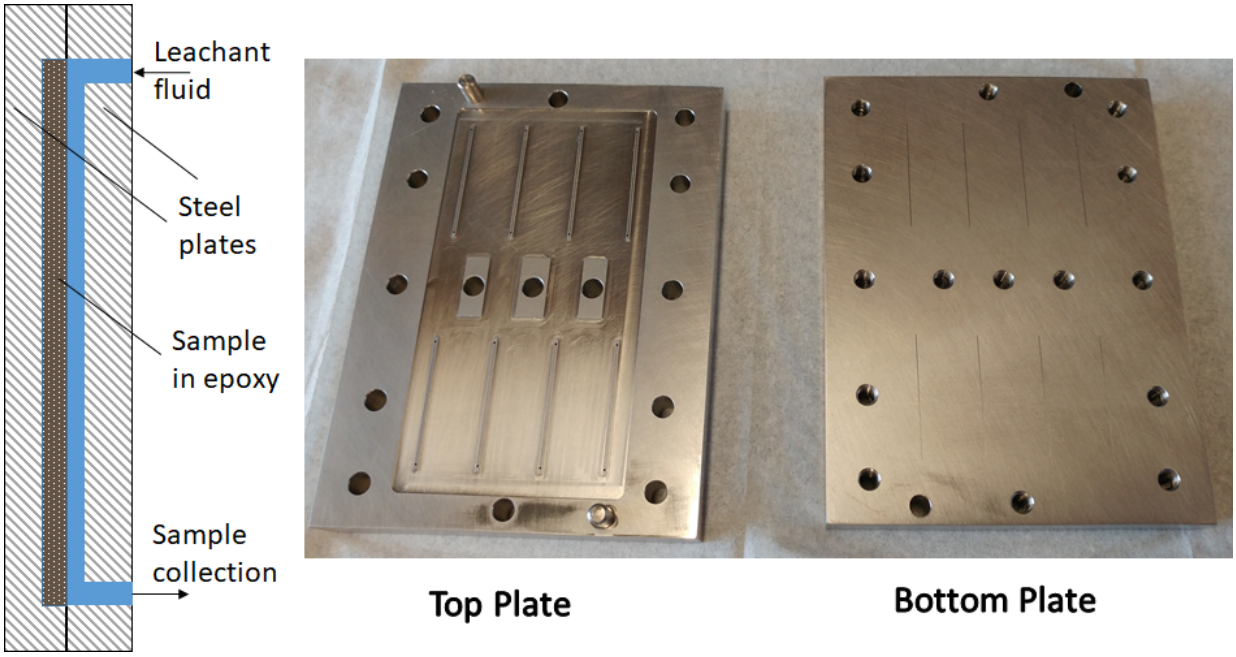

Figure 4-2: Left: Schematic representation of the steel microfluidic device. Right: Photograph of the steel device

In both thin-sections and the steel device, the goal of each experiment remains

the same: obtain reproducible measurements of the leaching concentrations and estimates of the surface areas of the mixture components. The greater the difference in surface areas between experiments, the more information is gained about leaching behavior. See Section 6.3 for a rigorous examination of the best experiments to perform. It must be reiterated that the experimentalist is not able to freely choose the solid phase surface areas present in an experiment. By definition, the mixtures considered in this work are difficult to separate, and so manipulation of the mixture surface areas is likewise challenging. In the microfludic form factor, sampling bias is leveraged to generate composition differences between channels and provide for the performance of independent experiments. The small (μg) solid sample contained in each channel is unlikely to be representative of the broader mixture and in this manner independent experiments can be performed on any mixture, regardless of the difficulty of separation. Of course, the more significant the differences between the channels, the low the condition number of the linear problem in Eq. 3.15 and the more stable the rate estimates will be in the presence of experimental uncertainty. Therefore, if it is possible to produce enriched mixture fractions via separation, the leaching of these fractions will likely be more valuable experimentally than leaching of the complete mixture.

4.1.1 Sample Preparation

Thin Section

Thin sections of the hydrothermal material were sourced from an outside vendor (Spectrum Petrographics; Vancouver, WA). These consisted of the powder material dispersed in epoxy (Epotek 301) and mounted on a glass slide. The thickness of the epoxy layer was approximately 30 microns. For planning the route of the microfluidic channel, a coordinate grid was engraved on a metal frame that held the thin section. A light microscope (Olympus BX 51) was used to study the section the locations of experimentally interesting features were recorded using this grid. Scanning electron microscopy (SEM) was performed on some thin section samples, but severe charging

artefacts were encountered and it was not found to have great utility. Using a vector graphics program, the desired path of the fluid channel was drawn by referencing the coordinates of the notable features. A cast of PDMS of the same approximate dimensions as the thin section was then made, and the fluid channel formed on one side using a laser cutter and the vector image. Skin biopsy punches of 1mm diameter were used at both ends of the channel to create holes through the PDMS for fluid inlet and outlet. The channel-side surface of the PDMS and sample surface of the thin section were treated for 30 seconds each by sweeping over them with a corona discharger. After treatment, bonding between the device and section was performed using a polyacrylate vice equipped with a recessed area to hold the section. After contacting the device and section, pressure was applied for one hour using the vice. Following bonding, threaded ports were placed over the fluid inlet and outlet ports and secured by adding uncured PDMS. These ports accepted the compression fittings and fluid lines for the syringe pump and sample collection vial.

Steel Device

Sample powders were packed into the sample channels of the bottom plate, then epoxy (Epotek 301 or 377H) was added via pipette to cover the powder. The plate was placed in a vacuum chamber for curing, to help reduce the occurrence of air bubbles in the epoxy. After curinng, the excess epoxy remaining on the device was ground away with successively finer grits of silicon carbide paper, with the final step being 2500 grit (8 micron). Once the surface of the epoxy was flush with the surface of the steel, a non-aqueous suspension of 3 micron diamond particles was used until the scratches in the steel from the previous steps were largely removed. Final polishing was performed using a 1 micron diamond paste with a non-aqueous lubricant. Polishing at this step proceeded until sharp reflections could be seen in the steel. The condition of the steel surface was used as a gauge of the level of polish of the sample surface. After polishing, the plate was cleaned by rinsing with hexanes to remove remaining lubricant and waste material.

The previous steps prepare the surface for microscopic analysis. Electron mi-

croscopy was preferred to light microscopy for the steel device, as the steel blocks transmitted light. To combat charging of the sample, an epoxy with a graphite additive (Epotek 377H) was used for later samples in this work, and the backscatter electron detector was used rather than the secondary electron detector. The sample channels were partially mapped for each experiment; the processing of these images is discussed in Chapter 5. To prepare for flow experiments, a silicone gasket is fit to the recessed portion of the top plate visible in Figure 4-1, and the plates are joined and screwed together. The top plate integrates the threaded ports for fluid handling between the syringe pumps and sample collection vial.

4.1.2 Common Procedure

Flow experiments for both form factors proceeded identically. The leachant fluid, an aqueous solution of nitric acid of known pH, was held in a 10 mL syringe. The syringe was housed in a syringe pump (Harvard PHD Ultra) to control the flow rate (0.1 mL/hr for all thin section samples, 0.1 or 0.3 mL/hr for the steel device) and connected to the channel inlet with hard plastic tubing (Cole-Palmer 0.01" - .254mm ID). Under these conditions, the residence time of the fluid in the exterior tubing was on the order of 10 seconds, and the residence time in the channel was on the order of 10 seconds. The outlet fluid was pooled for a set amount of time, most commonly 3 or 12 hours, at which point the sample vial was sealed and replaced with a new vial. Concentration measurement was performed using ICP-MS. The microfluidic samples were diluted 1:100 in 1M nitric acid prior to analysis, to ensure adequate volume for analysis. All samples reported here, in both thin section and the steel device, were created from the same batch of hydrothermal material created using the procedures described in[21].

4.2 Leaching Results

The hydrothermal material was investigated using the microfluidic technique in both form factors. First, the results from the thin sections will be briefly summarized,

including comments on the reliability and durability of the devices. Then the results and refinements of the steel device will be presented.

4.2.1 Thin Section Leaching

In further developing the thin section technique for multicomponent systems, the focus was on experimental reproducibility and reliability. Given the data requirements for studying mixtures, and the relatively small difference expected between channels, it is necessary to minimize the failure rate of experiments and the experimental variance in order to produce a practical investigative technique. These goals were not met with the thin sections. Shown in Figure 4-3 are the leaching results for six separate channels on five unique sections of the same material.

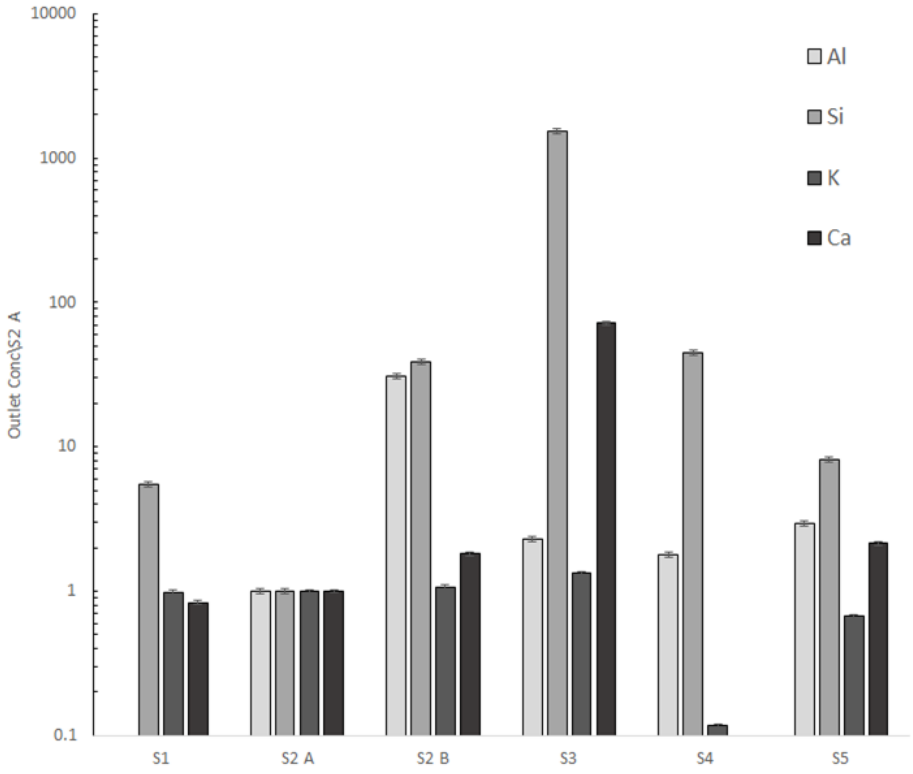

Figure 4-3: Outlet concentrations for several elements measured for six different channels on five different thin sections of the same material. All results are normalized to those of Section 2 A, to show the variance between channels.

Experimental reproducibility was poor across the studied sections, in particular for the polyvalent species and especially for silicon, where the variance across this data set is measured in factors of a thousand. These differences are far larger than would be expected due to random variance of sample surface composition; taken at face value they suggest a material that is already strongly segregated, which is known to be false. One potential explanation for the anomalous variance in silicon is extra leaching from the PDMS, which has been observed by other researchers under certain conditions[15]. In general, the large variance in leaching concentrations is likely a product of the poor bonding of device and thin section at the boundary of the channel. These large experimental variances leave the absolute leaching results with little quantitative utility, however an advantage of the microfluidic technique is the static nature of the surface which allows qualitative statements on leaching behavior to be made. Figure 4-4 shows the effect of acidic leaching of the hydrothermal material.

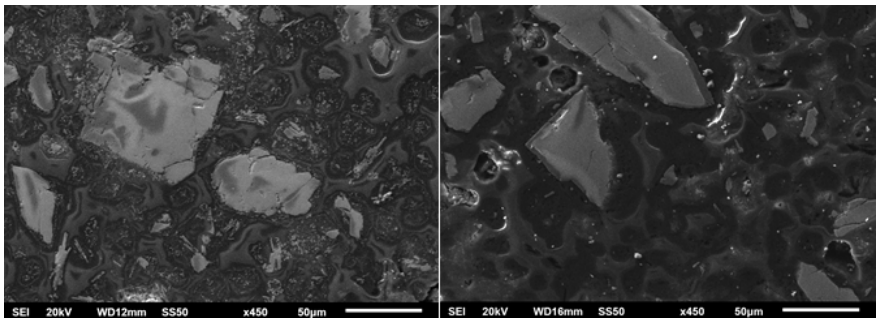

Figure 4-4: Left: A micrograph of the hydrothermal material in thin-section before leaching, note the presence of minor phases around the large feldspar features. Right: A micrograph of the same material after leaching (pH 5 nitric acid, 4 hours) the minor phases are absent.

The images given in Figure 4-4 exhibit one of the more persuasive arguments in favor of microfluidic leaching techniques. Eliminating the anonymity of the surface serves to ground the observed chemical behavior in very visual terms. This also offers some insight into the relative stabilities of the phases under the leaching conditions, and can therefore help to bound reasonable values for the leaching rates. The information given by Figure 4-4 while important, is not inherently actionable. The

calcium-aluminum-silicate-hydrate (CASH) phases which dissolved are believed to be the primary source of the material's fertilizing ability, given the relatively inert nature of feldspar on its own[22, 21]. It is the rate of release from these phases, however, that determine how and in which contexts the material can be used.

Imperfect bonding near the channel edge created dead spots for flow outside the main path of the fluid. In these areas, seen to extend up to multiple channel widths from the nominal edge of the channel, a Si-rich precipitate was observed. Examples of this precipitate are given in Figure 4-5.

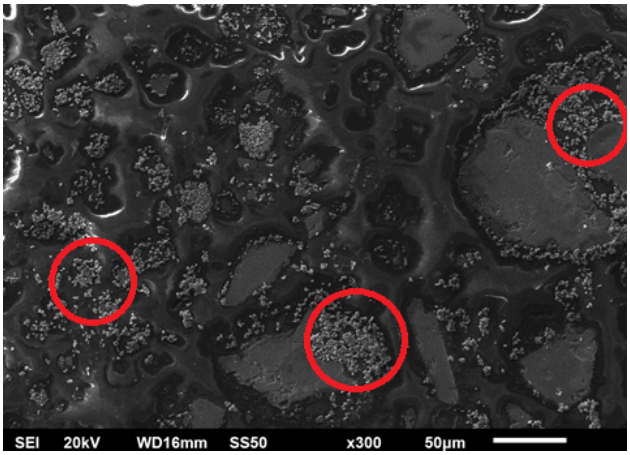

Figure 4-5: A micrograph of the hydrothermal material after leaching (pH 5 nitric acid, 4 hours). The region shown was outside the main path of the channel and not intended to be subjected to the leaching fluid. The red circles denote examples of the silicon precipate which can be observed throughout the micrograph.

The presence of this precipitate outside the fluid channel confirms the the presence of leaching fluid in these areas. This result makes it impossible to effectively estimate the surface area of the components exposed to leaching, and renders the model of Eq. 3.15 incompatible with the reality of the fluid dynamics of the experiments. While the surface of the thin section is highly polished, it is not homogeneous, and the different surface chemistries encountered preclude identical adhesion across the device. Given the dimensions of the microchannel, even macroscopically small areas of leakage can represent very large increases in the total area of leaching, rendering

the concentration measurements unreliable indicators of the leaching behavior of the surface in the channel.

Device reliability was a major obstacle for the thin section experiments. The preparation procedure laid out above is long, taking several days per section, and only a few opportunities for parallelization are available. This time investment is further challenged by the high failure rates at each step of the procedure; the bonding between the PDMS and thin section can fail immediately, it can fail under flow, the glass can crack under the pressure applied for bonding, the channel can be misaligned with its intended path, and fluid can leak from the handling ports if their mounting is weak. All of these failure modes were observed experimentally, and not all of them were able to be sufficiently mitigated over the course of the project. Notably, the strength of the bonding between the PDMS and thin section remained an everpresent concern and, as the nature of the chemical changes induced by the current supplied by the corona discharger are not well understood, improvements to this weakness were slight. Experimentally, this also limited the obtainable flowrates, as no thin section device passed a volumetric flow above 0.1 mL/hr without leaking. The challenges and limitations identified in this section strongly motivated the creation of an alternate platform for the microfluidic technique.

4.2.2 Steel Device Leaching

The steel device reduced the failure rate of experiments from roughly 50% to about 8%. Remaining failures were almost entirely leaks from the fluid inlet ports, due to the plastic fittings being somewhat incompatible with the steel threads. Channel dimensions and locations were standardized, and this prevented misalignment errors. A gasket isolating the channels prevented any small leak in one channel from impacting the other experiments, and the absence of active material outside of the channel path prevented such a leak from introducing additional sources of the leached species, beyond what was present on the sample surface.

These improvements presented themselves in a greatly reduced experimental variance, as shown in Figure 4-6.

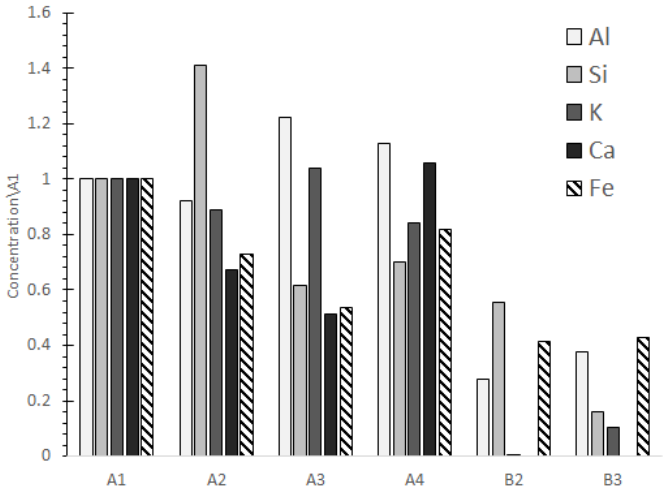

Figure 4-6: Species outlet concentrations measured using the steel device for 6 separate channels. A1-A4 held the sample material, B2 and B3 contained only epoxy.

In comparing Figures 4-6 and 4-3, a drastic reduction in experimental variance is seen. While the variance in the silicon signal in the thin section experiments was on the order of 1000, for the steel device it is at worst a factor of 2. The potassium and aluminum signals are generally within a 20% range, which is a more reasonable variation to explain with surface effects. A consistent iron background is seen in the blank channels, however the presence of the material in the A channels appears to increase the leaching of iron from the steel. Additionally, correlation is seen between the signals of calcium and iron; this is concerning as, per the model, all species should be independent.

Micrographs of the sample surface post-experiment showed the presence of a highly amorphous, Si-rich precipitate phase intermittently covering the sample. One example of this phase is shown in Figure 4-7. From EDS analysis, the gel was found to contain a large and variable amount, 15-45wt%, of the polyvalent species in the system, Ca, Fe, Cr, and Ni. The composition varied spatially, and the gel deformed under the electron beam.

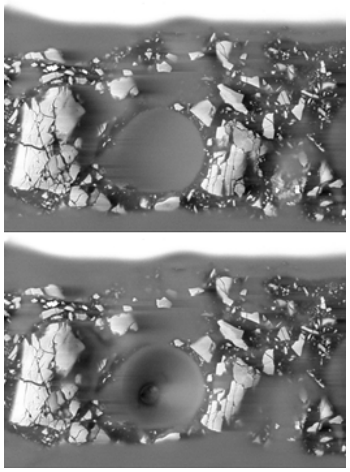

Figure 4-7: Top: A micrograph of the Si-gel in a channel of the steel device. Bottom: The same area after analysis via EDS, the gel has deformed from the action of the electron beam.

The presence of this gel in the channel, while not conclusive evidence of homogeneous reactions, suggests such reactions occur. As stressed during development of the model, the suppression of homogeneous reactions is of utmost importance; they violate nearly every simplifying assumption of the model, and the surface leaching rates cannot be related to the flow-averaged concentration if they are present. The aqueous chemistry of silicon in the presence of calcium is poorly understood, and the presence of iron, chromium, and nickel in the gel also adds to complexity of developing any kinetic model for its formation. Tripling the volumetric flowrate to 0.3 mL/hr, while a simple solution to a complex problem, did succeed in suppressing formation of this gel. It was never observed in a sample at this higher flowrate.

The gel was emblematic of more widespread issues with silicon measurement, partly due to its complex aqueous chemistry, but also as consequence of the choice of ICP-MS for measuring the sample concentrations. Silicon is not an element that is well-suited to ICP analysis; at low pH, it exists in water as amorphous quartz[68] with low solubility compared to higher pH[67]. Additionally, it is poorly aerosolized by the nebulizer leading in to the plasma torch, and thus subject to sampling errors. The calibration curves for silicon tended to be largely flat - signifying that the con-

centration of silicon in the sample did not have a large effect on the signal measured by the ICP. It was therefore desirable to find a method to increase the instrument's sensitivity to silicon, in order to better quantify its leaching behavior.

4.2.3 Silicon Stabilization

Silicon is known to complex with organic species in solution[84, 73, 134], and this was seen as a mechanism by which it's detection via ICP-MS could be improved. Two organic molecules, oxalic acid and tetramethylammonium hydroxide (TMA), were investigated. Several solutions of silicon at known concentrations (0.1, 1, and 10 ppm) in 1M nitric acid were prepared as a control set, with no additive, and with known concentrations the additives. Figure 4-8 shows the ratio of signal increase over the control samples for each of the additives.

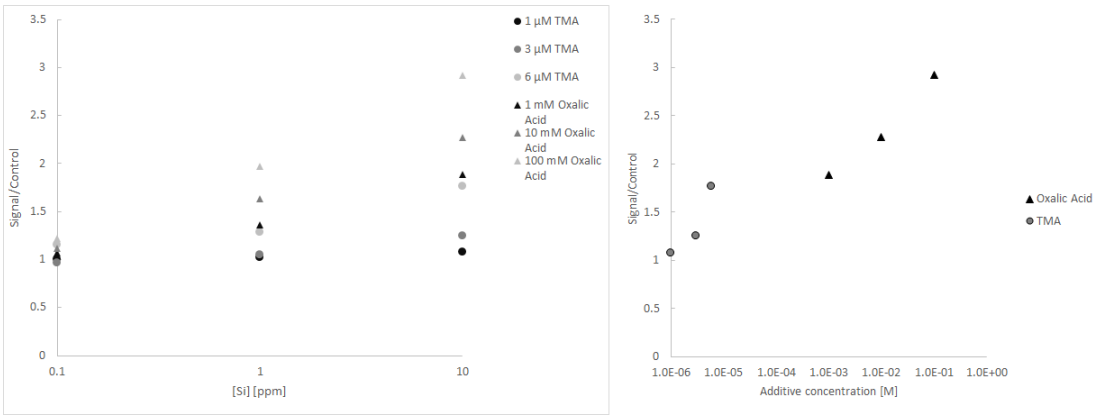

Figure 4-8: Left: Fractional increase in the Si signal for each Si and additive concentration. Right: Signal increase at 10 ppm Silicon vs. additive concentration

Both the oxalic acid and TMA were found to be effective at increasing the silicon signal. The TMA was found to be approximately 16,000 times more effective than oxalic acid, per molecule, at increasing the silicon sensitivity. This metric of effectiveness is important, as soot can form on the plasma torch if the sample contains too much carbon.

With these results, the increased reproducibility shown in Figure 4-6, and the suppression of the Si-gel formation, the major experimental challenges with the mi-

crofluidic leaching technique were resolved.

4.3 Discussion

The transition from single-use thin sections to the reusable device greatly improved the experimental utility of the microfluidic technique. With the results presented in this chapter, there was confidence that concentration measurements could be performed with enough precision to be useful in calculating the leaching rates. The final accuracy of this calculation depends both on the concentration measurements, and the surface area estimations covered in Chapter 5. In this project, it was found that this second task, estimating the phase surface areas, was much more difficult than addressing the experimental challenges with concentration measurements. These measurements, while necessary to study the kinetics of multicomponent systems, do not suffer from the increased complexity discussed in Section 1.2, and as such are not expected to become more difficult as the number of system components increases, so long as homogeneous reactions can be suppressed and the analysis technique chosen can measure species independently.

Chapter 5

Phase Classification in Microfluidics

As described in Chapter 3, two experimental quantities are necessary to enable the calculation of individual leaching rates from multicomponent systems in microfluidic leaching experiments: the phase surface areas, and the leached species concentrations in the effluent. The leaching measurements reported in Chapter 4 cover this second quantity, and this chapter details the methods employed to estimate the surface areas of separate mineral phases present in those microfluidic leaching experiments. As this estimation is the key obstacle in the rigorous extension of microfluidic leaching to multicomponent systems, considerable effort was devoted toward this problem. The results of three main avenues for classification: shape, machine learning, and chemical composition are described below.

5.1 Imaging of Microfluidic Samples

Early procedures for the microfluidic leaching of minerals were carried out using mineral thin-sections [19]. Thin-sections, 30μm-thick slices of minerals mounted in epoxy on glass slides, are commonly used in petrology and many techniques for analysis via optical microscopy have been developed [16]. Due to the random assortment of mineral features across the area of the section, alignment of desired features with a micro-channel bonded to the surface was poor, and a more robust microfluidic device was developed for this work.

The steel microfluidic device ensure alignment of the fluid channel and sample surface, and allowed microscopic imaging to focus on a narrower formation of features. Several classical technique from optical microscopy, notably the use of polarized light, are not possible with the current device due to its opaque nature. Following from this limitation, the vast majority of microfluidic samples were characterized using Scanning Electron Microscopy (SEM).

5.1.1 Sample Preparation

The powder samples were packed into the 150μm-wide sample channels on the bottom plate of the device. A small excess of powder was allowed to remain above the level of the channel lip to avoid the sample settling below the channel lip later on. A two-part epoxy that was either optically clear (Epotek 301-1) or electrically conductive (Epotek 377H) was prepared and spread over the powders in the channel. Vacuum was applied for 1-2 hours to allow the epoxy to impregnate the samples thoroughly. The sample plate was then removed from vacuum and the epoxy was allowed to cure. Following curing, the sample plate was ground with 1600-grit silicon carbide sandpaper until the epoxy was nearly flush with the channel edge and with 2500-grit silicon carbide sandpaper until the epoxy was exactly flush with the channel edge. Lubrication for grinding was provided by kerosene or mineral oil, with no difference in grinding quality noted between the two. Polishing of the exposed powders was performed in two steps, the first being a non-aqueous 7μm diamond suspension, and the second, final, polishing step being a 3μm diamond paste. After polishing, the plate was cleaned with hexane to remove leftover polishing media and lubricant.

5.1.2 Electron Microscopy

The sample plate was analyzed using a Jeol 6610LV SEM. Imaging was performed using an accelerating voltage of 20kV using the backscatter detector, due to its lower susceptibility to charging artefacts over the secondary electron detector. The sample plate was arranged such that the sample channels ran horizontally across the field

of view and magnifications were on the order of 300x. Images were taken using a 2-minute scan rate, and were staggered down the length of the channel without overlapping. For certain samples, interference from sample charging was significant enough to require the use of low-vacuum conditions. For these samples, imaging was performed at chamber pressures between 20 and 25 psia. EDS measurements were taken at a fixed working distance of 10 mm, at an accelerating voltage of 20kV, and exclusively under high-vacuum. Minimum detector counts were 100 thousand for point analyses, and 1 million for elemental maps. An example micrograph taken with the SEM is given below in Figure 5-1.

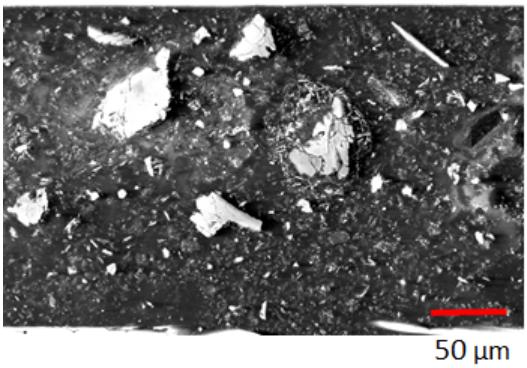

Figure 5-1: Example micrograph of the hydrothermal material

5.2 Image Segmentation and Analysis

To separate mineral features in the sample channel from the channel walls and epoxy, an automated image segmentation and object measurement routine was created in MATLAB. The routine operates in 5 basic steps:

1. Determine image scale
2. Image pre-processing
3. Binarize image using Otsu thresholding
4. Image post-processing
5. Detect and measure objects in binary image

5.2.1 Determine image scale

Each sample micrograph contains an information overlay containing the scale bar and scale text. For accurate assessment of sample surface areas, the scale of each image must be set according to this information. This overlay is separated from the image as the first step of image analysis and processed independently. This is necessary to prevent the objects in the overlay from being interpreted as mineral features during later stages of processing. A visual schematic of the process flow is given in Figure 5-2.

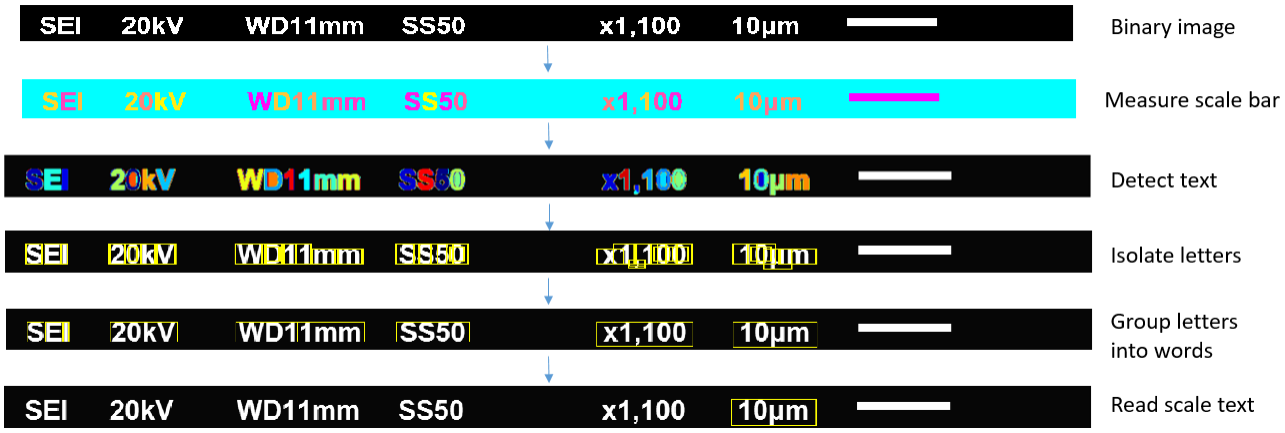

Figure 5-2: Process used to determine scale of sample micrographs

Once separated, the overlay is converted to a binary image and the image objects measured. The object with the widest bounding box in the bottom-right quadrant of the image is assumed to be the scale bar, an assumption that always resulted in choosing the correct scale for this work. The scale text is located through its fixed position relative to the scale bar, and the individual letters are grouped into words. Optical character recognition (OCR) is used to read the numerical value and units of the scale text. By dividing the number given in the scale text by the pixel length of the scale bar, the image scale is set in units of scale units per pixel. All following measurements of image objects are converted to physical quantities through the use of this scale.

5.2.2 Pre-processing

Pre-processing of the main image is intended to remove digital noise and improve contrast in order to enhance the accuracy of the binary image. A linear filter is applied, which averages the values of pixels in a 5-width square. This helps to reduce the effects of image 'grain', a false texture visible in the image due to electrical perturbations effecting the signal from the electron detector, while slightly increasing the difficulty of detecting objects of coincident size with the filter. The final step of pre-processing is to improve the image contrast by saturating the upper and lower 10% of the brightness levels. This step essentially spreads the image histogram to occupy a greater portion of the available 255 brightness values. While this does not create any new information, it does allow an easier visual comparison between the adjust image and the eventual binary image.

5.2.3 Binarize image

Creating a binary image converts the grayscale pixel values into logical values of 0 or 1. Thresholding via Otsu's method[99] is used to create the binary image; a pixel brightness value is chosen and all pixels below this value are extinguished while those above are set to 1. This simplicity belies the fundamental importance of this step. All decisions regarding which image features are objects which should be measured occur in this step, and the pre-processing steps are there to ensure that the binary image represents experimental intuition as to which features to include as closely as possible.

5.2.4 Post-processing

Before measuring the image objects, the binary image is processed once more to remove noise. Morphological opening, a technique to remove small objects while maintaining the size and shape of larger objects, is used to remove the small star-like binarization noise that commonly afflicts the background of the binary images. The size threshold for removal was set by determining a lower limit of physical size which

could be reliably characterized using the microscopy conditions, $4\mu m^2$, and converting this to a pixel size threshold using the image scale found in Section 5.2.1. A second noise filter was implemented following the investigation of cluster analysis for object classification. The mechanism of operation and experimental results of this filter are given in Section 5.3.3.

5.2.5 Object Measurement

Image objects are defined as being 8-way connected components of bright pixels. That is, in the binary image, an object is a white pixel and all white pixels in the 8 neighboring positions, and all of their neighboring white pixels; and so on until no neighboring pixels are both bright and not already part of the object. Objects, then, are connected components as defined by graph theory[55]. Informally, each object can be viewed as the 'islands' of white in the 'sea' of black in the final binary image. A comparison between an initial SEM micrograph and the final image objects is given in Figure 5-3.

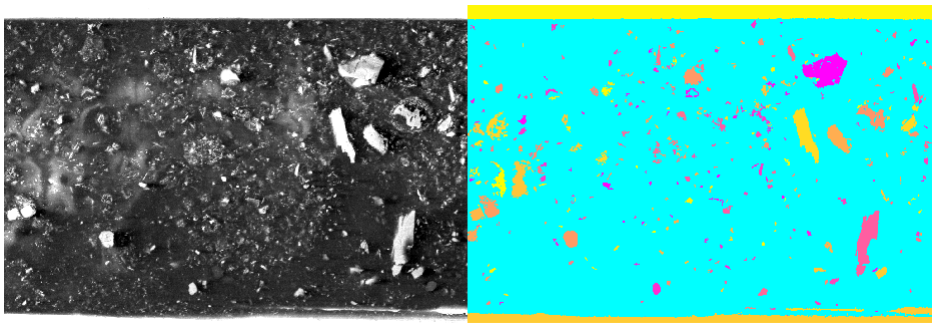

Figure 5-3: Left: Initial sample micrograph. Right: Image objects, labeled by color.

Measurements of the properties of these objects proceed via pixel counting and limited mathematical manipulation. The area of the objects is defined as the number of pixels they contain, which must be converted to a physical measurement through the use of the image scale. At this stage, 15 properties of each object are measured, including area, perimeter, solidity, euler number, centroid loacation, major and minor axis lengths, and eccentricity. These properties are gathered into a table and can

then be used in concert to create shape factors of varying complexity, with the goal of classifying the parent object into the mineral categories present in the sample. At this point in the analysis, all information that can be gained from the sample images is accessible and the challenge is no longer one of measurement, but of classification.

5.3 Classification via Shape Factors

Classification of the measured objects solves the identity problem introduced in 1.2. The microscopy procedure laid out above provides a large amount of information on the appearance of each object, notably size and shape, which may offer an avenue to classify the objects by mineral identity. Shape factors provide a method to condense this information into a set of values from which conclusions can be drawn.

A shape factor is a dimensionless, quantitative, descriptor of an object which is dependent on that shape of the object, but independent of the size (or scale) of the object[105, 27]. The use of shape factors to perform object classification inherently assumes a significant difference in shape exists between objects of different mineral identity, and that this difference can be adequately described using a reasonable number of quantitative descriptors. Shape factors have been successfully utilized for object identification in biological applications[114, 94, 137], which motivates their application to another natural system.

5.3.1 Simple Shape Factors

Simple shape factors, as defined in this work, include information from at most three object properties. Examples include aspect ratio, circularity and elongation[41]. Multiple shape factors were calculated for each object and different combinations thereof were plotted simultaneously. 5-4 shows the results for the plot of aspect ration vs. circularity for hydrothermally altered potassium feldspar.

For this material, simple shape factors were not found to be sufficient to distinguish any of the seven major phases present in the hydrothermal material. This failure motivated enlistment of more complex metrics of shape.

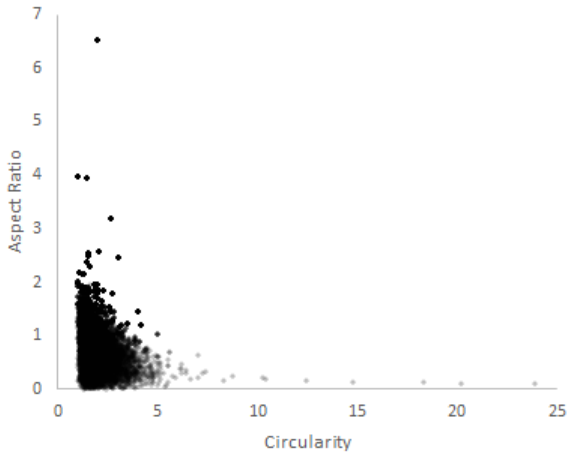

Figure 5-4: Aspect ratio vs. circularity for a representative sample of hydrothermally altered potassium feldspar

5.3.2 Complex Shape Factors

Complex shape factors, as defined in this work, are those that require more than three object properties to calculate. The main one employed here was taken from [105] and uses information from the object perimeter, area, feret diameters, and number of corners in its calculation.

A histogram of the Podczek shape factor values calculated for the same objects as in 5-4 is given in 5-5. The use of this more complex relation did not produce visually distinct regions of object properties which could be identified as comprising distinct mineral features. To better examine possible patterns in the shape factor data, algorithms for cluster analysis were applied to the results of both the simple and complex shape factor analyses.

5.3.3 Cluster Analysis

Cluster analysis is a data analysis technique used to quantitatively study the structure of data. This allows non-obvious groupings of data points to be defined, and was applied to the object shape factor data to test for obscured structure. In brief, these algorithms compare a measure of the distance between data points to a criterion distance for cluster formation - points that are closer to each other than to

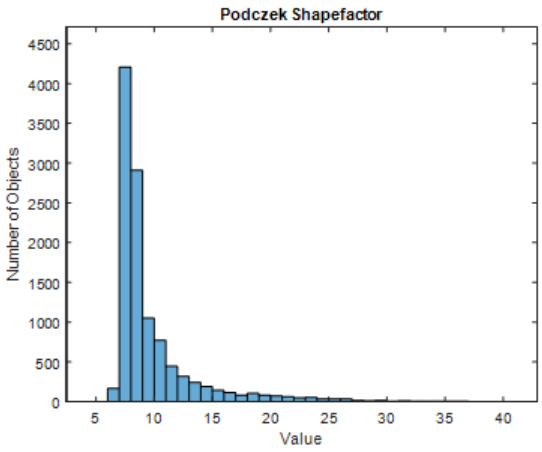

Figure 5-5: Histogram of the Podczek shape factor values calculated for hydrothermally altered potassium feldspar

other points are grouped as a cluster. DBSCAN has two parameters, the maximum distance between points for them to be considered part of the same cluster (ϵ, and a minimum number of points needed to form a cluster. OPTICS is substantially the same algorithm, but abstracts the distance parameter to allow for the examination of cluster structure. The euclidean distance used in this work generalizes well to higher dimensions, and this enables many shape factors and object properties to be used simultaneously for classification. As a greater number of dimensions are used to describe each data point, the data naturally becomes more sparse[1]. This can aid in clustering, with the caveat that data visualization beyond three dimensions is increasingly difficult.

Analysis of the shape factor data in two dimensions, aspect ratio and circularity, and three dimensions, via adding the Podczek shape factor, could not produce clustering behavior of use in the positive identification of image objects. While it is difficult to show images of the direct clustering output via DBSCAN, due to the large number of permutations of the parameters, plots of the reachability distance calculated via OPTICS - the smallest value of ϵ at which a point would form and propagate a cluster - offer greater insight. Clusters appear as valleys in reachability distance plots, with deeper valleys signifying denser clusters. Points with larger reachability distances form the 'mountains' in these plots, and separate the different clusters

from one another. A representative reachability distance plot for 4-dimensional shape factor data (aspect ratio, circularity, Podczek, and area) of a sample micrograph of hydrothermally altered potassium feldspar is shown in 5-6.

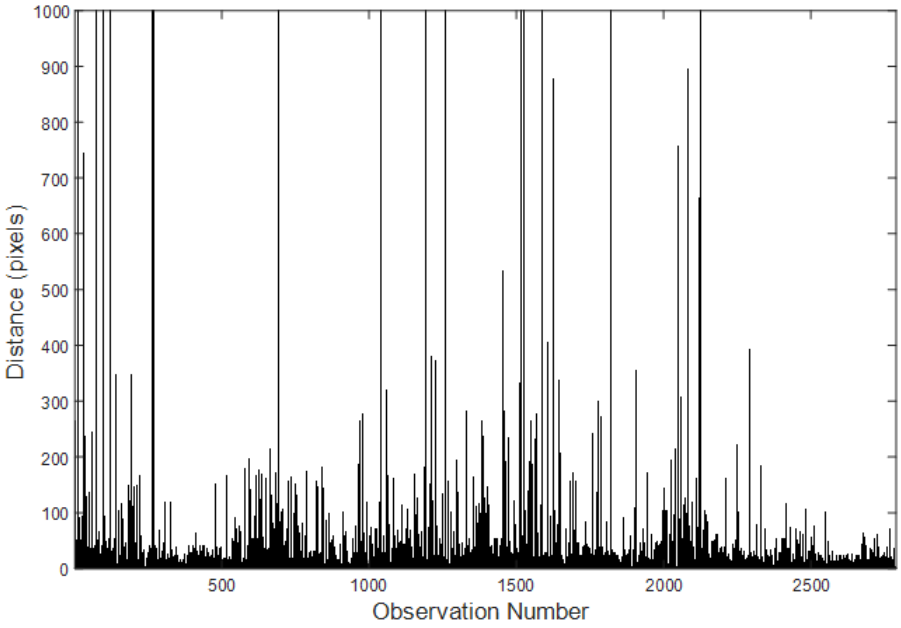

Figure 5-6: Reachability distances of objects in micrographs of hydrothermally altered potassium feldspar. Data dimensions are object area, major and minor axis lengths, and convex area. The minimum cluster size is 3 points.

The reachability distance plot shows few clear valley-type signals for clusters. A large number of clusters can be formed using a very small distance parameter, as shown by the heavily populated bottom edge of the graph. Small increases to the distance parameter will cause many of these clusters to merge, as shown by the relatively low barriers between the identified valleys. The few features with very large reachability distances are feldspar features, which have very large areas.

Sharp changes in the slope of the sorted reachability distance plot can identify ϵ values at which separate cluster structures would be found. The sorted complementary plot to 5-6 is shown in 5-7.

The gradient of reachability distance changes continuously, rather than at discrete points. This leaves no obvious choices for the values of ϵ which will produce a natural grouping of the data. This suggests that such a grouping is not present, and hard boundaries between the properties of objects of different mineral identity do not exist.

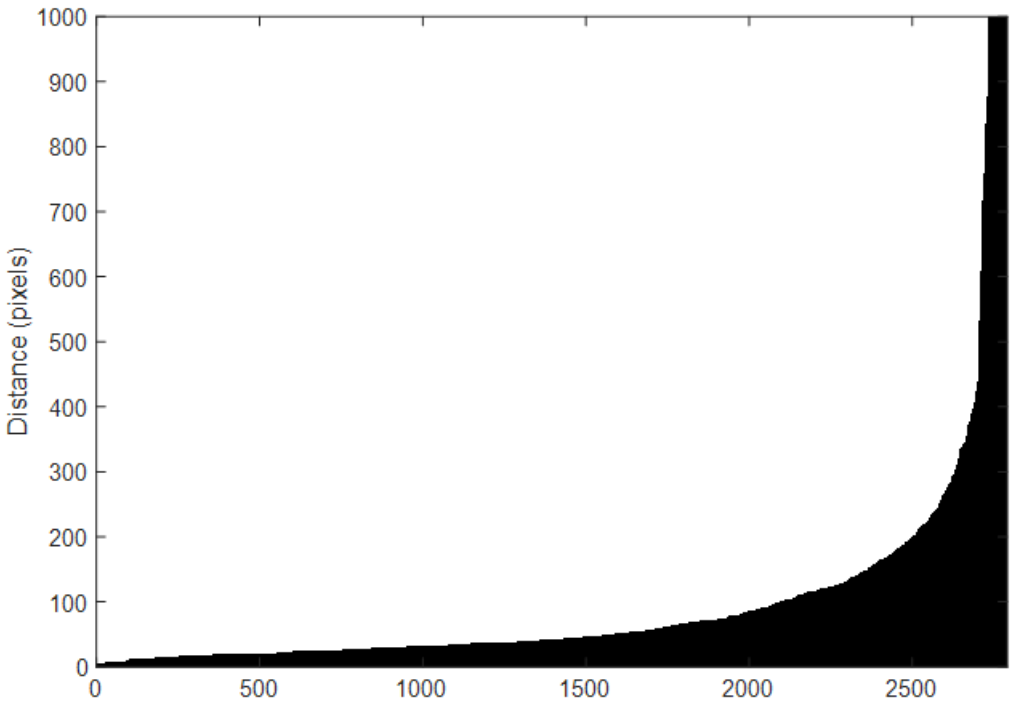

Figure 5-7: Sorted reachabilities distances of objects in micrographs of hydrothermally altered potassium feldspar. Data dimensions are object area and centroid coordinates. The minimum cluster size is 3 points.

However, the large number of clusters present at very small reachability distances did provide a reliable and powerful method to remove noise objects from the images.

Noise Removal

The DBSCAN algorithm classifies unclustered points as noise in the underlying structured data. Ironically, in this work, it was found that noise objects in the image were much more similar and easy to cluster than the objects representing true features. This allowed the implementation of a further refinement step in image post processing, where noise remaining after other post-processing steps could be effectively removed. Reductions in the number of detected objects routinely exceeded 80% using the centroid coordinates and object areas as the data dimensions. An example image of the filter in action is given in 5-8.

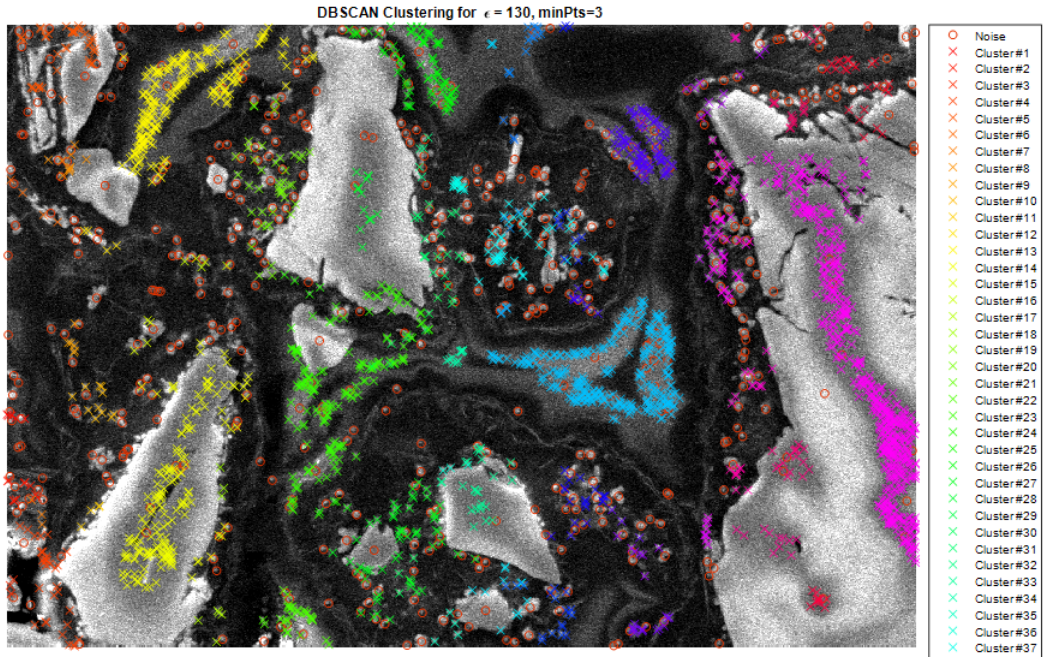

Figure 5-8: Clustering of image objects by centroid location and pixel area. The true image features were found to remain unclustered -labeled 'Noise' - with high probability.

5.3.4 Shape Variance under Rotation

Following the failure of shape information to provide a reliable method of object classification, it becomes necessary to explain why classification via shape appears to fail in the case of polished mineral powder surfaces, when it is successful in other applications. One possible explanation is that the underlying assumption - that significant and quantifiable differences in shape exist between objects of different mineral identity - is incorrect. This would represent a strong rejection of one of the hypotheses of this work, as traditional image analysis techniques would not be sufficient to allow the extension of the microfluidic leaching technique to multicomponent systems, and such a statement requires further explanation. The single-cluster structure observed in the shape factor data strongly supports that the variance of shape *among* like-mineral features is of similar magnitude to (if not greater than) the variance of shape *between* mineral classes in the microfluidic section. This may naturally arise as a

consequence of the procedure used to produce the sections, and not be present in the original sample.

Dispersal of the powder sample in epoxy creates a random orientation of objects of each mineral identity, and the grinding and polishing steps effectively destroy information about the shape of those objects. In essence, each three-dimensional object in the sample is cut by a randomly oriented plane, and the cross section produced by this cut is the surface visible through microscopy. The shapes of these sections can vary drastically depending on the angle of the cut, and as such can prevent the use of shape factors from positively identifying samples even in cases where the three dimensional powders are of different shapes. This effect can be most easily described using simple shapes, herein cubes and cylinders, but it applies, and may be even more significant, for more complex shapes. The cross-sections of a cube taken from its intersection with a randomly-oriented plane, and the same for a cylinder are shown in 5-9.

The aspect ratio vs. circularity plot of a sample of 300 randomly-generated cross sections is shown in 5-10. There is significant overlap in the shape factor ranges for these cross sections, with the variance of the aspect ratio and circularity between cubic and cylindrical sections being within 3% of the variance of these metrics for cubic sections alone.

For completeness, the Podczek shape factor for the sections was also calculated and a histogram is shown in 5-11.

These results for primitive shapes underscore the difficulty in using shape information to classify objects from images of sectioned samples. While not conclusive evidence for the same behavior in the complex shapes of real mineral powders, these observations nonetheless apply equally to all non-spherical shapes, and it cannot be assumed *a priori* that any arbitrary collection of particle shapes in a sample will be free of this difficulty. Further, the natural variety of shapes that comprise real samples naturally imparts variance to metrics of shape before considering the range of values possible for a random assortment of cross-sections. Shape alone is therefore unlikely to be a sufficient metric for solving the identity problem and enabling the

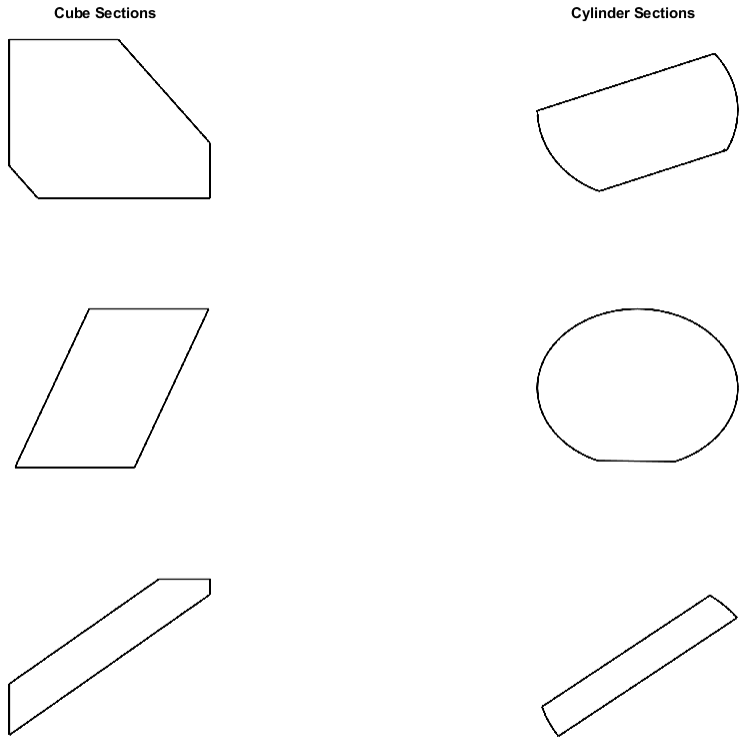

Figure 5-9: Example cubic and cylindrical cross-sections generated with random cutting planes

extension of the microfluidic leaching technique to multicomponent systems.

While more shape factors exist than were used in this work, there is only a limited amount of novel information accessible through other shape metrics. Many shape factors are highly correlated with others, such as elongation, variously defined as the square root of the ratio of the second and first image moments or the aspect ratio of the bounding box, is essentially equal to the aspect ratio calculated in this work. Eccentricity is also similar, only using the axes of the bounding ellipse instead of the bounding rectangle. Compactness, a quantity which has seen increased discussion in the public sphere due to its application to congressional redistricting[136], is fundamentally similar to circularity, as they can both be defined as the ratio of the object area to the area of a circle with the same perimeter as the object. More esoteric

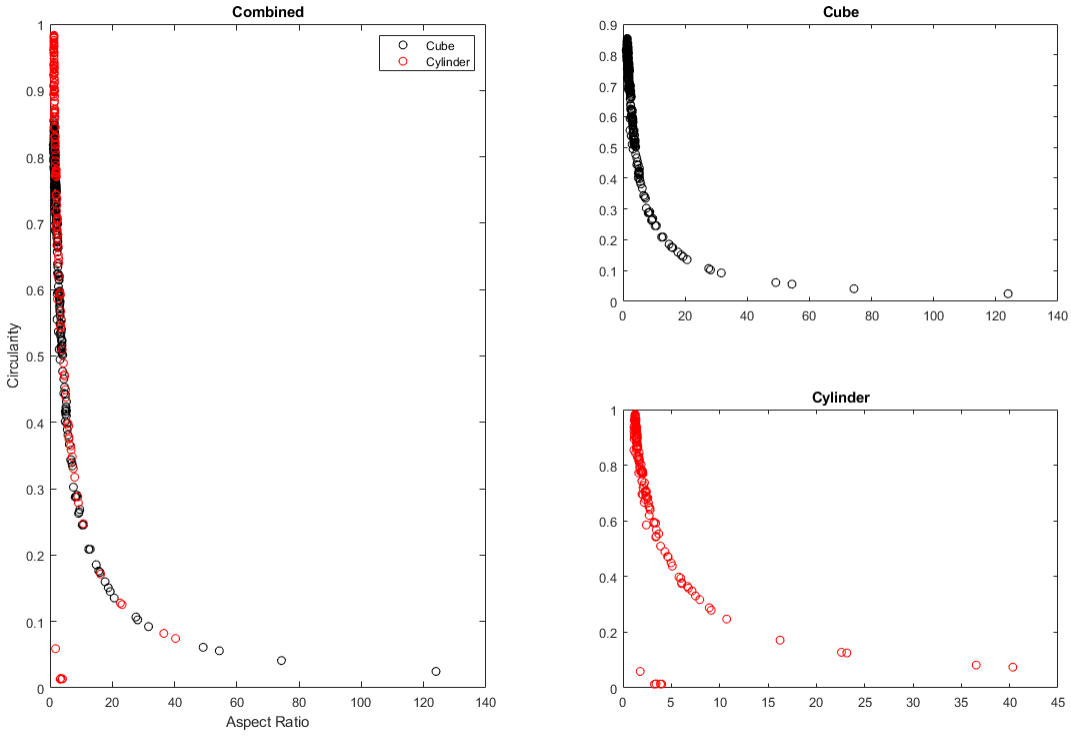

Figure 5-10: Plots of aspect ratio vs. circularity for cubic and cylindrical cross sections separately (right) and in a hypothetical mixture (left)

quantities such as convexity, waviness, and sphericity, essentially measure the irregularity of the object boundary, a feature which is already captured by circularity. While it cannot be conclusively proven that no shape factor, or combination thereof, exists which will enable reliable classification of image objects in sectioned mineral powders, there is no evidence or theoretical framework to support the existence of such a quantity or combination of quantities.

5.4 Classification via Convolution Neural Networks

Machine learning, in the form of Convolution Neural Networks (CNNs) would seem to be an ideal tool to use for mineral object classification, given its prevalence in object classification for images of macroscale objects[46, 49, 62]. Briefly, CNNs function by transforming the input data by multiplication with some weighting terms,

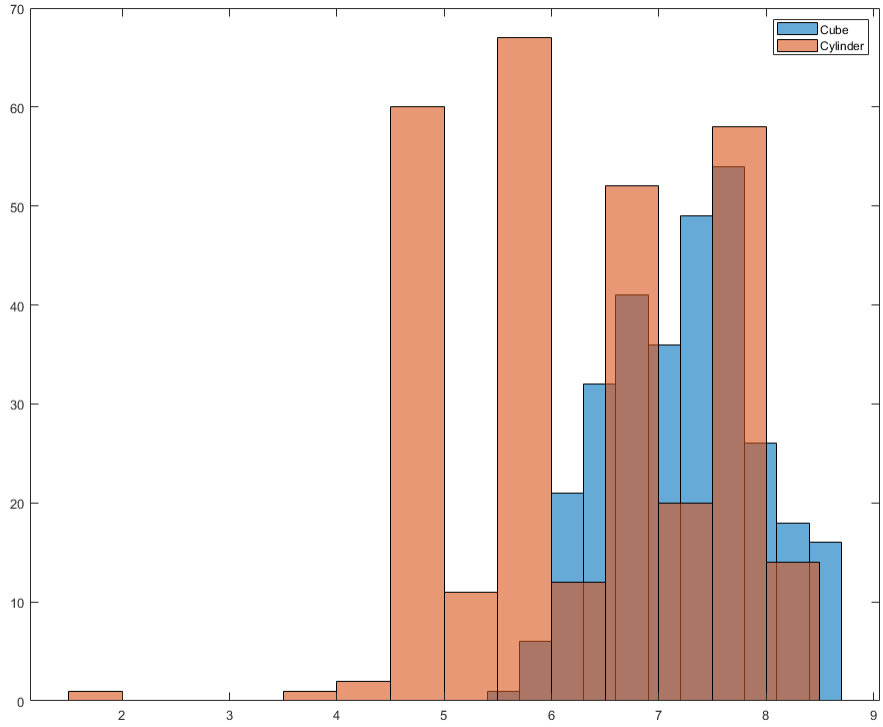

Figure 5-11: Histogram of the Podczek shape factor values calculated for the cubic and cylindrical sections

followed by a filtering layer which approximates nonlinear behavior, and then finally a sub-sampling operation which reduces the size of the output data. At the end of the network, a decision vector of several values is produced and these values are compared to those found for known features to determine the correct classification for the data. At each stage in the network, the values of the weighting terms must be chosen, and choosing them correctly produces the clearest distinction between different data categories for the output decision vector. The process of optimizing these terms is called training. This section is not concerned with the broader properties and applications of CNNs, only with their application to the task of classifying image objects by mineral identity. Applying CNNs directly to the micrographs allows information beyond object shape to be used for classification. Topological features, such as the number of holes in an object, as well as subtler variations in pixel brightness in ob-

ject interiors that were not accessible through shape factors can be leveraged by the network. These extra sources of information may allow CNNs to outperform shape factor in classification tasks.

A CNN requires training with relevant data to allow for accurate classification. In the context of classifying these image objects, training data consists of images with each object pre-labeled with the category to which is belongs. The amount of data required is generally large, on the order of thousands of examples per category of classification, and a similar magnitude of negative examples which belong to no category[29, 23]. Generating this data to train the network is a key challenge in the use of CNNs to solve the identity problem in microfluidic systems.

5.4.1 Network Training

Training images were generated by hand-labeling regions of SEM micrographs of hydrothermally altered potassium feldspar set in epoxy in the sample channels of the steel microfluidic device. Labeling consists of drawing bounding boxes around each object in an image and defining the category to which they belong. An example of a labeled training image is shown in 5-12.

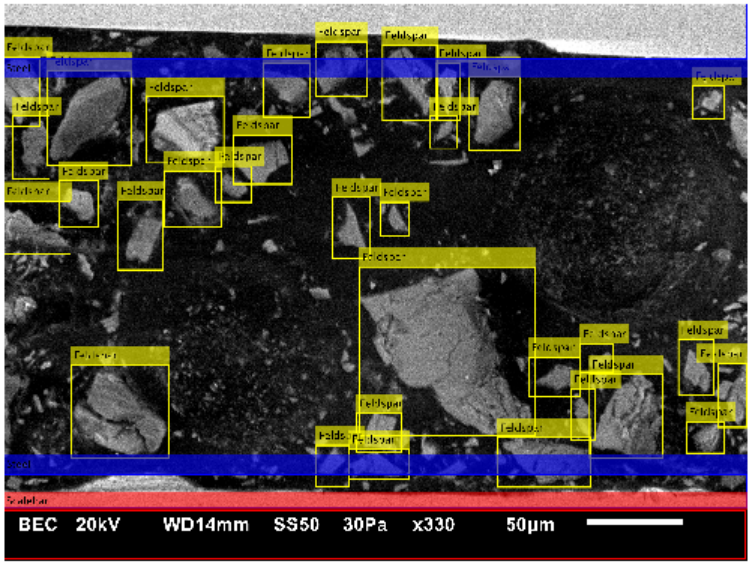

Figure 5-12: Micrograph labeled for CNN training

Of the sample constituents only feldspar was labeled in the training images, as it comprises most of the larger and easier to identify objects. Thirty-one such images were created for use in network training, representing roughly eight-hundred examples of feldspar objects.

Given the time investment required to collect the images and, further, to label the features, it was found that not enough training images could be created in a reasonable amount of time to train an entirely new CNN. This motivated the adoption of a transfer learning approach, where a commercial network, AlexNet[69], previously trained to classify pictures of animals and other common objects, was retrained using the labeled images.

5.4.2 Transfer Learning

Transfer learning has the potential to reduce the amount of training data required for reliable classification performance by orders of magnitude[128]. This is due to a large amount of the training process imparting general image manipulation techniques, such as edge detection and feature extraction, that are broadly applicable to most image classification tasks. By using a pre-trained network, only features specific to the problem of classifying mineral sections need to be reinforced by the training data.

Following a transfer learning approach, the set of training images described in 5.4.1 were used to retrain AlexNet. The 'black box' nature of CNNs imparts difficulty to showing the progress of the training procedure, as was done for the image segmentation and object detection routine. The results of applying the retrained network to SEM micrographs of hydrothermally altered potassium feldspar are shown in 5-13.

The accuracy of classification was found to be poor. This is likely due to the training data-set being too small for the differences between features to be adequately learned. As feldspar is most heavily represented in the training images, it is the most likely feature to suffer from over-fitting. Classification accuracy could likely be improved by creating a larger set of images, however this is not guaranteed, and there is no method to accurately estimate the size of the training dataset that would be

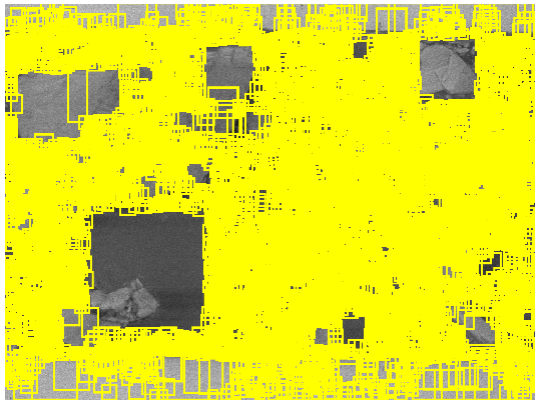

Figure 5-13: Image analyzed with the retrained AlexNet. Yellow boxes surround each feature the network identified as feldspar

needed to achieve an arbitrary classification accuracy. As feldspar was only one of the six major mineral constituents of the hydrothermally altered feldspar, it seems likely that a much larger number of training images could be required, than could be produced given the time, material, and financial constraints of the project.

These results do not provide confidence for the further use of CNNs to provide a solution to the problem of mineral feature classification in powder sections. Scalability is poor, as an entirely new training dataset must be produced for each mixture, and the required sizes of these datasets is not immediately approachable, if not prohibitive. This barrier only grows as the number of mixture constituents increases.

5.5 Classification via EDS

Information on the chemical composition of image features provides a strong discriminating factor for classification. The SEM used for acquiring sample micrographs was equipped with an EDS system and software. Mappings of the elemental signals for carbon, potassium, aluminum, calcium, silicon, and iron were produced for samples of epoxy-mounted hydrothermally altered potassium feldspar in the steel microfluidic device. These maps were acquired simultaneously with backscatter micrographs, of the kind shown in 5.2, with a horizontal resolution of 256 points, compared to the 5120 points of the sample micrographs. This resolution was a compromise between

data coarseness and acquisition time, with each map requiring twenty to twenty-five minutes to produce. Doubling the dimensions would necessitate mapping times approaching or exceeding one hour, which was not practical for the number of images required for this work.

5.5.1 Elemental Signal Ratios

The mechanism to transform elemental signals to identity metrics is the calculating of ratios of elemental signal intensities. This is defined as the ratio of the average intensities of the signals of two different elements over the pixels corresponding to characterized object. Each elemental mapping was converted to grayscale and resized to match the resolution of the SEM images. The limits on map resolution excluded features smaller than the pixel size of approximately 1.3μm from the classification procedure. Features smaller than 13μ in one dimension, approximately 10 pixels on the elemental maps, were excluded from this analysis, as the quality of the average elemental signal is less subject to random noise as more pixels are used in its calculation. These constraints reduced the scope of application of this technique to the study of the feldspar fraction of the material, as it is the only constituent with features consistently above these minimum size thresholds.

The potassium-aluminum and potassium-silicon ratios were calculated for each of approximately 30 features in a representative micrograph that were above the minimum size threshold. These objects included the steel walls of the channel, feldspar pieces of various size, and some features which were difficult to visually classify. A plot of the K/Al ratio versus the K/Si ratio of these objects is given in 5-14.

There is a distinct clustering of feldspar objects towards the origin, at both low K/Al and K/Si ratios. Stoichiometric feldspar has atomic ratios of K/Al and K/Si of 1 and 0.3 respectively, but there is no relation between the mapping signal intensity and a physical quantity such as atomic percent; the maps are fundamentally qualitative. The strong grouping of most of the feldspar signals in one area provides the best classification performance of the methods investigated in this work. This result, while encouraging, exists in a small sampling of objects due to the inherent limitations of

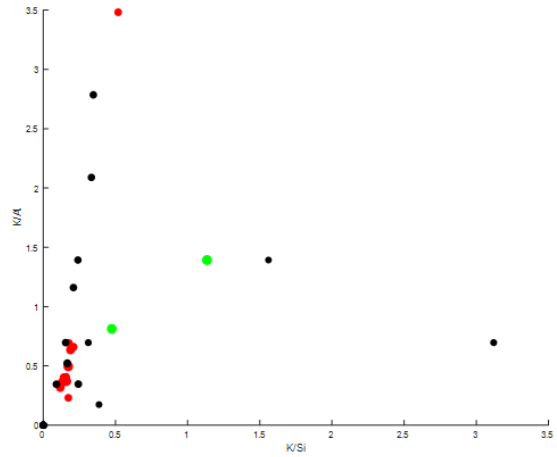

Figure 5-14: Elemental signal ratios for objects measuring at least 13μ in one dimension in a micrograph of a hydrothermally altered potassium feldspar sample. The points are colored according to their visual classification: Red: Feldspar, Green: Steel, Black: Unclassified.

the technique, and it cannot be stated how it would perform with the hundreds of features that the other classification methods encountered.

5.6 Discussion

The analysis of images of sectioned, multicomponent, powders was found to be insufficient to enable classification of the present features and the extension of the microfluidic leaching technique to multicomponent systems. The difficulty does not arise in image acquisition, segmentation, object detection, or object measurement, but in the use of object properties as proxies for identity. Each technique investigated, shape factor analysis, CNN classification, and elemental ratios via EDS, was found to be inadequate for producing reliable measures of object identity. This failure to solve the identity problem introduced in Section 1.2 renders the leaching results presented in Chapter 4 of little use in calculating the leaching rates.

Shape factors, both simple and complex, did not provide enough contrast between features, producing crowded plots without distinct groupings. An attempt to explain the failure of these common discriminants found that the sectioning of randomly oriented solids, of distinct and uniform shape, reproduces the difficulty encountered

experimentally. Shape becomes unreliable for identification following random sectioning, as distinct features are lost during the dimension reduction. This result places doubt on the ability of any conventional shape factor to provide a reliable identification method. Topological features of the constituents of three-dimensional sample powder are lost during sectioning, which creates a fundamental barrier to the use of these sections to identify the parent objects. Any future scheme to use shape information as a pathway for identification in sections must involve quantities which are invariant under random sectioning, which may not exist for all shapes, suggesting that shape cannot provide a general solution to this classification task.

Convolution Neural Networks show promise for the identification of common macroscale objects in photographs, but had very poor accuracy when tasked with classifying sectioned powders. The limiting factor is believed to be the size of the training data set. A large time investment is required to acquire and label images required for training, and it cannot be known *a priori* how many images are required to produce a usable tool for classification. In this work, over eight hundred examples of sectioned feldspar were provided to the commercial CNN AlexNet for retraining, with the results shown in 5-13 suggesting many more would be required. The problem of shape variance noted above may also play a role, as shape is the most prominent information provided by the training images. Training the network that shape is unreliable, and more subtle surface features such as cracks, texture, or uniformity are more important appears to require a prohibitive number of training images. Furthermore, the investment in creating this training data is non-transferable, each new sample material would require the process to begin anew, reducing the prospects for machine learning, in its current form, to take part in a general solution to the classification problem.

Elemental mapping provided the best results of the classification methods investigated. Chemical information provides a much stronger method to discriminate between features than shape, as it is, to a first order, entirely independent of shape. Commercial microprobe systems exist which automatically map petrological thin sections and identify classes of minerals[64]. However, such machines are highly special-

ized and generally not available to the researcher. Even with the use of such machines, the time required for elemental mapping of a sample at micrometer resolution is prohibitive, generally orders of magnitude longer than is required to obtain a micrograph, itself an order of magnitude longer than a photograph from light microscopy. The minimum feature size that can be mapped is inversely proportional to the time of acquisition. Similarly, the signal-to-noise ratio increases with mapping time. While this method was able to produce the most recognizable correlation between object identity and measured properties, this results came after discounting the majority of features in the image because they were too small to be mapped. Ultimately, elemental analysis via EDS was not able to be adapted to form a practical solution to the classification problem.

5.7 Conclusion

Image analysis was hypothesized to have the potential to enable the quantitative extension of the microfluidic leaching technique to multicomponent systems. This part of the hypothesis cannot be supported by the evidence gathered during this investigation. Shape data, machine learning, and elemental mapping all failed to provide reliable and tractable avenues to solved the identity problem. While it is possible that these failures are the result of the choice of system, that the hydrothermally altered feldspar is too complex or otherwise ill-suited to this kind of classification, it is nonetheless a real system requiring characterization. The reduction of experimental variance and resolution of other barriers to concentration analysis presented in Chapter 4 cannot close the system on their own. These leaching results are, unfortunately, of no use without the corresponding surface area estimates.

Future work to solve this hard problem of classification should focus away from shape. Optical microscopy may provide more opportunities than electron microscopy for performing this characterization. In sectioned samples on transparent substrates, the use of polarized light enables structural information to aid in discrimination. Color, essentially a proxy for chemical information, can also be a powerful tool for

differentiating in systems containing ammenable chemistries. It is likely that no single solution exists which will find success in all systems, as such, careful consideration of the aspects which most strongly differentiate system components from one another, and how they may manifest in imaging, is likely to produce the best results.

Chapter 6

Framework for Multicomponent Bulk Leaching Rate Determination

The key problem when attempting to estimate individual contributions to non-specific measurements is one of identity. Extra information is needed to be able to separate an overall value into meaningful, physical, quantities. This core problem is encountered and addressed in both the microfluidic and bulk leaching pathways in this work. In the microfluidic case previously discussed, phase identity is assigned through analysis of microscopic surface images. In the bulk case, size heterogeneities prevent the easy application of microscopy as a general solution to the problem of identification; instead, the particle size distribution (PSD) of the mixture is decomposed into the constituent PSDs. This decomposition, detailed in 6.2, allows the assignment of identity and calculation of component areas based on size alone.

6.1 Continuum Model and Rate Calculation

A schematic of the bulk leaching apparatus is shown in 6-1. The continuum model that describes this apparatus will be developed in this section. Strong similarities exist between the models for the bulk and microfluidic cases, as reducing the effect of homogeneous reactions requires similar experimental conditions.

The leaching of a thin packed bed of mineral powder can be described by the

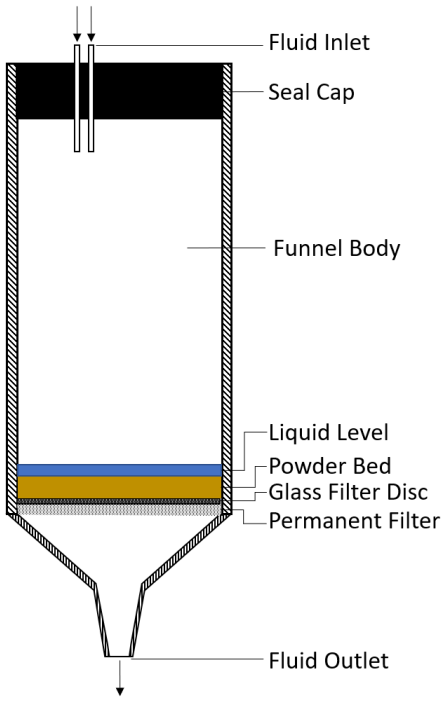

Figure 6-1: Schematic of the bulk leaching apparatus. The filter funnel had an approximate volume of 30 mL and the retained liquid volume was on the order of 7 mL.

classic packed-bed reactor design equation[38]:

$$\frac{dN}{dW} = R \tag{6.1}$$

Where N is the species molar flowrate, W is the mass of heterogeneous substrate on which the reaction occurs, and R is the specific rate of reaction.

For the multi-phase, multi-component leaching studied in this work, Eq.6.1 can be manipulated to a form closer to the model of the microfluidic case. The species molar flow can be written as the product of a concentration and volumetric flowrate, assuming one average flowrate and perfect mixing. Dividing by the specific surface area changes the basis of the equation from mass to surface area:

$$\dot{\mathbf{q}}\frac{d\mathbf{U}}{d\mathbf{A}} = \mathbf{r} \tag{6.2}$$

where $\mathbf{A}$ is the vector surface areas of the phase present in the bed and $\mathbf{r}$ is the

matrix of leaching rates per unit area.

Assuming further that the rates are constant, Eq. 6.2 can be integrated to yield:

$$\dot{\mathbf{q}}(\mathbf{U}_A - \mathbf{U}_0) = \mathbf{r}\mathbf{A}_T \tag{6.3}$$

where $\mathbf{U}$ is the vector of species concentrations, U_0 and U_A are the average concentrations at the inlet and outlet, respectively, $\dot{q}$ is the volumetric flowrate, and r is the vector of leaching rates per unit area, and A_T is the total bed area.

Assuming the inlet is free of leached species, Eq. 6.3 can be rearranged to solve for the rates as:

$$\mathbf{r} = \dot{\mathbf{q}}\mathbf{U}_A\mathbf{A}_T^{-1} \tag{6.4}$$

Which is the same as the inversion solution to the microfluidic model described in eq. 3.14. All the same solution concerns raised in 3.5 apply and the rate calculation can be performed using the same parameter estimation techniques on a mixed effect model as described in eq. 3.17. The simplifications that lead to the models being identical also necessitate that the experimental conditions are symmetrical. Notably, neglecting diffusion and assuming constant rates, in the case of a microchannel, enforces a perfect mixing and uniform flow through the sample in the bulk apparatus. Uniform flow is enforced as a method to achieve uniform sampling of the surface rates; if different areas of the bed experience preferentially higher or lower flow, then the outlet concentration will not be representative of the leaching behavior of the flow overall. For this reason, all bulk experiments in this work were performed using a thin bed of uniform thickness. This complication was not experienced in the microfluidic case, as the entire surface was guaranteed to be sampled due to the strict confinement of the channel walls.

6.2 Surface Area Determination

The volume-weighted particle size distribution of a solid powder mixture is very accessible experimentally. This motivates its use as tool for pre-leaching analysis of powder samples and as a tool for discerning component surface areas. The 93 distinct size ranges and their corresponding fraction values correspond to the volume percent of the mixture that exists with the same diffracting power as a sphere with a diameter contained within the bounds of the size range. This measurement technique is fundamentally volume-based. Care must be taken to address uncertainty when performing nonlinear transformations of basis, such as generating an area- or number-based distribution from the volume distribution. In order to make use of the particle size distribution for the purposes of estimating areas, it is necessary to rigorously address this issue.

Non-linear transformations of basis cause non-linear propagation of error. Consider the simple case of a uniform volume distribution $P_v(z)$ across a range of sizes $z \in [ab]$. Each point has some associated variance $\sigma^2_{P_v}(z)$, which is assumed, without loss of generality, to be zero-mean and identically distributed. The point estimate and error of the surface area calculated from this distribution are:

$$A(z) = P_v(z)\frac{\alpha(z)}{z}V \tag{6.5}$$

$$\sigma^2_A(z) = \left(\frac{\alpha(z)V}{z}\right)^2 \sigma^2_{P_v}(z) + \left(\frac{P_v(z)V}{z}\right)^2 \sigma^2_\alpha(z) + \left(\frac{P_v(z)\alpha}{z}\right)^2 \sigma^2_V \tag{6.6}$$

Where $A(z)$ is the surface area present at size range z, $\alpha(z)$ is the surface area to volume ratio of the particles multiplied by z, and V and σ^2_V are the total volume of the solid sample and the variance in this quantity, respectively.

The first term inside in Equation 6.6 is the carried uncertainty from the initial error in the volume-based distribution, while the second term is the additional uncertainty due to doubt about the exact shapes of the particles, as a function of their size. In all real cases, this error can be quite significant due to the need to estimate particle shapes from finite samples. The final term captures uncertainty due to imperfect

estimation of the total volume of the sample. From the form of equation 6.5, it is seen that the estimated area will be greatest, relative to the measured distribution, towards the smaller end of the size range, with the discrepancy growing as α increases. The error grows in a similar fashion; relative error in the area estimation can be no lower than that of the volume-normalized distribution, but will in general be larger due to the added shape and volume uncertainty. These three sources of uncertainty: PSD measurement, shape estimation, and total volume estimation, must be carefully managed in order to obtain useful measurements of total mixture surface areas.

In order to extend the above analysis to allow for the calculation of the surface areas of individual mixture components, an extra piece of information is necessary. The prevalence of each phase at each size range is needed in order to partition the total area calculated for a particular size range among the mixture constituents. Estimation of this prevalence can be performed by deconvolution of the mixture particle size distribution.

A volume-normalized particle size distribution of a component i is defined as collection of the ratios of the volume of component i at some size z to the total volume of component i across all size ranges.

$$P_{v,i} = \frac{V_i(z)}{V_i} \tag{6.7}$$

If particles are conserved when solids are mixed, the volume-normalized particle size distribution of the resulting mixture can be written as a linear combination of the component PSDs:

$$P_v = \sum_i f_i \frac{V_i(z)}{V_i} = \sum f_i P_{v,i} \tag{6.8}$$

Where f_i are the volume fractions in the mixture of the different components, which may be calculated from the weight fractions, w_i, and component densities, ρ_i, as:

$$f_i = \frac{\frac{w_i}{\rho_i}}{\sum_i \frac{w_i}{\rho_i}} \tag{6.9}$$

If the individual $P_{v,i}$ and f_i are known, then the volume fraction of each component

at each size range can be calculated:

$$I(z) = \frac{P(z) \circ f}{P_v(z)} \tag{6.10}$$

Where $I(z)$ is the identity distribution, $P(z)$ is a stacked vector of the component PSDs, f is the vector of volume fractions, and $\circ$ denotes the Hadamard (elementwise) product.

The identity distribution has m entries at each size range, corresponding to the fraction of each component present at that size range. Regardless of whether the generating distributions are volume-, area-, or number-normalized, the identity distribution will contain the same values for the same mixture. Naturally, this distribution is subject to propagated uncertainty due to imperfect knowledge of P, P_v, and f.

Quantifying the uncertainty of I is necessary for the creation of confidence bounds on the surface area estimates, which are in turn necessary for bounding the error in the rate estimates. Given the nonlinear nature of I, the propagation of uncertainty will be estimated using a Taylor expansion. The final expression is given here, with the derivation presented in A.1.

$$\Sigma^I(z) = J_I(z)\Sigma^{P,f}J_I(z)^T \tag{6.11}$$

Where Σ^I denotes the covariance matrix of I, J_I is the jacobian of I, and J_I^T is the transposed jacobian.

With the identity distribution defined, the full model for estimating surface areas from mixture particle size distributions is:

$$A(z) = I(z) \circ P_v(z) \circ \frac{\alpha(z)}{z} V \tag{6.12}$$

Where A contains m columns, each holding the area estimates for each solid phase as a function of the particle size range. These estimates are subject to the total uncertainty:

$$\sigma_A^2(z) = \left(P_v(z) \frac{\alpha(z)}{z} V \right)^2 \Sigma^{I^2} + I(z)^2 \sigma_A^2(z) \tag{6.13}$$

6.3 Design of Experiments

As previously discussed, the amount of data required to obtain reliable estimates of leaching rates can be quite large. Additionally, the process for obtaining the surface area estimates necessary to perform the calculations is quite involved, as shown in Section 6.2. These circumstances motivate a careful design of experiments (DOE) approach to gathering data, in order to maximize the value of the information obtained from each trial.

The independent variables in each trial are conveniently represented by a vector, with one entry for each component that contains the surface area of that component. Across multiple trials, these vectors are concatenated to form the text matrix, where each column of the matrix is the area vector for one trial. Maximization of the information gained from each trial is equivalent to maximizing the distance between experimental conditions and the orthogonality of the vectors. In vector form, this is the minimization of the dot product between the columns of the test matrix. In the ideal case, the dot product for every combination of two vectors would be identically zero, representing an orthonormal set of vectors and guaranteeing that each trial is providing only novel information. However, constraints are placed on the obtainable values of the independent variables determined by the ability to manipulate the component surface areas. Therefore, it is very unlikely that such a set of experiments could be designed in most cases and it becomes necessary to develop a method to maximize information gain within the constraints of the experimental system.

Within the context of powder mixtures, separation based on particle size is commonly performed by sieving, and such methods may be employed to generate samples for analysis. For a mixture of components with different particle size distributions, sieving the mixture will produce separate mixtures with distinct compositions. Careful choice of the sieve mesh is necessary to maximize the experimental value of the

produced mixtures.

Considering the case of a mixture of m mixture components, for which the overall PSD, identity distribution ($I(z)$), and shapefactors ($\alpha(z)$) are known, the total area of each component between size bounds z_{min} and z_{max} is given by summing Eq. 6.12 within those size bounds:

$$a(z) = \sum_{z \in [z_{min}, z_{max}]} P_v(z) \circ I(z) \circ \frac{\alpha(z)}{z} V \tag{6.14}$$

z_{min} and z_{max} are bounded by the smallest and largest measured size ranges, respectively, for the PSD. The choice of z_{min} and z_{max} is equivalent to the choice of $m-1$ intermediate sizes, within the support of the PSD, D, which will serve simultaneously as z_{min} for a larger mixture fraction and as z_{max} for a smaller mixture fraction. These sizes, effectively sieve mesh sizes, should be chosen such that the resulting mixture fractions form a test matrix which is as close to orthogonal as possible. This can be written as the optimization problem:

$$\begin{aligned} & min \sum_{k=2}^{m} \sum_{j}^{k-1} \left(A(\phi)^T A(\phi)_{kj} \right)^2 \\ & s.t.\ \phi \in D \end{aligned} \tag{6.15}$$

Where ϕ is the vector of $m-1$ intermediate sizes, and A is the matrix with columns given by a in 6.14.

This construction seeks to identify the best sieve sizes to minimize the sum of the squared dot products of the columns of the test matrix. While there is no generalization of the inner product to collections of vectors, the smaller this sum, the greater the linear independence between experiments and therefore the greater the information value of those experiments. Local minima to 6.15 can be computed directly, but for experimental convenience it is helpful to provide additional constraints. Constraining the volume fraction between entries of ϕ to be above a minimum value may be necessary to provide enough sample to experiment with. Depending on the

sieves available, it may also be necessary to restrict ϕ from holding certain values.

6.4 PSD Validation for Framework Dissolution

Leaching can occur through migration of ionically-bound constituents, such as potassium or sodium from feldspar, or via destruction of the covalently-bound framework, comprised of aluminate and silicate tetrahedra in feldspar. Framework dissolution naturally causes a decrease in the volume of a particle subject to it, and, taken to its conclusion, the destruction of said particle. If this leaching mechanism is present and rapid enough in the system under study, the alteration of particle size provides an avenue to validate leaching rate estimates in the bulk case.

Consider a solid particle mixture, for which the particle size distribution of the total mixture and of each phase is known. Under conditions of framework dissolution, the mixture particle size distribution will change due to the changing volume of each constituent particle, and the change will be a function of the dissolution rates of each phase. Comparing the PSD of a mixture pre- and post-leaching therefore provides information on the rates of framework dissolution. Further, if the relationship between particle size and leaching rate is known, or can be accurately estimated, for each phase, then the change in the mixture PSD provides further constraints on the values of the phase leaching rates.

A method for the quantitative prediction of the post-reaction PSD of a dissolving mixture is developed below. For any size range in the distribution, there are three mechanisms that change the volume fraction it contains:

1. Smaller particles exit to the next smaller size range
2. Larger particles enter from the next largest size range
3. The total volume of the mixture is decreasing

For the shrinkage of particles, where particle shapes can be assumed to be constant and to simply scale with time, the items above permit a simple mathematical description.

The rate of change of the characteristic dimension of a particle can be written as:

$$\frac{dR}{dt} = \frac{-k(t)}{\rho_m} \frac{f(R)}{\frac{dV}{dR}} \tag{6.16}$$

Where R is a representative shape measure, t is time, k is the leaching rate of a framework element per unit surface, ρ_m is the molar density of that element in the solid, $f(R)$ is the function which describes the surface area of the particle shape, and V is the volume of the shape.

It follows that the total volume loss from leaching can be written, for a single mixture component, as:

$$V_{loss} = \int_{t_0}^{t_f} \frac{-k(t)}{\rho_m} SA(t)\, dt \tag{6.17}$$

Where V_{loss} is the volume loss during leaching, and SA(t) is the total surface area of the mixture component over time.

Eq. 6.17 must be calculated for each mixture component and the results summed to obtain the total volume loss from leaching. This value could also be obtained experimentally if the total volume of the remaining powder can be measured after leaching, such as by weighing when the density is known.

These two equations, Eq. 6.16 and Eq. 6.17, provide the location and scale, respectively, of the mixture PSD post-leaching. While it is necessary to solve both Eq. 6.16 and Eq. 6.17 to accurately predict the entire distribution, in practice Eq. 6.17 is simply a multiplicative constant, and all the relevant information on the kinetic behavior of the mixture components is contained in Eq. 6.16. An examination of the units of this equation, length per time, provides insight to its utility as a second line of evidence for validating leaching rates. Eq. 6.16 describes a velocity, along the support of the PSD, at which a single class of features moves. As before, in 6.2, we consider that the overall mixture PSD is the linear combination of the component PSDs, and this combination is changing as the underlying component distributions move along the support at different, kinetically-determined, velocities. The utility of this result is most obvious when considering the simple case of a multi-peaked mixture PSD, where

each peak corresponds to a unique mixture component. Distance between these peaks would change upon leaching by the difference if their velocities, as calculated in Eq. 6.16. In more complicated, and more realistic cases, of broader PSDs with significant overlap between mixture components, the utility is greatest as a way to check the feasibility of the rates calculated using Eq. 6.4, by comparing the shift of features to those predicted by the rates.

The most convenient application of Eqs. 6.16 and 6.17 is straightforward, and does not require extensive knowledge of the particle shapes. The quantity $\frac{f(R)}{\frac{dV}{dR}}$ is a constant for any shape described by one-dimension, and can be approximated as a unique constant for each value of R in the distribution, if desired. From there, the change in size of any particle from leaching is:

$$\Delta R = \int_{t_0}^{t_f} \frac{-k(t)}{\rho_m} \frac{f(R)}{\frac{dV}{dR}} \, dt \tag{6.18}$$

The size of a particle after leaching can then be described by the sum of the original size, and the change due to reaction given above. The effect of this size change on volume depends on the particle shape, but is proportional to the cube of the fractional change in the dimension.

$$\Delta V \propto \frac{R^3 - \Delta R^3}{R^3} \tag{6.19}$$

Eq. 6.19 describes the fraction of volume retained by a particle of size R after undergoing a scaling by amount ΔR. This is a curve, with smaller particles losing a greater fraction of their volume than larger particles. The elementwise product of this curve with the original PSD gives the fraction of the original volume that remains in each size range after leaching. This new PSD must be normalized, formally through the use of Eq. 6.17, but practically simple division by the sum of its entries is sufficient. In complete form, the PSD of a material undergoing a size-altering leaching reaction without change of shape is:

Chapter 7

Phase Classification in Bulk Powders

Unlike in the microfluidic case, the surfaces of bulk samples are anonymous. That is, there is no feasible way to assign an identity label to a distinct feature, and properties of groups of objects must be considered instead. Despite the differences in approach, the goal of classification remains the same as discussed in Chapter 5, to obtain an estimate of the surface areas of individual mixture constituents that can be used in Eq. 6.4 to calculate the leaching rates. This is performed by decomposing the particle size distribution of a mixture into a linear combination of the PSDs of the mixture components, and then calculating the identity distribution - the fraction of volume at each measured size range that belongs to each component - which solves the identity problem described in Section 1.2. The definition of the identity distribution in Section 6.10 follows directly from the deconvolution of the PSD, and therefore its suitability as a tool for analysis of a mixture relies on how accurately this mathematical representation captures the mixture PSD. Uncertainty due to the failure of Eq. 6.8 to represent reality is not captured in Eq. 6.11, and is difficult to quantify without quantitative knowledge of the mechanism by which a mixture differs from the ideal case represented in Eq. 6.8, information, if known, which would enable the development of a more suitable model for the mixture. Experimental evidence of the close agreement between the actual mixture PSD and the PSD predicted by Eq. 6.8 is therefore required before using the identity distribution to calculate mixture component surface areas and presenting such evidence is the focus of this chapter.

Two experimental developments are presented in this chapter: the validation of the representation of a mixture PSD as a linear combination of the components PSDs for several systems, and the presentation of surface area estimation results for systems of mixed mineral powders. The first supports the use of the PSD-based framework for estimating component areas, and is a necessary part of employing this framework for any system. The second outlines the results, including uncertainties, that were obtained using this method for model systems of mineral mixtures.

7.1 PSD Deconvolution

Samples containing varying amounts of feldspar powders and quartz sand were prepared in order to test the validity of the model presented in Section 6.2. Validation proceeds by comparing the measured PSD of a mixture to the PSD predicted by Eq. 6.8, given the component PSDs and mixture composition. Deviations from the assumed linear combination indicate the violation of the assumptions used to produce the model, with the most important being the conservation of particles across mixing. This assumption essentially enforces conditions of no aggregation or flocculation; phenomena which are strongly dependent on the surface interactions of the solids and the solvent and can not be assumed to be negligible in a system without evidence.

7.1.1 Binary Mixtures

Three classes of binary mixtures were studied, mixture of nickel compounds, mixtures of feldspar powders, and mixtures of feldspar powder with quartz sand. These different classes serve to probe a diverse set of size ranges and solid interactions, in order to provide a broader test of the model's validity. The materials were suspended in distilled water and the suspension pumped through a laser diffraction particle size analyze (Beckmann Coulter LS13320).

Nickel compounds

Mixtures of nickel silicate and nickel oxide, at 20, 40, 60, and 80 wt.% silicate, were prepared by mixing known amounts of the pure powders. The oxide and carbonate were purchased as powders, while the silicate as-received was in millimeter-sized pieces. The silicate was ball-milled for one minute in an alumina jar using steel balls to create a powder which could be mixed with the other compounds. The PSDs of the pure components are shown in Figure 7-1 and comparisons between the measured and predicted PSDs for the mixtures are shown in Figure 7-2.

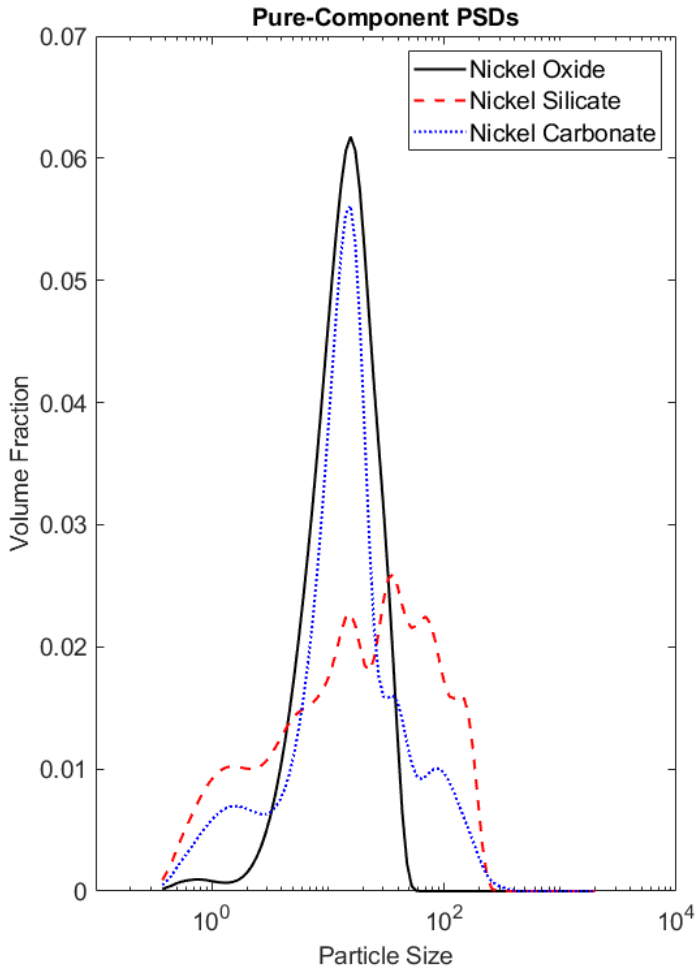

Figure 7-1: PSDs of the pure Nickel powders

The PSDs of each compound exhibit a large amount of overlap, that is, signifi-

cant fractions of each distribution lay in size regions where multiple compounds have significant presence. Size-separation techniques, such as sieving, would therefore be unable to achieve a high amount of separation for most of the mixture.

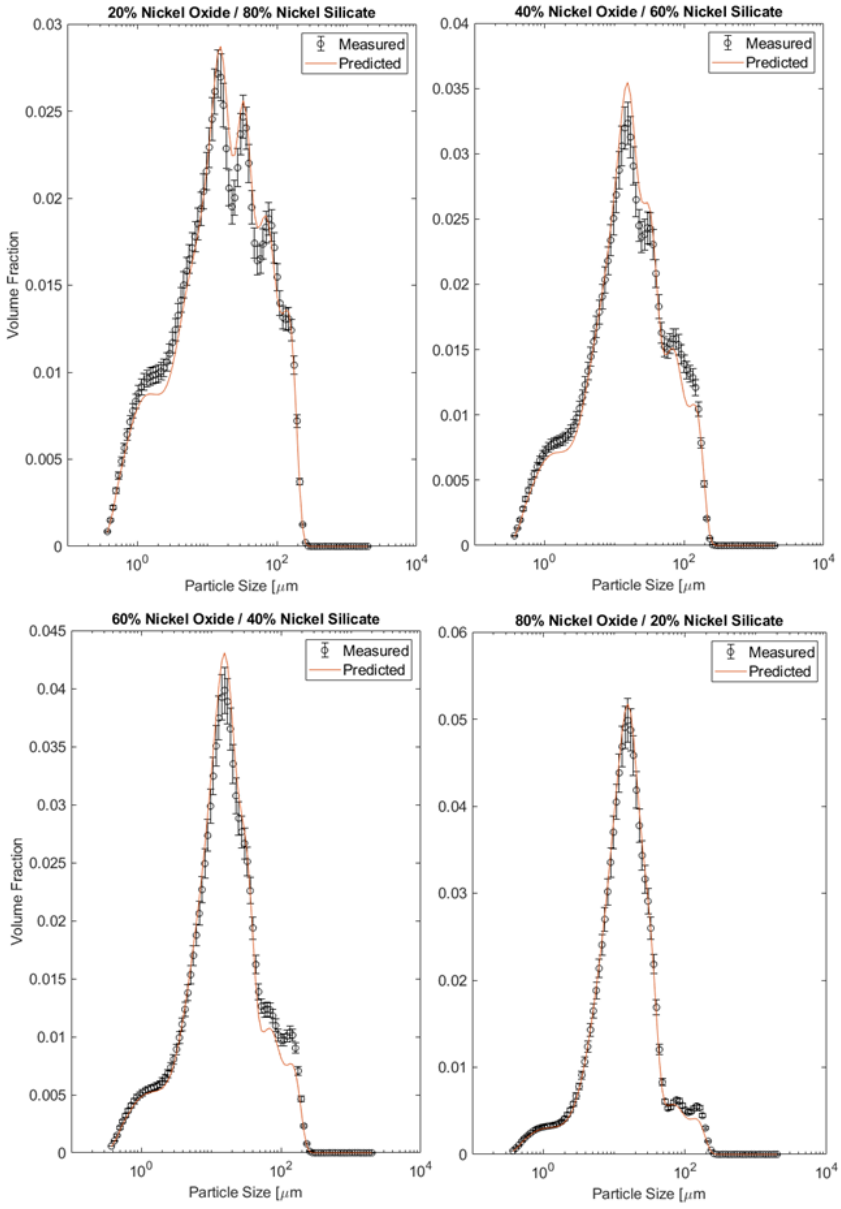

Figure 7-2: Comparison of measured PSDs and those predicted by Eq. 6.8 for mixtures of nickel silicate and nickel oxide. The density of each component used for prediction was found via liquid displacement: Ni_2SiO_4= 4.9 g/cm^3, NiO=6.7 g/cm^3

Agreement between the measured and predicted mixture PSDs is good overall, with an average absolute error of 6.7% across the four mixtures which is roughly

coincident with the approximately 5% standard error in the measured values. The error is greater at the two intermediate compositions (40-60: 7.8% and 60-40: 8.1%) than the extreme compositions (20-80: 6.8% and 80-20: 4.7%), which suggests some degree of interfering interaction between the oxide and silicate particles, such as agglomeration. However, given the coincident magnitude of the error in the prediction relative to the variability in the measurement, this interaction does not harm the validity using Eq. 6.8 to describe the system, and identity distributions calculated from Eq. 6.10 remain valid for this system. The results for the identity distribution calculation are given in Figure 7-3.

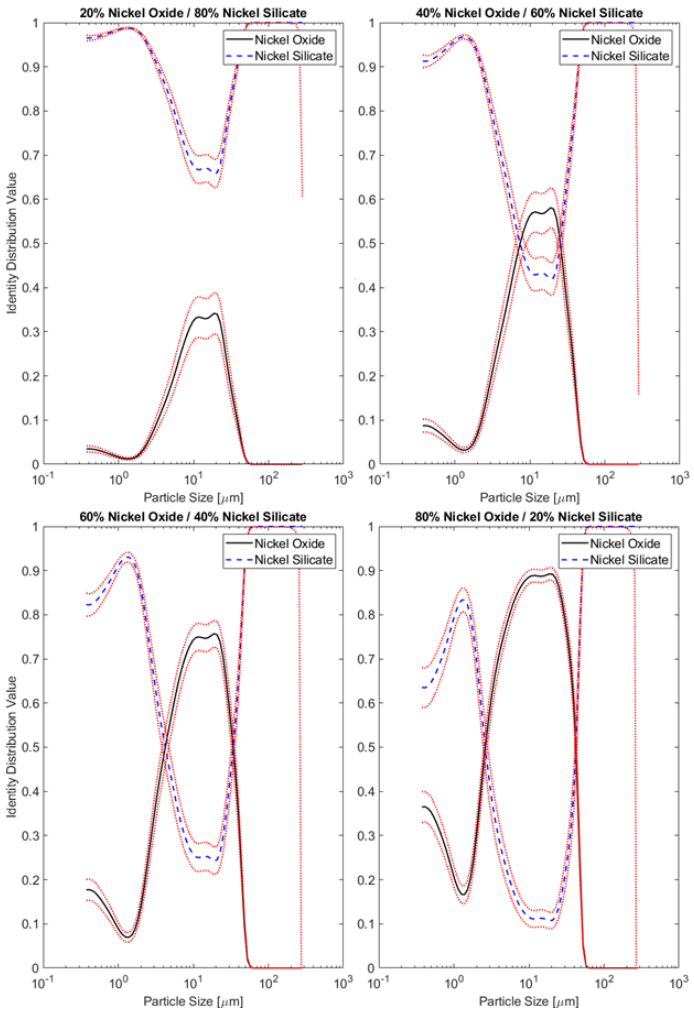

Figure 7-3: Identity distribution values for the mixtures of nickel oxide and silicate calculated using Eq. 6.10. The dotted lines are the upper and lower bounds of the 95% confidence interval for each component, calculated using Eq. 6.11.

For the nickel oxide-nickel silicate system, the values obtained for the identity distribution are intuitively plausible, the value for nickel oxide vanishes away from the peak in the PSD of the pure nickel oxide, and the confidence intervals are narrow. The large increase in uncertainty at the highest size range is an artefact of the vanishingly small value of the total mixture PSD in this region With these results, the identity problem is solved for this system. With knowledge of the shape of the particles, the surface area of oxide and silicate in each mixture can be estimated and the leaching rates of the oxide and silicate calculated from leaching experiments without the need to separate the mixture.

Feldspar powders and quartz sand

Binary mixtures of two potassium feldspar powders, designated EBT13 and FSB02, were created with compositions of 25 wt.%, 50 wt.%, and 75 wt.% EBT13. The PSDs of the pure components and mixtures were measured, and compared to those predicted using Eq. 6.8. In addition, mixtures of FSB02 and quartz sand were prepared in the same composition levels. The pure component PSDs are given in Figure 7-4 and results of the comparison for both mixture types are given in Figure 7-5.

Significant overlap is observed in the particle size distributions of the feldspar powders. Mixtures of these powders would therefore be difficult to separate using common size-based methods, which underscores the need for a tool to calculate individual component properties without requiring separation. The overlap, and similar chemistries, of the feldspar powders also increases the likelihood of particle agglomeration, which would render Eq. 6.8 invalid. As a test of the validity of this model in real mineral systems, these conditions are ideal.

Very strong agreement is seen between the model and measured results, in all cases, at sizes below approximately 250 μm. The average error across all six mixtures is 17.1%, with the three feldspar powder mixtures having an average error of 2.0% and the three mixtures containing sand having an average error of 28.4%. Features larger than μm - exclusively quartz in these mixtures - were poorly suspended in the water flowing through the optical cell, and therefore the particle size measurements

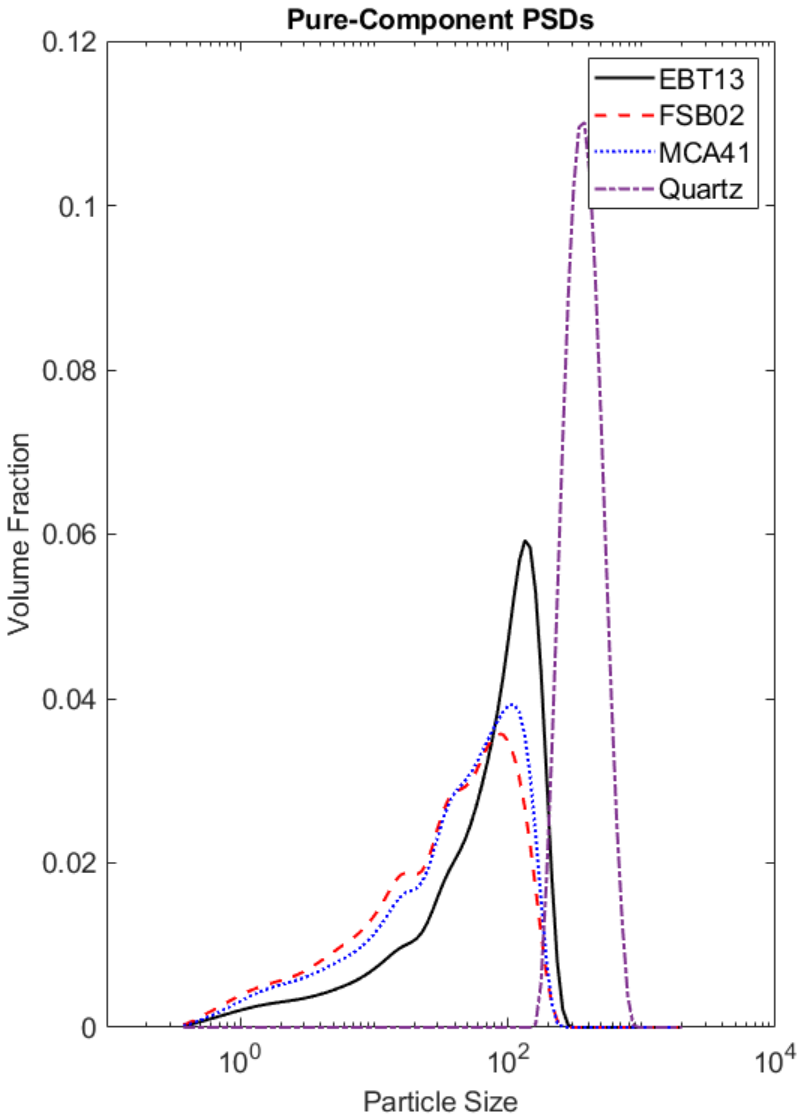

Figure 7-4: PSDs of the pure felsdpar powders and quartz sand

are less reliable at these sizes. This effect originates from the large density difference between quartz and water and is likely limited to the larger sizes due to the settling velocity of the particles increasing with the square of the particle size in accordance with Stokes' law[122]. The close overall agreement of the computed and measured PSDs, in mixtures without quartz and at sizes below 250 μm, lends confidence to the structure of the model, a linear combination of the component PSDs can be used to accurately represent the mixture PSDs in, at least some, mineral systems of two

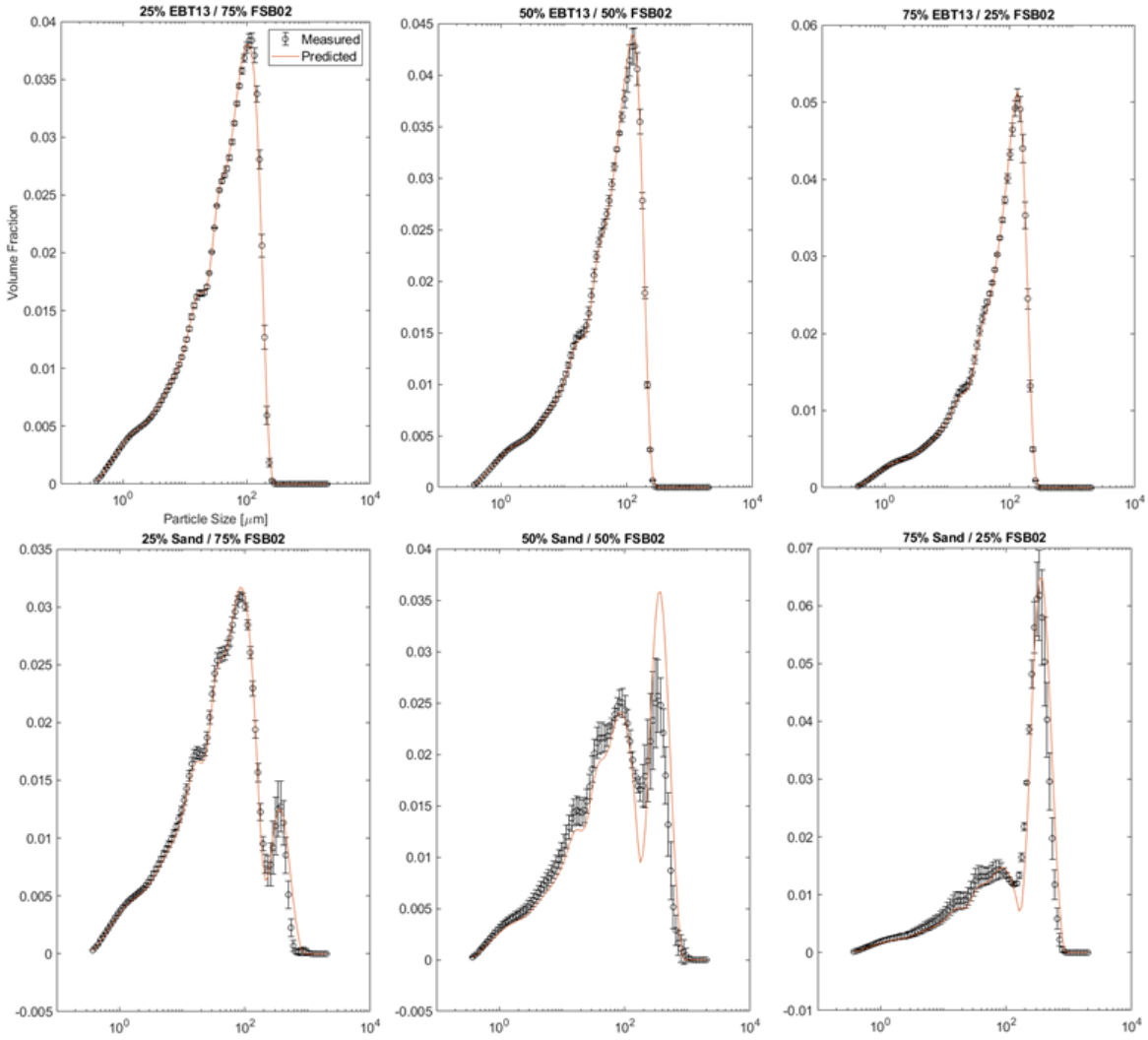

Figure 7-5: Comparison of measured PSDs and those predicted by Eq. 6.8 for mixtures of feldspar powders (EBT13 and FSB02) and quartz sand. The density of each component was measured to be: EBT13= 1.2 g/cm^3, FSB02=1.02 g/cm^3, quartz=2.65 g/cm^3

components. The identity distributions of the mixtures are given in Figure 7-6.

As above, the values of the identity distribution are plausible given the pure-component PSDs shown in Figure 7-4, and the confidence intervals are generally narrow. The PSDs of the sand and FSB02 only have a narrow region of overlap at a particle size of around 100 μm, which is shown clearly in the rapid inversion of the identity distribution at this size for the mixtures containing sand. The measurement difficulties with the quartz which cause poor agreement between the measurement and

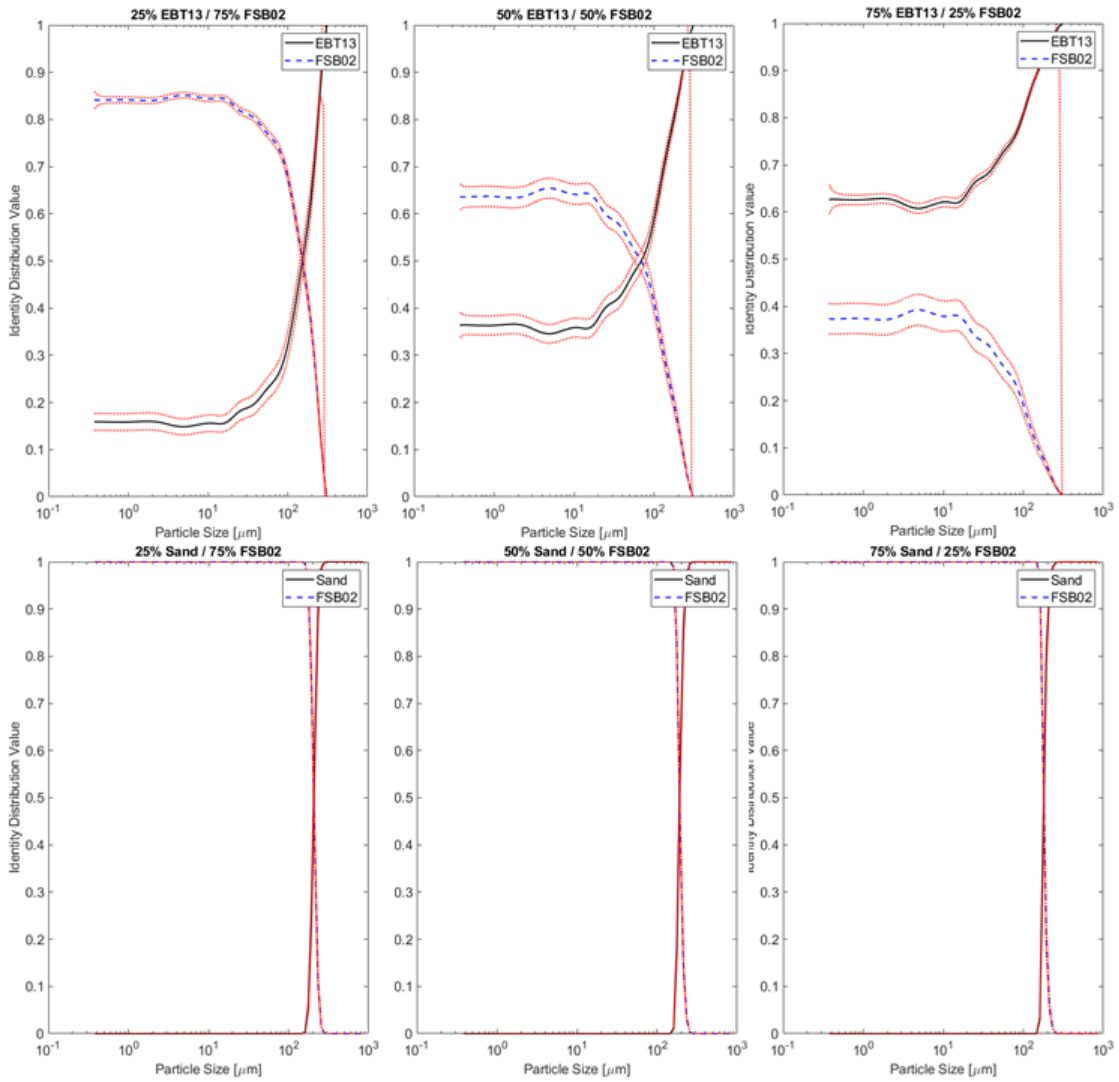

Figure 7-6: Identity distribution values calculated for the mixtures of feldspar powder and sand

model at larger size ranges do not manifest themselves in a larger confidence interval for the identity distribution because they occur in regions where there is essentially only one possible identity for the particles; there is no question that the larger particles are quartz, as the other components of the system do not have particles that large. However, these measurement difficulties will manifest in the accuracy of the surface area estimate which can be obtained with the uncertainty in the size distribution of these larger particles.

7.1.2 Ternary Mixtures

While binary mixtures are the simplest systems which can benefit from the analysis and methods developed in this work, mixtures with a greater number of components are more likely to be encountered in real scenarios. Ternary mixtures are the simplest extension of the framework towards these many-component systems. A ternary mixture of the two feldspar powders, EBT13 and FSB02, and quartz sand was created by mixing equal weights of each, and the Eqs. 6.8 and 6.10 were used to calculate the predicted PSD and identity distribution, which are shown in Figure 7-7 below.

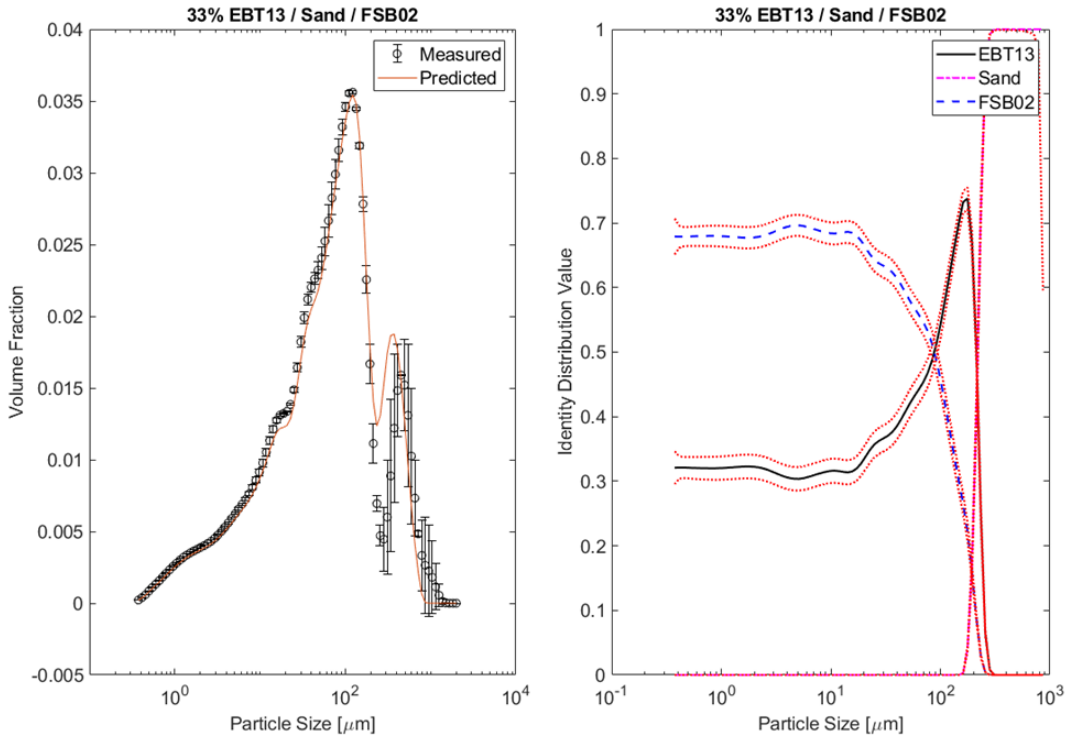

Figure 7-7: Left: Comparison of measured PSDs and those predicted by Eq. 6.8 for a ternary mixtures of two feldspar powders (EBT13 and FSB02) and quartz sand. The density of each component was measured to be: EBT13= 1.2 g/cm^3, FSB02=1.02 g/cm^3, quartz=2.65 g/cm^3. Right: The identity distribution calculated for the ternary mixture.

As before, agreement between the measure and modeled mixture PSD is good for particle sizes below 250 μm. The presence of a third component does not appear to negatively affect the utility of the identity distribution for the feldspar powders, as shown by the close agreement between the identity distribution shown in Figure 7-7

and that shown for the binary mixture of 50% EBT13/FSB02 in Figure 7-6.

7.2 PSD Estimation via Microscopy

In systems with significant overlap in particle size between mixture constituents, measurement of the individual PSDs is a non-trivial task. Various schemes can be imagined to obtain approximations of the individual distributions from the mixture. One option is fractionation of the mixture by size, followed by measurement of the fraction composition and PSD. This may produce good results if fractionation is facile and size-specific, and recovery rates are high. Another is optical granulometry, direct observation and measurement of the particles via microscopy, with the PSD being computed directly from the observed geometry[88]. Similar to the case of classifying minerals from a mixture in a microfluidic channel, this method requires that mixture constituents can be identified visually. This second method was employed for this work, as it also provides information on the particle shape, which is necessary to use Eq. 6.5 to calculate surface areas.

7.2.1 Experimental and Analysis Procedure

To prepare the powders for granulometry, approximately 300 milligrams of powder were added to a clean glass vial. The vial was filled with heptane, capped, and shaken vigorously to suspend the powder. Before settling could occur, a sample of the suspension was drawn into a pipette and dropped onto a clean glass slide. Several repetitions of suspension, sampling, and addition to the slide were performed until the slide was coated entirely with heptane. The slide was then placed in a drying oven at 60°C until the heptane evaporated, leaving the previously-suspended powder as separated particles on the glass. The prepared slides were then imaged using a Olympus BX51 microscope, and the photographs analyzed with a custom MATLAB routine to estimate the volume-based particle size distribution. Examples of the microscope images are given in Figure 7-8.

The image analysis routine to estimate the PSD is similar to that described in

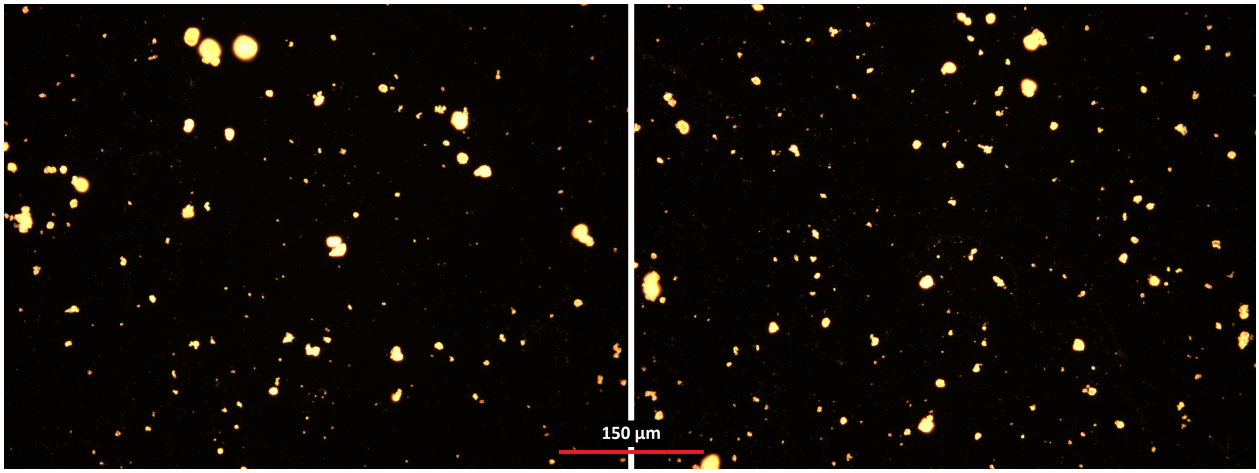

Figure 7-8: Two example images of nickel carbonate drop cast on a glass slide, viewed in dark-field

Chapter 5. Images are taken in dark-field to increase contrast between the background and the particles and facilitate particle identification. Each image is then binarized, and the contained objects detected and measured in the same manner as described in Section 5.2.5. To convert the measurements of the two-dimensional image objects to estimates of the volume-based distribution, some assumptions must be made about the shape and orientation of the particles.

- The major axis of the particle is oriented along the surface of the glass, perpendicular to the viewing angle
- The out-of-plane depth of the particle (d) is commensurate with the in-plane minor axis length of the particle

The first assumption is grounded in mechanics, it is unlikely that an extended body would rest stably on a surface if the longest dimension was perpendicular to the surface. That is, the most stable configuration for a three-dimensional body on a plane is the one which produces the widest contact with the plane and the shortest height above it. The second assumption is one of necessity, traditional microscopy and photography give very little information on the out-of-plane extent of an object, and therefore an assumption must be made. Given the restrictions and reasoning of the first assumption, it is logical to assume that this third measurement,d is of

the same general magnitude as the shorter of the two visible dimensions. If d were much greater than the visible minor axis length, the particle would be unstable on the glass. However, there is no minimum value of d which can be prescribed, and therefore enforcing this assumption will tend to produce an overestimate of the particle volume. To correct for this, d is estimated as half the minor axis.

With the results of the particle measurements obtained via image analysis, and the assumptions above, an assumption of the particle shape is required. An ellipsoid was chosen, as rounder shapes are more common in natural systems exposed to weathering[75]. The three axes of the bounding ellipsoid of the particle were taken to be the visible major and minor axis lengths, and d. The particle volume is then estimated as the volume of this bounding ellipsoid. Object solidity, the fraction of the convex hull of the image object that is filled, was used as a correction factor to the volume of the ellipsoid to account for concavity. As solidity is an area-based metric, the full correction was to multiply the volume of the ellipsoid by the solidity raised to the three-halves power. After these calculations, the obtained quantity, in cubic pixels, was converted to a physical estimate through the use of the image scale. This manner of estimation was applied to each particle visible in an image, and the results of multiple images were combined to produce the PSD estimate. A rolling average over ten points was used to smooth the obtained distribution estimate. This procedure was applied to photographs of drop-casts of nickel carbonate and nickel silicate, to assess the suitability of the technique for estimating PSDs of individual components in mixtures.

7.2.2 Nickel compounds

Comparison between the PSD for the nickel oxide and carbonate obtained through laser diffraction and granulometry is shown in Figure 7-9.

For the oxide, overall agreement is excellent, though there is a clear minor feature at small particle sizes. For the carbonate, overall agreement is poor, although the main peak is resolved fairly well. Systematic overestimation of the volume of individual particles appears to have occurred, due to the slight slight the main peak towards

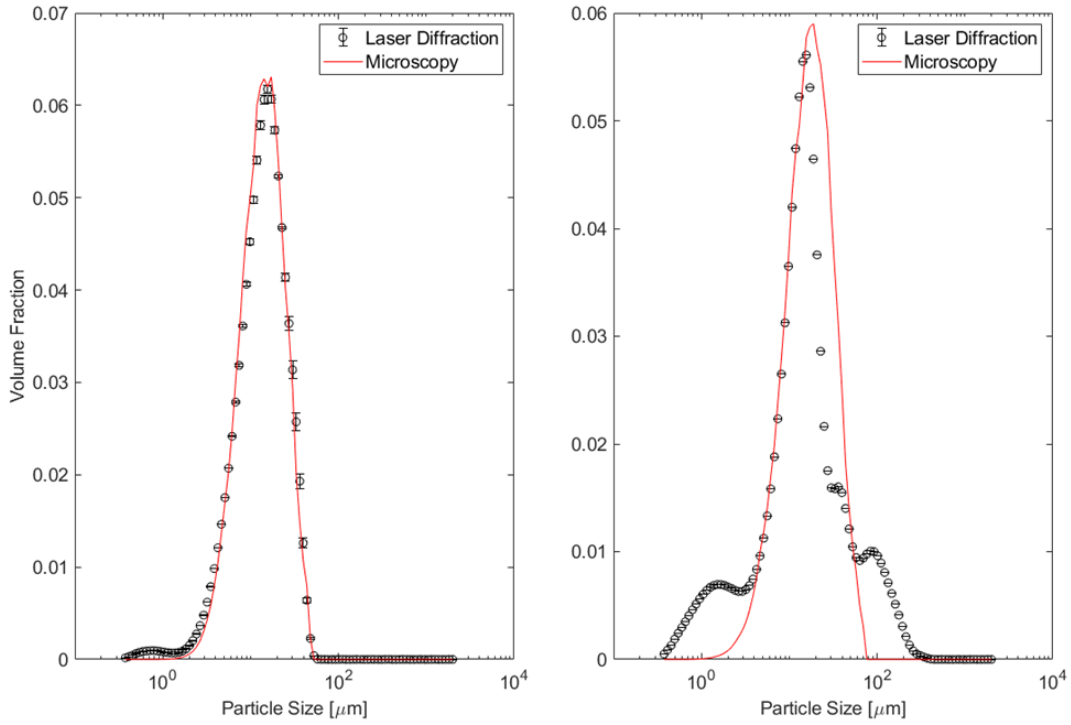

Figure 7-9: Comparison of the PSDs obtained via laser diffraction and optical granulometry for nickel oxide (left) carbonate (right)

the larger size ranges. Two significant inadequacies are apparent in the regions above and below the main peak. The error at larger size ranges is likely due to inadequate sampling; across the thirty images used to estimate the PSD, not enough of the larger $10^2\mu$m features were observed. This is to be expected, as, based on the laser diffraction PSD, such features are three orders of magnitude less common than those near $10^1\mu$m. In addition, these larger features are more likely to settle out the initial suspension before it can be sampled, leading to another source of systematic undersampling bias. At the lower end of the size domain, approaching and below one micron, a significant limitation of this method is encountered. The resolvable depth of field for an optical microscope is inversely proportion to the magnification[117], which creates difficulties in producing a focused image of three-dimensional particles at magnifications high enough to preserve these very small features through the image analysis procedure. At the highest magnification (20x) which allowed for focusing most of the objects in

the field, a one-micron wide particle is only about three pixels wide. Additionally, as the range of the width of the PSD increases this optical technique becomes less applicable to a naive first-sampling of the powder. This is shown cleary by the results obtained for the nickel silicate powder, given in Figure 7-10, which has a more uniform PSD than the carbonate.

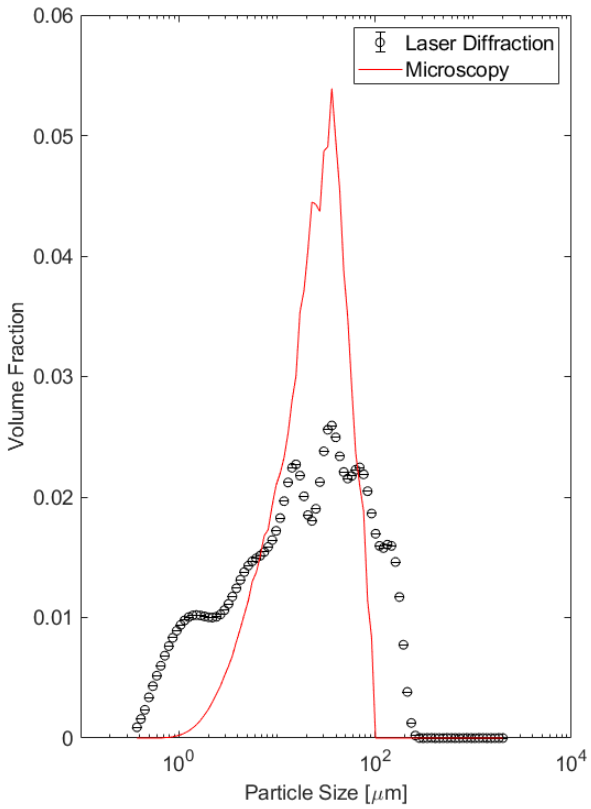

Figure 7-10: Comparison of the PSDs obtained via laser diffraction and optical granulometry for nickel silicate

The wider PSD creates extra difficulty in microscopic examination, as it reduces the fraction of particles which can be optically focused at any magnification level. One remedy to address these shortcomings is to restrict the domain under study by sieving the powder into multiple narrower domains. Smaller features may then be captured better at higher magnifications, leading to stronger results in the micron and sub-micron regimes. Undersampling bias is a persistent challenge at the larger size ranges, and may require analyzing large number of images to acquire good results.

7.3 Discussion

The results shown in Figures 7-2, 7-5, and 7-7 show that such a decomposition can accurately represent the overall mixture particle size distribution. This success enables the use of the identity distribution of Eq. 6.10 to quantify, with uncertainty, the identity of previously anonymous particles in a mixture. As seen in Figures 7-3 and 7-6, the confidence intervals for this classification are narrow, which reduces the amount of uncertainty propagated to surface area estimates through the use of Eq. 6.12, directly reducing the uncertainty in the leaching rates calculated with Eq. 6.4.

A method of estimating component PSDs via microscopy, through analysis of the images of drop-cast powders, was presented. This procedure can provide usable first estimates of size distributions, and is particularly suited to samples with a narrow, unimodal PSD. Challenges remain to improve the accuracy of the technique for particles of approximately one micron, and for larger particles which are rarely found in the microscopic images. More advanced confocal microscopy techniques give some information on the out-of-plane extent of objects[102], and may be suitable to provide more detailed volume estimates. Despite these shortcomings, the total error between the microscopic technique and the standard laser diffraction method was around 50%, which is suitable for a first-pass estimate of surface areas and leaching rates, if no other avenue is available.

7.4 Conclusion

Decomposition of mixture particle size distributions into linear combinations of the PSDs of their components offers an avenue to solving the identity problem in bulk systems. The analysis developed in Chapter 6, and the results presented here, reduce the solution to the problem of leaching rate determination in multicomponent, interfering systems to the determination of two quantities. For any system for which the linear decomposition of the mixture PSD is suitable, the chemical leaching behavior can be fully specified given knowledge of the component PSDs and their $\alpha(z)$ shape

factors. This simplifies a complex, multiscale, multiphase problem to the simple, but by no means easy, task of quantifying the geometry of the mixture constituents. Fundamentally, the only challenges remaining for bulk systems, are the development of appropriate measurement techniques to access these quantities.

Chapter 8

Surface-to-Volume Estimation via Microscopy

A key parameter for calculating phase surface areas using Eq. 6.12 is $\alpha(z)$, the function of particle size which describes the surface-to-volume ratio of the mixture components. This function depends on the shape of the particles, and therefore requires observation of the shape to estimate. Direct observation of the particles via microscopy is a straightforward and accessible technique to access particle shape, and this motivates the development of a method for estimating $\alpha(z)$ using microscopy.

8.1 Framework for Estimation

In Eq. 6.5 $\alpha(z)$ is defined as the average ratio of the surface area of a particle to the volume of that particle multiplied by the size range in the PSD domain the particle inhabits. This construction means the quantity $\alpha(z)/z$ is the full surface area to volume ratio for a mixture component, at size range z. An advantage of this definition is the $\alpha(z)$ value for any shape defined by a single measurement (sphere, cube, and all platonic solids) is simply a constant. For shapes of two separate measurements, such as cylinders and square prisms, where z is one of the measurements, $\alpha(z)$ will be a constant plus a multiple of the ratio of shape dimensions. The pattern continues for shapes of three unique measurements, where $\alpha(z)$ assumes a value of a constant plus

multiples of the ratios of z to both other dimensions. For systems where particles are well described by such simple shapes, calculating $\alpha(z)$ reduces to choosing an appropriate basis shape, which defines the constants, and calculating the aspect ratios of the particles across the range of sizes in the PSD. Corrections to account for extra area due to surface roughness or cracks could be introduced by increasing the constants present in the expression. Such well-ordered systems are not the norm for natural systems, such as soils and mineral mixtures, however, and a more general approach suitable for irregularly-shaped particles must be developed.

Leveraging the particle volume estimation procedure developed in Section 7.2, and extending it to estimate particle surface areas as well, will allow the estimation of $\alpha(z)$ for arbitrary particle shapes. For heterogeneous particles, this naturally involves an averaging of the surface to volume ratio of different particles in a size class, as individual particles are not distinguishable objects. Accepting the estimate of the particle volume derived in Section 7.2, surface areas can be estimated without the need for defining a reference shape.

Analysis of the microscope images allows measurement of the projected areas of the particles. In transforming this projecting to the surface area of three-dimensional shape, multiple options are available. Defining a convenient reference shape, as was done for estimating particle volumes in Section 7.2 is possible, although unnecessary for obtaining reliable estimates. In the interest of making the fewest assumptions, the projected area of the particle will be transformed into a three dimensional shape via the simplest method, and it will be shown that the maximum error for using this simple method is acceptable. The area of the image object is assumed to form two faces of a solid, separated from each other along the viewing axis by a distance d. The edges of these faces are joined, forming a three dimensional solid whose cross section is that of the image object; this essentially creates a cylinder whose ends are the shape observed through the microscope rather than circles. The solid formed is, rigorously, the extrusion of the shape observed via microscopy by a distance d into the viewing plane. The surface area of this shape is then equal to twice the area of the faces, which are directly measurable, plus the product of the perimeter of the face

and d.

This 'cylindrical' approximation for the shape, while simple, has desirable estimate error properties that make it attractive. The lower bound on error is zero, if the true shape is a cylinder or cube, with an upper bound of approximately a factor of two, if the true shape is a tetrahedron and d is estimated in the manner as in Section 7.2. For particles with a spherical shape, the relative error is equal to half of the ratio of d to the true diameter, *i.e.* an error of 50% in estimating d only produces an error of 25% in the estimated area. Even when the true particle shape is far removed from a cylinder, the error in the area estimate is controlled largely by the relative magnitudes of the estimate of d and the true depth of the particle. This is critically important as there exist no general technique to quantify particle surface areas, and so no direct comparison to reality can be performed on the estimates of α. Gas adsorption techniques, widely used to measure specific surface areas, require mixtures to be separated to measure individual components, precluding their use for systems which are difficult or undesirable to separate. Such techniques can also suffer from dramatic overestimation, as free gas molecules can access fine particle pores that may be inaccessible to a leachant solution[97, 70]. There is also an effect similar to the coastline paradox[50], where different surface areas are measured depending on the size of the adsorbed gas molecule[97].

8.1.1 Nickel Compounds

The area estimation procedure described above was performed concurrently with the volume performed in Chapter 7 for samples of nickel carbonate and nickel silicate. Sample preparation and microscopic analysis for these samples were identical to those described in that chapter. Results for surface-to-volume estimation for the nickel compounds are shown in Figure 8-1.

Similar trends are seen between the reference platonic solids and the nickel compounds, although the areas estimated for the powders are much higher than those of the geometric objects. This is consistent with the focus on concavity above, as it is not surprising that real shapes, that are not confined to be strictly convex, can

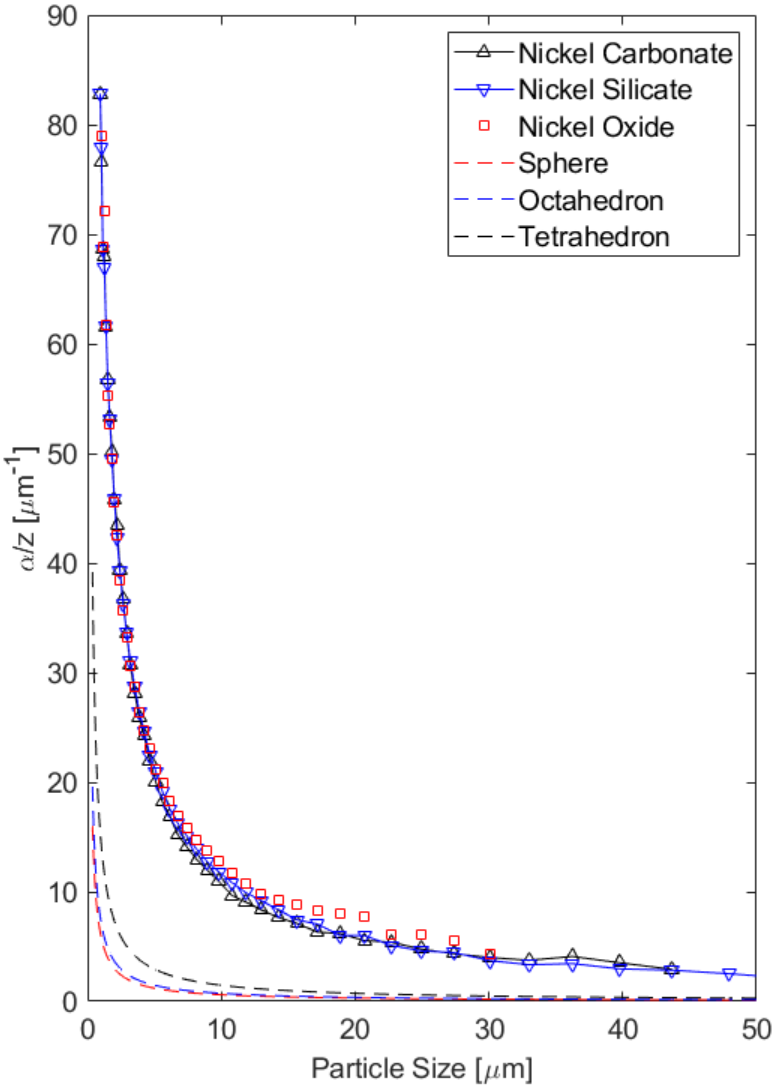

Figure 8-1: Comparison of the $\alpha(z)/z$ values obtained for the nickel compounds with those of several platonic solids

have much larger surface areas than platonic solids. These results underscore the danger in assuming convenient reference shapes to calculate particle properties, as particle shapes are rarely so convenient and their properties are therefore difficult to calculate. While the trend in the values of $\alpha(z)/z$ across the domain is encouraging, there is some concern in the similarity between the different nickel species. While the carbonate and oxide are likely well-described by this procedure, the silicate powder

has a more complex shape, and that complexity appears to have been lost to some degree through the image analysis transformations. It is also possible that true values of α for the compounds are close and the technique is simply not sensitive enough to distinguish between them. As mentioned in Chapter 7, the issues with representative sampling at the ends of the domain remain unchanged here as the technique relies on microscopy. For this reason, the estimates of α end around 50 μm, because there were not enough particles of this size present in the microscope images. The limitations of microscopy may help to explain the similarity between the results as well, given that particles with similar settling velocities (itself dependent on the surface-to-volume ratio of the shape) would be likely to be sampled in the drop-casting procedure to attach the powder to the microscope slide.

8.1.2 Phase Discrimination

Optical microscopy is a powerful technique for phase discrimination, and especially so for nickel compounds. A stark difference in the color of the nickel silicate and oxide was observed. This difference was most pronounced in the blue channel of the full color image, as shown in Figure 8-2. These differences could be used to create a mask for the optical PSD estimation procedure, enabling the estimation of component PSDs from the mixed sample.

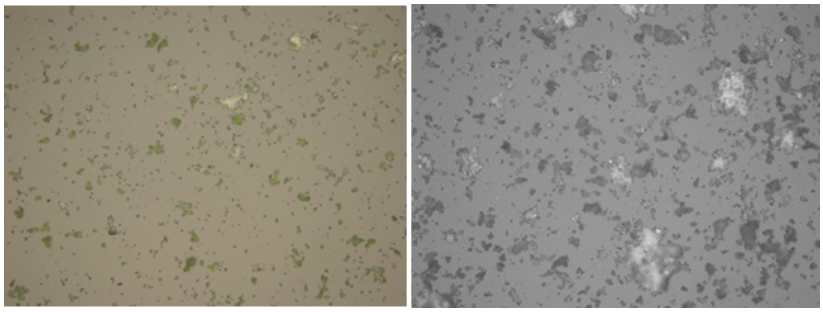

Figure 8-2: Left: Full color image of a mixed nickel oxide/nickel silicate sample. Oxide particles are the dark green features. Right: A grayscale image of only the blue channel of an image of the mixed sample. This exaggerates the color difference between the oxide and silicate.

8.2 Discussion

The results shown for dark-field, reflected-light microscopy are encouraging. Trends of α with particle size follow similar trends as those of platonic solids, suggesting that particle shape does not vary greatly across the range of particle size. Values of α are much larger than would be expected for reference shapes of convex polyhedra, showing the importance of considering concavity when estimating the surface area. Deviations from idealized, strictly convex, shapes affect estimation of the surface area much more, on average, than estimates of the volume. This is easy to understand when considering the focus of this chapter, surface to volume ratios, and how such quantities scale with feature size. Small deviations from an ideal shape, *e.g.* indents, protrusions, cracks, etc. add or remove very little volume compared to their effect on surface area. Furthermore, surface imperfections are fractal in nature[71], and exist at too many scales to permit a facile method for true surface area measurement. Returning to the coastline paradox, one must decide at which scale to estimate surface areas, and remain consistent with this choice.

In this sense, there is much more to solving this problem than obtaining a perfect surface area measurement. Recall that in 6.4 the mixture component surface areas appear as linear weighting terms to the leaching rates, and that the product of the rates and the areas is constrained to reality by measurement of the leachate concentration. Therefore a constant factor of systematic over, or under, estimation of the component surface areas will scale the calculated rates estimates by the reciprocal of this factor while maintaining their relative magnitudes. The key is that the error in the area estimate does not differ greatly between mixture components, as, if this is not true, then the ratios between rates is compromised and the information gained from this process is of lesser value. Effort for the development of area estimation techniques should therefore prioritize convenient estimate error properties, as done in this work, rather than striving for the unobtainable goal of perfect accuracy.

There one major weaknesses of the cylindrical method of approximating surface areas using optical microscopy. Only the projected area of the particle is visible, and

only from one side. Given the argument of preferred orientation of the particles made in Section 7.2.1, this prevents all information about the concavity of the particle from being known. The perimeter seen through the microscope is comprised of the points of greatest extent of the particle across all cross-sections along the path of the light. Additionally, the condition of the surface visible to the microscope is unknown, with regard to roughness, and the surface on the opposite side is likewise occluded. These shortcomings will cause the method, on balance, to underestimate the surface area of highly concave and asymmetric particles. Particles with such significant irregularity will present a difficult challenge to any estimation method, as, by virtue of possessing such complex surfaces, they defy reduction to a simple model.

8.3 Conclusion

Microscopy provides one of the few feasible methods of direct interrogation of particle size and shape. As such, it is uniquely situated to assist in the creation of a tractable solution to the identity problem in bulk powder systems. However, it must be noted that shape and size are not simple quantities. The complexities of particle size analysis and general solid characterization remain difficult to resolve to this day. Instruments which produce simple answers, such as the volume-based PSDs given by laser diffraction particle size analyzers, obscure much of the complexity of the physical nature of powders. Mathematics itself provides few general tools suitable to the analysis of concave shapes compared to convex shapes[146, 101]. Any future work in this arena must proceed fully informed on these points. Future adjustments to the area estimation procedure could include more complex techniques, such as incorporating 3-dimensional information gathered from confocal microscopy[102] and future modeling work could identify more general reference shapes or algorithms with more desirable error properties than the one presented in this work. Lastly, while the area and volume estimation procedures given in this chapter and in chapter 7 are applicable to any system, there are likely many mixtures where the accuracy of area and volume estimates could be significantly improved through system-specific refinements

to the procedures.

Chapter 9

Determination of Leaching Rates under Conditions of Mutual Interference in a Bulk Powder Mixture

A mixture of nickel oxide and nickel silicate was chosen as the test system for the extended bulk leaching method. The pure components, as well as two binary mixtures, were leached in the apparatus shown in Figure 6-1. In this chapter, the leaching results of the bulk method developed in Chapter 6 for this system will be presented. The supporting results for surface area determination and framework dissolution are presented in Chapters 7, 8 and 10.

9.1 Experimental Conditions

In all experiments, approximately 0.5 g of powder was placed in the bulk leaching apparatus, on top of a disposable glass filter disc. The powder bed was spread to a uniform thickness before the filter funnel was sealed. The leachant solution was stored in a sealed glass beaker and the flow rate was set using a peristaltic pump. Acidic leachant solutions were prepared using nitric acid, while basic leachant solutions were

prepared using sodium hydroxide. Flowrates were either 5 mL/min, for the pure nickel silicate, or 10 mL/min for all other experiments. The leachate solution was collected over three minute intervals for a total of 10 samples in 30 minutes. The hold-up volume inside the funnel was estimated from the difference in fluid volume of the first sample (at 3 minutes) and the average of the remaining samples, and was found to be approximately 4 mL in all experiments. From these results, average resident times of 48 and 24 seconds, for the pure nickel silicate and all other experiments respectively, were calculated. These are slightly higher, but still comparable, to the 10-20 second residence times in the microfluidic channel.

As in the microfluidic case, it is necessary that homogeneous reactions are suppressed, as the model in Eq. 6.3 only incorporates heterogeneous reactions. Additionally, channeling through the bed must be reduced, in order to ensure that the outlet concentration represents the leaching of the entire bed. The first constraint is supported by the use of low residence times, to keep the in-situ concentration low. Powder beds were kept thin and uniform, with the goal of reducing the pressure gradient across the bed and the formation of preferential paths for flow through the bed.

9.2 Leaching Results

Each sample was diluted 1:10 in 1M nitric acid before analysis via ICP-MS. This normalized the pH between the basic and acidic samples and kept the total species concentration close in magnitude to the concentration of the ICP internal standard (1 ppm indium).

9.2.1 Pure-Components

Pure powders of nickel oxide and nickel silicate were leached separately to serve as references for the leaching rates of the mixtures. Figure 9-1 gives the time series data for the pH 11 and pH 2 leaching experiments for the pure powders.

The obtained signals vary smoothly with time in the case of a basic leachant

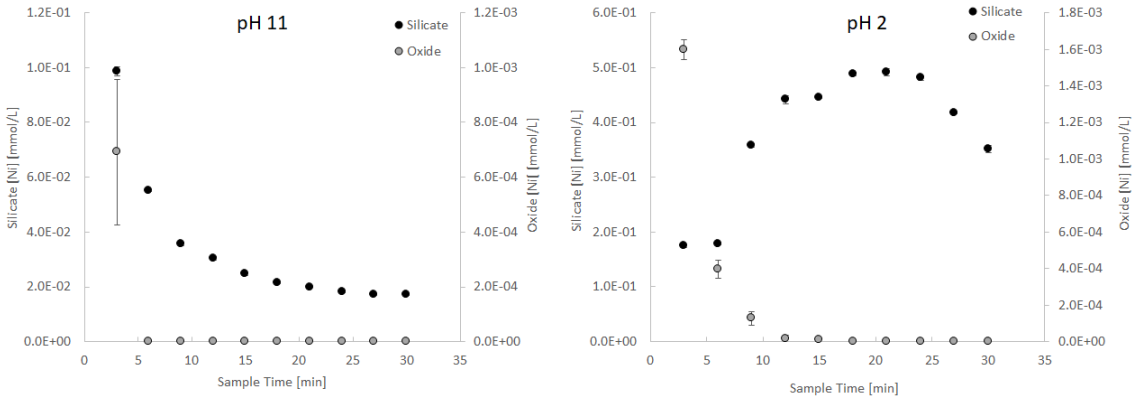

Figure 9-1: Left: Outlet concentrations of nickel from leaching of pure nickel silicate and nickel oxide with pH11 sodium hydroxide. Right: Outlet concentrations of nickel from leaching with pH2 nitric acid. Concentrations from the silicate are plotted on the left axis, and oxide on the right axis.

solution. In contrast, the silicate signal in acidic solution appears to approach a constant value within a modest variance. These differences in pH hint at a change in the mechanism of dissolution between acidic and basic conditions, as would be expected for a silicate material given the complex pH-dependent speciation of silicon. In both cases, the oxide signal drops below detectable limits before the end of the 30-minute runtime of the experiment. The concentrations in the acidic case are roughly 1 order of magnitude larger than those measured in the basic case, for this reason the acidic regime was chosen for the leaching of the binary mixtures.

9.2.2 Binary Mixtures

Two binary mixtures were created by mixing known amounts of the pure oxide and silicate powders. One was 60 wt% silicate, and the other 40 wt% silicate with the balance being nickel oxide. The PSDs of these mixtures were shown to agree well with the mixing model, as shown in Figure 7-2, and these compositions were chosen to simulate poor separation of a binary mixture of equal weights of both components. The leaching results for these mixtures are given in Figure 9-2.

The concentration profiles follow a clear decreasing trend starting with the sample taken at 15 minutes. As the mixtures appear to have not fully reached steady

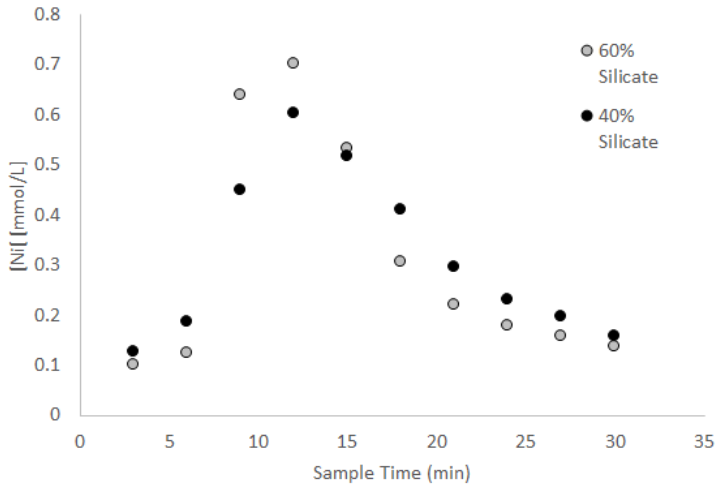

Figure 9-2: The outlet concentrations of nickel measured during leaching of the binary mixtures with pH2 nitric acid.

leaching behavior during the 30-minute window, the data in this region was fit to a simple decaying exponential with a constant offset to identify the steady-state concentration. These fits are given below in Figure 9-3. Of course, running a longer leaching experiment would be preferable to relying on an empirical fit to extract a steady concentration. The experimental runtime was decided after the results of the pH 11 leaching experiments, and then the pure component and mixture leachings were all performed before measurement of the concentrations of the samples from any of these experiments.

The fits agree with the data to high accuracy. There remains some danger in extrapolating an empirical result beyond the domain of the data, however, as the concentrations are expected to drop to a steady value, the form of the model is likely to be sufficient. The steady concentrations for the pure components and binary mixtures were converted to molar flows of nickel by multiplication with the volumetric flowrate. These molar flows are plotted in Figure 9-4 versus the weight fraction of silicate, as that is the more active component of the mixture. A strong linear relationship is seen between the weight fraction of silicate and the nickel flowrate, which is to be expected given that the steady concentration from the oxide was observed to be zero.

From the results shown in Figure 9-4, and the pure component leaching results,

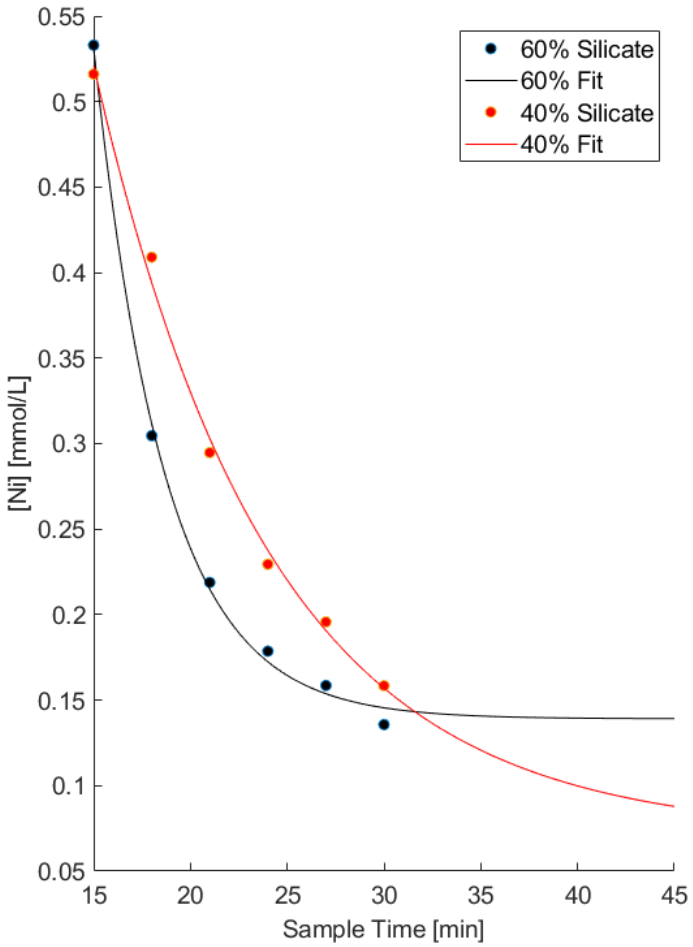

Figure 9-3: Fits for the regression of the steady leaching concentration from the mixture leaching results. The fitting function was a decaying exponential plus a constant term.

the bulk model should be able to describe the leaching in the system. Fundamentally, the model is a summation of linear relationships between the surface area of mixture components and the molar flow of the leached species. For the case of this mixture, the oxide relationship is a rather uninteresting factor of zero, and the entire leaching behavior is due to the silicate content. However it should be stressed that the only reason this is known to the reader, at present, is the results shown for pure-component leaching experiments which could not be performed on a general solid mixture. The task of using only the mixture leaching experiments to calculate the leaching rates

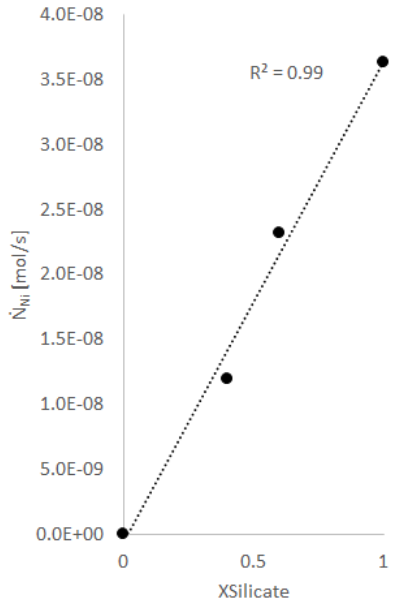

Figure 9-4: Steady molar flow of nickel leaving the powder bed vs. the nickel silicate weight fraction.

shows the true utility of this work, and for this task the behavior of the oxide cannot be assumed to be unimportant.

There are two fundamental limits to consider in the problem of determining multicomponent leaching rates: equal importance and extraneous variables. In the equal importance limit, the total leaching rate, importantly *not only* the intrinsic leaching rate, of each phase is of coincident magnitude. The equivalent plot of the nature of Figure 9-4 would be a roughly horizontal line near the regions of the mixture's natural composition. In the extraneous case, all of the leaching behavior is due to a subset of the phases, and the remaining phases contribute nothing, chemically, to the mixture's leaching properties. In the first case, the methods developed in this work are somewhat tedious - if the leaching behavior is not observed to change within the experimental ability to separate the mixture, then the answer is simply that leaching rate is similar between all phases. In the second, less rigorous methods are strained. The presence of surface areas for non-reactive phases, of variables with no explanatory power, only serves to increase the confidence interval of the relevant phases by serving as a sink for system uncertainty. As discussed in Sections 3.3 and 6.3, the condition

number of the design matrix is likely to be large owing to ineffective separation, and therefore the effects of experimental uncertainty on the estimates of leaching rates will be magnified. It is for this reason that, while it may seem initially trivial, the calculation of leaching rates from a mixture with one significant component is an important test case.

9.3 Rate Calculation

The synthetic nature of the mixtures permits a slight simplification in the calculation of the rates. As the mixtures were created by mixing the pure powders directly, rather than created by sieving a mixture of the powders, the specific surface areas of the components in each mixture are identical. Practically, this means that the area calculation can be done once using the entire $\alpha(z)$ curve, and then scaled based on the mixture composition, rather than using portions of the curve depending on the size fraction of the mixture. Estimation of the α values for the silicate and oxide is shown in Chapter 8. The estimated surface areas and measured molar flows for each phase and trial are given in Table 9.1.

	Nickel Silicate [m^2]	**Nickel Oxide [m^2]**	**Outlet Molar Flow [mols/s]*1e8**
60 wt% Silicate	0.792	0.528	2.32
40 wt% Silicate	0.436	0.654	1.19

Table 9.1: The component surface areas and outlet molar flows for each trial of the mixture leaching experiments.

The results of different solution techniques of Eq. 6.3 to the system given in Table 9.1 are shown in Table 9.2. As expected, direct inversion does not produce a physically reasonable solution to the problem, as the rate of nickel release from the oxide is not negative. For a system which could be separated to a larger degree, with greater differences in surface area between trials, the inversion solution would be expected to produce stronger results. Treating the system as a parameter estimation problem and solving with the generalized maximum entropy (GME) technique produces a silicon leaching rate which compares very favorably to the rate measured from the pure

silicate. This is important, as it shows the technique is self-consistent, and comparison with any other measurement of rates is likely a matter of finding a common basis, as the measurement of phase surface area is likely to differ if different measurement techniques, such as BET, are employed.

	Direct Inversion	**GME Parameter Estimation**	**Pure Component Experiments**	**Literature**
Nickel Silicate [mol/m2/s]*1e8	3.5	2.6	2.7	2.7e-3[135]
Nickel Oxide [mol/m2/s]*1e8	-0.97	0.15	0	0[104]

Table 9.2: Rate estimates acquired by several methods for the leaching experiments of the binary mixtures

The silicate rates do not agree with those found in literature for the leaching of nickel silicate in pH 2 nitric acid. The authors of this study used a leaching setup very similar to the one used in this work, however they waited "several hundreds of hours" to measure the steady leaching rates. It is not surprising, then, that the rate measured here, after only 30 minutes, is much higher.

9.4 Discussion

The results shown in Table 9.2 represent, to the best knowledge of the author, the first demonstration of the simultaneous determination of intrinsic leaching rates from a mineral mixture. These estimates were self-consistent with measurements made on pure samples, and were performed with the minimum amount of experimental data required to make such an estimate. The nonphysical results obtained using direct inversion shows the care that must be taken to solve the system, and is the mathematical manifestation of the physical challenges in separating the mixture. There is no silver bullet to address this issue, its origins are in the structure of the linear inverse problem, and a careful assessment of solution techniques will always be warranted.

9.5 Conclusion

A practical, self-consistent, experimental method now exists for the extraction of individual leaching rates from experimental data containing the effects of multiple mixture components. While the bulk technique is not as flexible as the envisioned microfluidic technique, requiring some ability to separate the mixture, the problem of phase surface area assignment proved much more tractable for bulk systems. This tractability is key to the utility of the technique, as the complexity of the problem is shifted entirely to the measurement of directly observable geometric quantities. The full array of materials characterization techniques are available to facilitate these measurements, with greatly expands the opportunities for exploiting property differences to discriminate between phases. Color proved useful in the case of the nickel compounds, as seen in Figure 8-2 as the oxide was a much darker green than the silicate. Other techniques may be more useful for different systems, but by moving from a sectioned sample to a bulk one, the array of available characterization techniques is greatly expanded. While shape was found to be an unreliable in the microfluidic case, as shown in Section 5.3.4, there is ample opportunity to find a reliable one once the restriction of a microchannel is removed.

Chapter 10

Mechanism Determination in Bulk Powders

Many classes of minerals can leach species through multiple mechanisms. Broadly, these can be grouped into framework dissolution, where the mineral specimen is physically destroyed as the covalent framework of the crystal dissolves, and non-destructive leaching, where ion exchange occurs between the leachant solution and ionically-bound species in the framework[111, 54, 119]. It is the presence of these dual mechanisms that allows incongruent, non-stoichiometric, leaching behavior to exist over long times. This complicates the task of quantifying elemental release rates for multicomponent systems, as the leaching rates of different species from a single solid component cannot be assumed to follow the solid stoichiometry. In addition, in fertilizer applications, there are differences in the expected long-term behavior of systems undergoing each mechanism. For example, aluminum is the most common metal element in Earth's crust[110], and is toxic to many plants[144]. Fertilizer materials made using aluminum-containing minerals, such as feldspars, must therefore effectively sequester their aluminum content and prevent it from entering the soil. Having the ability to distinguish between framework release of aluminum and non-destructive leaching of aluminum, at the lab scale, provides key insights towards designing better pathways for fertilizer production from minerals. In the case of non-destructive leaching of aluminum, a rinsing or soaking step may be able to correct the

issue, but framework dissolution may require a more significant change to processing to alter the product chemistry. Any direct evidence of nutrient release mechanism that can be gathered at the same time as determining the leaching rates is therefore very valuable.

10.1 Framework Dissolution

As mentioned above, framework dissolution involves the loss of particle volume through the chemical destruction of the crystal lattice comprising the particle. In many minerals this framework is composed of silicate tetrahedra, or both silicate and aluminate tetrahedra, and so has some covalent character to the bonding[129]. Smaller species, such as alkali metal ions in the case of some feldspars, occupy voids in the silicate or aluminosilicate framework and serve to balance the charge of the lattice. Under leaching conditions, these species are able to substitute with charged species from the solution, such as protons or other metal ions, leading to the release of the original species from the surface, while maintaining the framework. Nutrient release via this mechanism should cause essentially no change in the volume of the leached particles. In contrast, nutrient release via destruction of the framework should be easily visible in the particle size distribution due to the destruction of particle volume. Equations governing the change of a PSD over time under conditions of framework dissolution were derived in Section 6.4, and results of applying this model to mineral systems are given in the following section.

10.1.1 Feldspar powder results

Mixtures of the feldspar powders MCA41 and FSB02 were leached with pH 1 nitric acid for 60 minutes at a flowrate of $15\frac{ml}{min}$ in the apparatus shown in Figure 6-1. The PSDs of the mixtures pre- and post-leaching were recorded, and the change due to leaching compared to that predicted by Eqs. 6.16 and 6.17 to check for evidence of framework dissolution. The results of this comparison are given in Figure 10-1.

Strong agreement is shown between the measured and predicted post-reaction

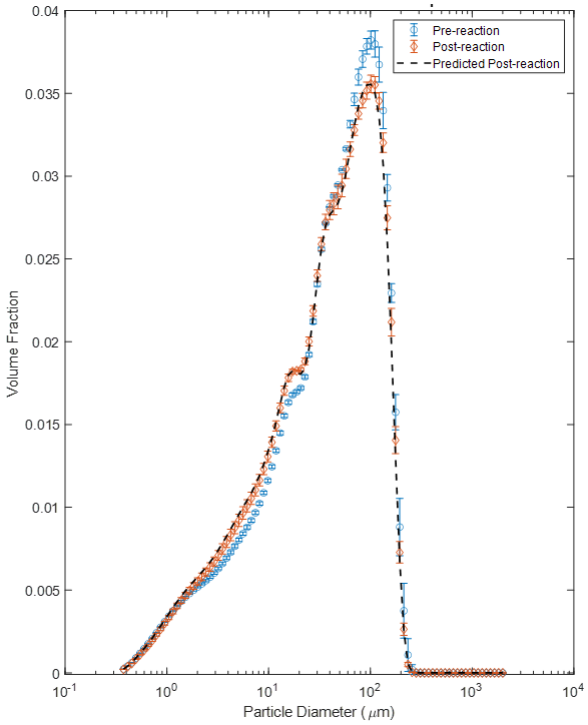

Figure 10-1: Comparison of the measured and predicted post-leaching PSD of a mixture of 75 wt% MCA41 and 25wt% FSB02. The pre-leaching PSD is included for reference

PSDs. The framework dissolution rate, as determined by the distribution method of Eq. 6.16 was $1.04 + -.14 * 10^{-10} \frac{mol}{m^2}$, which agrees well the literature rate of feldspar dissolution at $1.8 * 10^{-10}$[9] for these conditions. Given the very strong agreement across the entire distribution between the measured and modeled values, framework dissolution can be confidently stated to be the method of nutrient release in this mixed feldspar powder system. Furthermore, the rates of dissolution are similar for both constituents, as only one rate value was needed to produce this close agreement.

10.1.2 Nickel compound results

Separate samples of nickel oxide and nickel silicate were leached in the apparatus show in Figure 6-1 for thirty minutes at a flow rate of 15 $\frac{ml}{min}$. The leachant solutions were pH 11 sodium hydroxide for the oxide, and pH 2 nitric acid for the silicate. Figure 10-2 gives the comparison between the pre- and post-reaction PSDs and the prediction of the model described in Section 6.4.

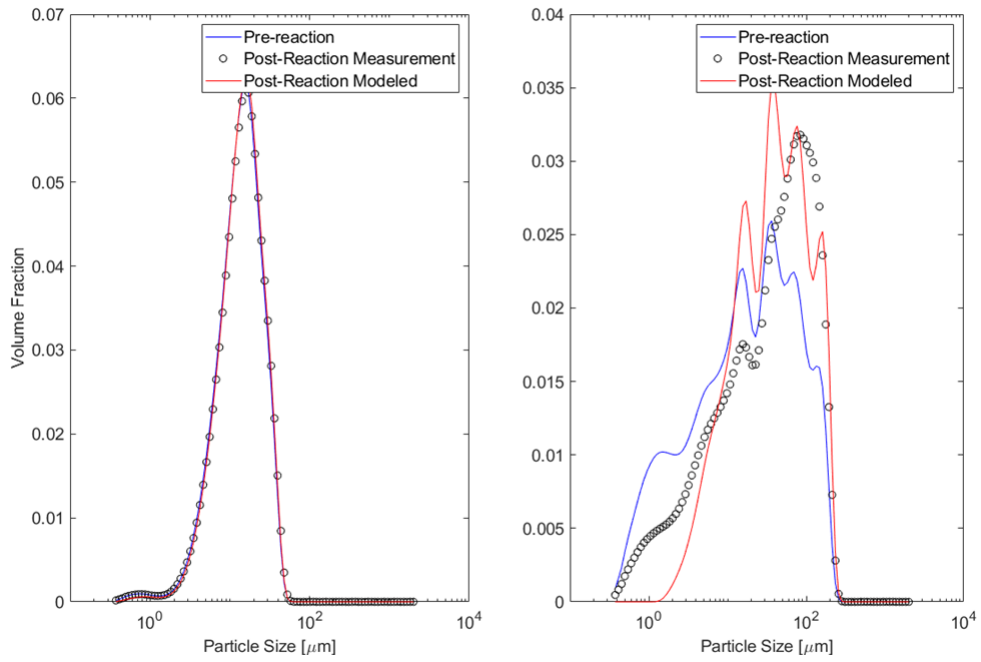

Figure 10-2: Comparison of the measured and predicted post-leaching PSD of nickel oxide (left, pH 11, 30-minutes) and nickel silicate (right, pH 2, 30-minutes). The pre-leaching PSD of each is included for reference

Nickel oxide shows strong agreement between the measured and predicted post-leaching PSDs. While the change in the PSD due to leaching is small, given the slow rate of leaching ($4.5 * 10^{-7} \frac{gNi}{m^2}$), a measurable difference in the PSD pre- and post-leaching exists. The sum of squared error (SSE) between the predicted PSD and measured post-leaching PSD is less than half ($2.9 * 10^{-5}$) that exists between the pre-reaction and post-reaction PSDs ($6.4 * 10^{-5}$). The error is most prevalent at the main peak, which has a modest over-estimate, and at small end of the domain, where the presence of smaller particles is underestimated. These errors are likely correlated; predicting the total extinction of the smallest particles forces the volume fraction of other particles to increase, in order to maintain the sum of the distribution at unity. The prediction for both the oxide and silicate maintains the general shape of the pre-reaction PSDs, including the multiple peaks present in the silicate distribution. However, the measured post-reaction PSDs show deeper transformations, with the multiple peaks of the silicate merging at the larger particle sizes. This is behavior is not unexpected, the model of Section 6.4 cannot account for changes of shape during

leaching, or creation of new particles, such as if a thin region of a larger particle is fully leached away and two smaller particles result. It also implicitly assumes that the pre-reaction PSDs are discontinuous, and as such it will always preserve independent peaks and other features until it predicts they would be completely dissolved. Examining the prediction error, shown in Figure 10-3, provides further support for this interpretation of the results.

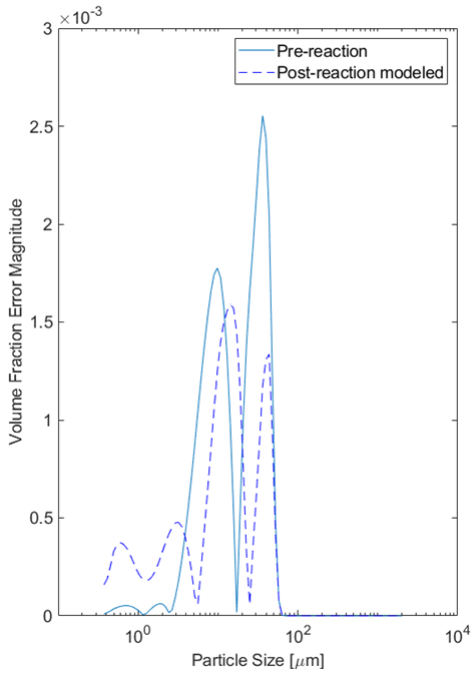

Figure 10-3: Comparison of the error magnitude between the post-reaction PSD of nickel oxide (pH 11, 30-minutes) and the pre-reaction PSD and modeled post-reaction PSD.

The shape of the curve describing the magnitude of error between the predicted post-reaction PSD and measured post-reaction PSD is incredibly similar to the curve describing the error between the pre-reaction and post-reaction PSDs for nickel oxide. This suggests that the pre-reaction PSD and predicted PSD have significantly similar shapes, and that the prediction is more appropriately scaled to match the post-reaction PSD. These properties originate from the modelling procedure, which is fundamentally a horizontal shift and rescaling of the original PSD.

10.2 Discussion

Modeling the change of a PSD under reactive conditions is a complex problem. The results given in this chapter for the procedure developed in section 6.4, show strong agreement in cases where dissolution is slow, and the pre-reaction PSDs have a limited number of independent peaks. Prediction in the case of nickel silicate, which has a multimodal PSD and dissolves orders of magnitude faster than nickel oxide, was poor. A key difference between the oxide and silicate, besides the dissolution rate, is particle shape. The silicate powder was prepared by ball-milling a larger powder, and this process created a non-uniform assortment of complex shapes. Given the merging of peaks seen across leaching, it appears that the dissolution process caused the splitting of some of the larger particles into multiple smaller ones. This helps to explain both the underrepresentation of larger particles in the measured PSD compared to the model, and the overrepresentation of smaller particles. The leaching of the feldspar powder mixture and nickel oxide did not display this behavior to a significant degree, likely due to both their simpler shapes and slower dissolution rates.

Given these results, certain limitations of the model become clear. Leaching times should be kept short enough that the splitting of larger particles does not become very prevalent. In addition, multimodal distributions will pose difficulties in resolving their post-reaction peaks. Lastly, there appears to be a systematic undercounting of the smallest particles, up to at worst a few microns in size. Depending on the values of the original distribution in this size regime, this limitation may be more or less hindering.

10.3 Conclusions

The model of Section 6.4 provides a second line of evidence for kinetic studies of bulk powders. Framework dissolution can be effectively identified when present, subject to certain limitations given the model's foundation. There exists a clear avenue for future work to incorporate the effects of distribution continuity, which will likely help

the model capture the merging of previously separate peaks at larger size ranges. The simplest procedure for this would be to simply join the mid points of the histogram bins with lines, rather than modeling the discontinuities at the bin edges. Care would have to be taken to ensure the distribution remains properly normalized, and any procedure to make the data continuous will be subject to some distortion. There may exist different best practices to perform this continuum transformation depending on the features of the distribution in question, even while it seems unlikely that any single method will be optimal for all cases. In the absence of continuous data, the discrete transformation provides strong agreement for feldspar powders, of the kind which comprise a large portion of earth's crust, and as such is likely sufficient for many of the common mineral components to be encountered in agricultural applications.

Chapter 11

Conclusions and Future Work

The goal of this project was to develop a practical experimental tool for the kinetic analysis of leaching reactions in multicomponent solid systems. That goal was achieved, although not in the manner that was initially proposed. The bulk method for multicomponent analysis developed in this project is significant, it represents the first rigorous and complete extension of traditional bulk leaching techniques to multicomponent systems. Experimentally, the entire suite of characterization techniques from materials science is available to solve the identity problem, creating a very robust analytical technique. However, the microfluidic leaching techniques provide many experimental advantages that make their extension to multicomponent systems attractive, and these advantages remain despite the failure of this work to find a path to effect that extension.

11.1 Microfluidics as a tool for kinetic analysis

The lack of a diffusive mechanism in solid mixtures predisposes them to spatial gradients in physical and chemical properties. This is the origin of sampling bias, which afflicts many measurements of solid properties and against which many specialized experimental procedures have been devised[89]. Microfluidic leaching harnesses this disruptive force to allow the design of independent leaching experiments and enable the calculation of intrinsic leaching rates without separating the parent mixture.

Nearly any solid system, for which the constituent particles can fit in a microchannel, can be analyzed in this manner. Only two constraints dictate the applicability of the method: that the mixture phases be impermeable in sectioned form, and that some metric exists with which to distinguish between them.

This second constraint is the more limiting. It was found that sectioning a sample substantially weakens the link between observed shape and identity, which reduces the utility of light and electron microscopy in discriminating phases. Shape factors, as metrics of particle shape, were therefore found to be unusable for the task of classifying features in the microfluidic channels. This is in contrast to their use in histology, where cell types can be accurately distinguished based on these metrics[94, 114, 138]. The difference is that a cell is a complete entity, where the objects seen the channel are sections of a larger whole.

Beyond shape, microscopy techniques allow easy access to topological features. Convolution neural networks provide a general way to combine these features with any relevant shape metrics and other visually accessible information available from microscopy. However, even these black-box models were found inadequate for the task of classifying mineral phases from a mixture. Of course, it cannot be stated that such an approach would never work, but within the size of the training dataset that could be produced, no example of effective phase segregation was found. If a large amount of training data is available then perhaps machine learning could be successfully applied, however reliance on such techniques to solve the identity problem in microfluidic systems prevents the use of these techniques for novel materials, where no such training data can exist. Future researchers in the pursuit of an extension of the technique to multicomponent systems, would be better served by focusing on any unique aspects of the system that may enable effective segregation - as was done in the bulk case with color.

Elemental analysis is an ostensibly general technique for phase identification, and has some commercial applications towards this end[64], however it was not found to be suitable for the hydrothermal material studied here. The heterogeneous size ranges present in the material, 100 μm feldspar features with single-micron-sized

CASH phases limited the use-fullness of EDS, as many of the smaller phases simply couldn't be sampled. With a monodisperse mixture, EDS may be more useful for phase classification. For mineral systems in particular, the similarities of the phase chemistries will always present a challenge. The wide range of substitutions available to many classes of minerals, and in particular calcium silicates[125, 142, 17], creates a moving target for the production of a composition metric to separate these phases. The time investment required for gathering composition data may be prohibitive for systems of many components, due to the number of experiments required. Further, any identification scheme must be developed in consideration of the number of phases it is tasked with distinguishing, and the number of experiments required to effect this.

Opportunities exist for shifting the difficulty of phase classification to other regions of the experimental procedure. By shortening the microfluidic channel, the total area requiring classification is reduced. In the extreme limit, it could be shortened enough to allow for manual identification of all phases present. This reduction comes at the cost of decreasing the total area of interaction between the fluid and solid, thereby lowering the outlet concentration. Practical limits are quickly reached regarding the minimum concentration amenable to analysis and the minimum sample volume that may be analyzed, and these give a firm lower bound on the area of the channel for a system of certain reactivity. A compromise between shortening the channel to allow for manual identification, and the difficulties in establishing automated classification metrics may be possible. If a representative area of the channel could be manually classified, then statistics could be used to predict the composition of the rest of the channel to within some error. It may be easier, for certain systems, to perform more experiments to reduce the effect of this error on the leaching rate estimates, than it is to develop a rigorous automated classification procedure for a longer channel. Such stochastic methods obviously rely on the ability of a human to reliably discriminate between phases, and it is implicitly assumed that the minerals are randomly distributed in the channel, which may not be the case for systems with strong chemical coupling.

11.2 Kinetic analysis in bulk powder systems

By avoiding the sectioning of the mixture particles, the bulk technique maintains any extant connection between particle size, particle shape, and particle identity. If the particle size distribution of a mixture can be accurately described by a linear combination of the particle size distribution of its components, then the identity distribution - the volume fraction of each component present at each nominal particle size - can be defined. This allows the accurate determination of the volume of each mixture constituent present in different size regimes, and this information is required in the intelligent design of experiments as, unlike in the microfluidic case, the mixture must be physically separated to enable independent experiments to be performed. The need for some degree of separation is an inherent weakness of the bulk technique, as is its reliance on describing mixture constituents are semi-regular and impermeable shapes. Under such conditions, the complex problem of chemical analysis of a multicomponent system is reduced to the estimation of directly observable geometric parameters. While still a challenging task, especially for mixtures with larger numbers of components, Highly amorphous systems, such as the hydrothermal material analyzed using the microfluidic technique, are poor test systems for this technique, as the mixture constituents do not exist entirely as separate entities. These extra constraints, that some separation ability exists and that particles are distinct and impermeable, are not crippling, and the bulk technique developed in this work is still applicable to broad classes of mineral mixtures and chemistries.

Extensions of the technique to handle softer materials and combined phases would be helpful in expanding the range of mixtures which could be analyzed. Soft materials, such as the silicon-rich gel phase encountered in the microfluidic leaching, pose a challenge to quantitative analysis as they defy quantitative description. The size of such features is difficult to define and their shape varies, two properties which make a geometric approach to quantifying the rates less applicable. The weight fraction of this phase could be used to report its prevalence, which would allow the calculation of a specific leaching rate rather than an intrinsic rate, however this would mandate both

a strong connection between the weight fraction and surface area, and the existence of method to accurately measure its weight fraction in a mixture. For crystalline phases, quantitative phase analysis (QPA) via x-ray diffraction can provide decent estimates of mixture composition[7], but it is less applicable to amorphous phases. Further, there is no guarantee that the surface area-to-weight relation remains constant, or nearly constant, between experiments. There is no obvious silver-bullet solution to the problem of amorphous materials and this mirrors the complexities of the materials themselves. Despite these difficulties, polymeric materials are very common in mineral systems containing silicon[28] and these geopolymers have rich chemistries to explore. Future work to extend the technique to these systems and unreliable geometries, would greatly expand the range of applicability of the technique. Combined phases, where individual mixture particles contain multiple mixture phases, pose another challenge. Such conditions may be encountered if a mixture is milled, or if a chemical transformation from one phase to another occurs incompletely. For this case, it may be helpful to consider a combination of descriptors of geometric and compositional information. If it is possible to distinguish the pure phases and combined phases in the mixture, then the weight fraction may provide some utility in the calculation of a correction to the phase volumes found using the methods described in this work. If the materials retain crystallinity, then QPA or another method could be used to calculate these weight fractions. This extension is only necessary if the combined phases comprise a large portion of the chemical activity of the mixture, if they are minor phases, or only a small portion of one or more of the major phases, then their effect is to modestly average the leaching rates of several phases. Depending on the accuracy desired, this shifting of the confidence intervals may not be sufficient to warrant the extra experimental effort required to resolve it.

11.3 Conclusions

Single component systems are rare in nature, and therefore the study of natural mineral and fertilizer systems necessarily encounters questions of the study of mul-

ticomponent systems. While the accuracy of measurement techniques has increased tremendously with technological progress, the difficulty in characterizing systems of multiple components has remained unchanged. It is not the ability to make accurate measurements of physical and chemical properties that frustrates the study of mixtures, but the fundamental structure of such problems. This is made concrete in the focus of this work on the identity problem, and developing solutions to it, for a given system. Regardless of the chemical nature of the system or form factor chosen for experimentation, some metric must be used to separate the contributions of the components. The success of any technique rests on the robustness and scalability of this metric. The microfluidic leaching technique, for all of its advantages, does not permit a ready solution to the identity problem and therefore could not be extended to the analysis of mixtures. Any future work must be directed towards closing this ability gap. In contrast, the bulk technique permits a straightforward solution to the identity problem for the case of a mixture of distinct particles. This enabled the rigorous extension of bulk leaching to mixtures, and the first simultaneous determination of leaching rates from experiments on mixtures. As the primary result of this work, this represents a solid foundation for the further extension to other classes of solid mixtures.

Appendix A

Supplemental Derivations

A.1 Derivation of Functional Uncertainty

A function $f(x)$ may be approximated as linear around the point μ_x through a Taylor-series expansion:

$$f(x) \approx f(\mu_x) + f'(x)|_{\mu_x}(x - \mu_x) + \frac{f''(x)|_{\mu_x}(x - \mu_x)^2}{2} + ... \tag{A.1}$$

If f is vector-valued function with a vector argument, this can be written as:

$$f(x) \approx f(\mu_x) + J(x)|_{\mu_x}(x - \mu_x) + \frac{H(x)|_{\mu_x}(x - \mu_x)^2}{2} + ... \tag{A.2}$$

where J and H are the Jacobian and Hessian matrices of f, respectively.

The variance of f is defined as:

$$Var(f) = E[(f(x) - f(\mu_x))^2] \tag{A.3}$$

Substituting the first-order Taylor expansion for f, and making use of the linear nature of the expected value operator:

$$Var(f) \approx E[(f(\mu_x) + f'(x)|_{\mu_x}(x - \mu_x) - f(\mu_x))^2] \tag{A.4}$$

$$Var(f) \approx E[f'(x)|_{\mu_x}(x - \mu_x))^2] \tag{A.5}$$

$$Var(f) \approx E[(f'(x)|_{\mu_x}^2 (x - \mu_x)^2] \tag{A.6}$$

The derivative term is a constant, and so can be moved outside the expectation:

$$Var(f) \approx (f'(x)|_{\mu_x}^2 E[(x - \mu_x)^2] \tag{A.7}$$

The quantity inside the expectation is the definition of the variance of x.

$$Var(f) \approx (f'(x)|_{\mu_x}^2 \sigma_x^2 \tag{A.8}$$

Likewise for the vector-valued function case:

$$\Sigma^f \approx J \Sigma^x J^T \tag{A.9}$$

Where Σ denotes the covariance matrix.

The use of a first-order Taylor expansion limits the applicability of this result to cases where the variance of the function arguments is not so large as to make a line a poor approximation to the function around the average values of the arguments.

A.2 Generalized Maximum Entropy parameter estimation

This section gives a brief overview of the GME parameter estimation technique as described in Golan et. al.[47].

The general linear model (GLM) may be written as:

$$\mathbf{y} = \mathbf{X}\boldsymbol{\beta} + \boldsymbol{\epsilon} \tag{A.10}$$

where $\mathbf{y}$ is the vector of T observations with noise, $\mathbf{X}$ is a $T \times K$ design matrix of known variables, and $\boldsymbol{\beta}$ is vector of K unknown parameters. $\boldsymbol{\epsilon}$ is an unobservable vector of random errors commonly assumed to be centered around zero and have finite variance.

Standard linear regression techniques estimate the values of $\boldsymbol{\beta}$ by minimizing some measure of the error terms $\boldsymbol{\epsilon}$. This works well in many instances, but can lead to overfitting when the number of parameters is similar to the number of data points, and to unstable solutions when the independent variables are correlated. For the GME solution, the GLM is reparameterized as the expected value of unknown probability distributions for $\boldsymbol{\beta}$ and $\boldsymbol{\epsilon}$ over a defined support.

$$\boldsymbol{\beta} = \mathbf{Z}\mathbf{p} \tag{A.11}$$

$$\boldsymbol{\epsilon} = \mathbf{V}\mathbf{w} \tag{A.12}$$

$$\mathbf{y} = \mathbf{X}\boldsymbol{\beta} + \boldsymbol{\epsilon} = \mathbf{X}\mathbf{Z}\mathbf{p} + \mathbf{V}\mathbf{w} \tag{A.13}$$

$\mathbf{Z}$ and $\mathbf{V}$ are the supports of the probability distributions for the parameters($\mathbf{p}$) and error terms ($\mathbf{w}$) respectively.

These supports define the acceptable range of values for the parameters and errors. This gives an opportunity to bias parameter estimates with prior information, for instance if the parameters are known to be non-negative, and to bound the error

terms to experimental confidence. In general, the domain of the parameter distributions should be wide and centered on zero, to avoid biasing the estimates if no prior information is known. The support for the error can be set to encompass +/- 3 standard deviations of the data, or some other acceptable metric, to prevent the model from overfitting noisy data.

The parameter estimates are produced by solving the following optimization problem:

$$max(H(\mathbf{p}, \mathbf{w})) = -\mathbf{p}' ln(\mathbf{p}) - \mathbf{w}' ln(\mathbf{w}) \tag{A.14}$$

subject to

$$\mathbf{y} = \mathbf{XZp} + \mathbf{Vw} \tag{A.15}$$

$$\sum \mathbf{p} = 1 \tag{A.16}$$

$$\sum \mathbf{w} = 1 \tag{A.17}$$

where $H(\mathbf{p}, \mathbf{w})$ is the Shannon entropy[115] of the probability distributions $\mathbf{p}$ and $\mathbf{w}$.

The point estimates of the parameters are then:

$$\hat{\boldsymbol{\beta}} = \mathbf{Z}\hat{\mathbf{p}} \tag{A.18}$$

The objective of the technique is to maximize the entropy, the uniformity, of the probability distributions of the parameters and error terms. The imposed constraints mandate that the values of the parameters model is satisfied, and that the distributions satisfy the consistency requirement and add to unity.

The maximum entropy distribution in a general sense is a uniform distribution. This means that, without the model constraining the values of the parameters, they will tend towards the center of the defined support in $\mathbf{Z}$. The overall entropy of the parameter distributions will be reduced to sharpen the distribution towards a different value, and this can be viewed as the transfer of information from the measurements

in $\mathbf{y}$ to the parameters. A key advantage of this construction is that the parameters *will not* over-fit data. if given realistic error bounds. The values of the parameters will be only as certain as required to satisfy the model within the bounds of the error, regardless of the number of data points provided. Collinearity affects this procedure less than other parameter estimation techniques, because only the unique explanatory power of a variable needs to be mapped to its parameter. If a variable is highly correlated with another, then the first variable is really the explanatory variable, and its parameter value will reflect the extent of this power. This property is tremendously useful for non-experimental data; that is, data from measurements where the independent variables can be observed, but not freely set, as is the case for surface areas in solid mixtures.

Appendix B

Figures

B.1 Continuum Model Comparison

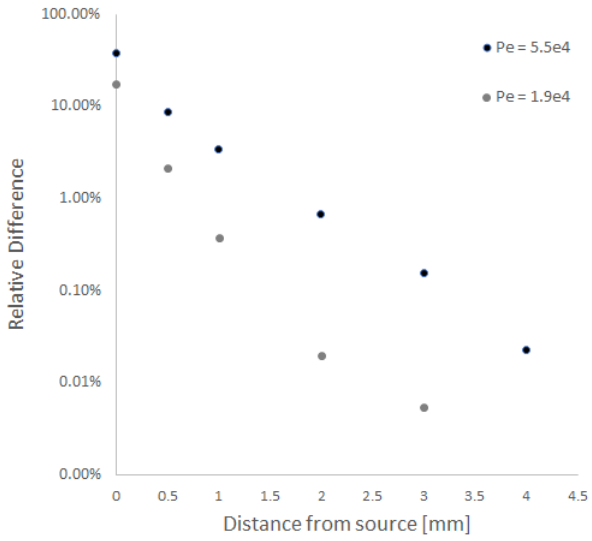

Figure B-1: The relative difference between the cross-section average and flow average (mixing cup average) concentrations in the microchannel as a function of distance from the last reactive surface.

Bibliography

[1] Charu C Aggarwal and Philip S Yu. Outlier detection for high dimensional data. In *Proceedings of the 2001 ACM SIGMOD international conference on Management of data*, pages 37–46, 2001.

[2] Daniel Ayalew Ali and Klaus Deininger. *Is there a farm-size productivity relationship in African agriculture? Evidence from Rwanda*. The World Bank, 2014.

[3] Mihael Ankerst, Markus M. Breunig, Hans Peter Kriegel, and Jörg Sander. OPTICS: Ordering Points to Identify the Clustering Structure. *SIGMOD Record (ACM Special Interest Group on Management of Data)*, 28(2):49–60, 1999.

[4] M A Badr. Efficiency of K-feldspar Combined with Organic Materials and Silicate Dissolving Bacteria on Tomato Yield. 2(12):1191–1198, 2006.

[5] Mateete A Bekunda, André Bationo, and Henry Ssali. *Soil Fertility Management in Africa: A Review of Selected Research Trials*, chapter 3, pages 63–79. John Wiley & Sons, Ltd, 1997.

[6] Samuel Benin. *Agricultural productivity in Africa: Trends, patterns, and determinants*. Intl Food Policy Res Inst, 2016.

[7] D_ L Bish and S A Howard. Quantitative phase analysis using the Rietveld method. *Journal of Applied Crystallography*, 21(2):86–91, 1988.

[8] Simon J Blott, Debra J Croft, Kenneth Pye, Samantha E Saye, and Helen E Wilson. Particle size analysis by laser diffraction. *Geological Society, London, Special Publications*, 232(1):63–73, 2004.

[9] Alex E Blum. Feldspar dissolution kinetics. *Chemical weathering rates of silicate minerals*, 1995.

[10] Camila Bonilla Cedrez, Jordan Chamberlin, Zhe Guo, and Robert J. Hijmans. Spatial variation in fertilizer prices in Sub-Saharan Africa. *PLOS ONE*, 15(1):e0227764, jan 2020.

[11] Glen D Brown, Satoshi Yamada, and Terrence J Sejnowski. Independent component analysis at the neural cocktail party. *Trends in neurosciences*, 24(1):54–63, 2001.

[12] S. C. Brubaker, A. J. Jones, D. T. Lewis, and K. Frank. Soil Properties Associated with Landscape Position. *Soil Science Society of America Journal*, 57(1):235–239, jan 1993.

[13] Jennifer A. Burney, Rosamond L. Naylor, and Sandra L. Postel. The case for distributed irrigation as a development priority in sub-Saharan Africa. *Proceedings of the National Academy of Sciences of the United States of America*, 110(31):12513–12517, 2013.

[14] P C Carman and J C Arnell. SURFACE AREA MEASUREMENTS OF FINE POWDERS USING MODIFIED PERMEABILITY EQUATIONS. *Canadian Journal of Research*, 26a(3):128–136, 1948.

[15] Sarah-Sophia D Carter, Abdul-Raouf Atif, Sandeep Kadekar, Ingela Lanekoff, Håkan Engqvist, Oommen P Varghese, Maria Tenje, and Gemma Mestres. PDMS leaching and its implications for on-chip studies focusing on bone regeneration applications. *Organs-on-a-Chip*, page 100004, 2020.

[16] F. Chayes. The Theory of Thin-Section Analysis. *The Journal of Geology*, 62(1):92–101, jan 1954.

[17] JJ Chen, JJ Thomas, , HFW Taylor Cement concrete ..., and undefined 2004. Solubility and structure of calcium silicate hydrate. *Elsevier*.

[18] E Colin Cherry. Some experiments on the recognition of speech, with one and with two ears. *The Journal of the acoustical society of America*, 25(5):975–979, 1953.

[19] Davide Ciceri and Antoine Allanore. Microfluidic leaching of soil minerals: Release of K+ from K feldspar. *PloS one*, 10(10):e0139979, 2015.

[20] Davide Ciceri and Antoine Allanore. Local fertilizers to achieve food self-sufficiency in Africa, 2019.

[21] Davide Ciceri, Marcelo de Oliveira, Dennis P Chen, and Antoine Allanore. Role of Processing Temperature and Time on the Hydrothermal Alteration of K-Feldspar Rock in Autoclave. *Mining, Metallurgy & Exploration*, 37(4):955–963, 2020.

[22] Davide Ciceri, Marcelo de Oliveira, Rebecca M. Stokes, Taisiya Skorina, and Antoine Allanore. Characterization of potassium agrominerals: Correlations between petrographic features, comminution and leaching of ultrapotassic syenites. *Minerals Engineering*, 102:42–57, 2017.

[23] DC Cireşan, U Meier ... on neural networks ..., and undefined 2012. Transfer learning for Latin and Chinese characters with deep neural networks. *ieeexplore.ieee.org*.

[24] Jenny Clover. Food security in sub-Saharan Africa. *African Security Studies*, 12(1):5–15, 2003.

[25] A Cottenie. *Soil and plant testing as a basis of fertilizer recommendations.* 1980.

[26] Gheorghe Craciun and Martin Feinberg. Multiple equilibria in complex chemical reaction networks: II. The species-reaction graph. *SIAM Journal on Applied Mathematics*, 66(4):1321–1338, 2006.

[27] Per-Erik Danielson. A new shape factor. *Computer Graphics and Image Processing*, 7(2):292–299, 1978.

[28] Joseph Davidovits. *Geopolymer Chemistry & Applications*. Institut Géoplymèr, Saint-Quentin, 4th edition, 2015.

[29] Anamika Dhillon and Gyanendra K. Verma. Convolutional neural network: a review of models, methodologies and applications to object detection, jun 2020.

[30] Reiner Dohrmann. Cation exchange capacity methodology I: An efficient model for the detection of incorrect cation exchange capacity and exchangeable cation results. *Applied Clay Science*, 34(1-4):31–37, 2006.

[31] Tamer Elkateb, Rick Chalaturnyk, and Peter K Robertson. An overview of soil heterogeneity: quantification and implications on geotechnical field problems. *Canadian Geotechnical Journal*, 40(1):1–15, 2003.

[32] A Enell, F Reichenberg, P Warfvinge, G Ewald Chemosphere, and undefined 2004. A column method for determination of leaching of polycyclic aromatic hydrocarbons from aged contaminated soil. *Elsevier*.

[33] Martin Ester, Hans-Peter Kriegel, Jörg Sander, and Xiaowei Xu. Density-based spatial clustering of applications with noise. In *Int. Conf. Knowledge Discovery and Data Mining*, volume 240, page 6, 1996.

[34] G L Fairs. The Use of the Microscope in Particle Size Analysis. *Chemistry and Industry*, 62(40):374–378, 1943.

[35] Food FAO and Agriculture Organization of the United Nations. World Agriculture: Towards 2015/2030 - An FAO perspective.

[36] Food FAO and Agriculture Organization of the United Nations. FAOSTAT Fertilizers Archive, 2017.

[37] Food FAO and Agriculture Organization of the United Nations. World Fertilizer Trends and Outlook to 2020. Technical report, 2017.

[38] H Scott Fogler. *Essentials of Chemical Reaction Engineering: Essenti Chemica Reactio Engi*. Pearson Education, 2010.

[39] A J Franzluebbers. Water infiltration and soil structure related to organic matter and its stratification with depth. Technical report.

[40] Karen Frenken. *Irrigation in Africa in figures: AQUASTAT Survey, 2005*, volume 29. Food & Agriculture Org., 2005.

[41] John J Friel. *Practical guide to image analysis*. ASM international, 2000.

[42] RL Galvez, AA Bandala, EP Dadios TENCON 2018-2018 . . . , and undefined 2018. Object detection using convolutional neural networks. *ieeexplore.ieee.org*.

[43] H Gao, B Cheng, J Wang, K Li, J Zhao, and D Li. Object Classification Using CNN-Based Fusion of Vision and LIDAR in Autonomous Vehicle Environment. *IEEE Transactions on Industrial Informatics*, 14(9):4224–4231, 2018.

[44] Yousef Ghorbani, Jean-Paul Franzidis, and Jochen Petersen. Heap leaching technology—current state, innovations, and future directions: a review. *Mineral Processing and Extractive Metallurgy Review*, 37(2):73–119, 2016.

[45] Audrey M Glauert. Practical Methods in Electron Microscopy. Technical report, 1975.

[46] I Gogul, VS Kumar 2017 Fourth International Conference On, and undefined 2017. Flower species recognition system using convolution neural networks and transfer learning. *ieeexplore.ieee.org*.

[47] Amos. Golan, George G. Judge, and Douglas Miller. *Maximum entropy econometrics : robust estimation with limited data*. Wiley, 1996.

[48] Ulrich E. Grauer and Walter J. Horst. Modeling Cation Amelioration of Aluminum Phytotoxicity. *Soil Science Society of America Journal*, 56(1):166–172, jan 1992.

[49] Joris Guérin, Olivier Gibaru, Stéphane Thiery, and Eric Nyiri. CNN FEATURES ARE ALSO GREAT AT UNSUPERVISED CLASSIFICATION. pages 83–95, 2018.

[50] Dorian A H Hanaor, Wojciech Chrzanowski, and Yixiang Gan. An approach for the in-situ specific surface area assessment of aqueous oxide particles. Technical Report 2, 2015.

[51] Robert M Haralick and Linda G Shapiro. Image segmentation techniques. *Computer Vision, Graphics, and Image Processing*, 29(1):100–132, 1985.

[52] DM Harper. *Eutrophication of freshwaters*. 1992.

[53] Simon Haykin and Zhe Chen. The cocktail party problem. *Neural computation*, 17(9):1875–1902, 2005.

[54] R Hellmann, CM Eggleston, MF Hochella Jr ... et Cosmochimica Acta, and undefined 1990. The formation of leached layers on albite surfaces during dissolution under hydrothermal conditions. *Elsevier*.

[55] Daniel S Hirschberg, Ashok K Chandra, and Dilip V Sarwate. Computing connected components on parallel computers. *Communications of the ACM*, 22(8):461–464, 1979.

[56] Tim Holland and Roger Powell. Thermodynamics of order-disorder in minerals: II. Symmetric formalism applied to solid solutions. *American Mineralogist*, 81(11-12):1425–1437, 1996.

[57] Norman J Hyne. *Nontechnical guide to petroleum geology, exploration, drilling, and production*. PennWell Books, 2012.

[58] Jordi Inglada. Automatic recognition of man-made objects in high resolution optical remote sensing images by SVM classification of geometric image features. *ISPRS Journal of Photogrammetry and Remote Sensing*, 62(3):236–248, 2007.

[59] M. L. Johnson and L. M. Faunt. Parameter estimation by least-squares methods, jan 1992.

[60] David S J Jones and Peter P Pujadó. *Handbook of petroleum processing*. Springer Science & Business Media, 2006.

[61] Anthony S.R. Juo and Kathrin Franzluebbers. *Tropical soils: properties and management for sustainable agriculture*. Oxford University Press, 2003.

[62] C Kanan and G Cottrell. Robust classification of objects, faces, and flowers using natural image statistics. In *2010 IEEE Computer Society Conference on Computer Vision and Pattern Recognition*, pages 2472–2479, jun 2010.

[63] Toshiyuki Katagi and T Katagi. Soil Column Leaching of Pesticides. *Springer*, pages 1–105, 2013.

[64] Nynke Keulen, Sebastian Næsby Malkki, and Shaun Graham. Automated Quantitative Mineralogy Applied to Metamorphic Rocks. *Minerals*, 10(1):47, 2020.

[65] Fareed A. Khan and Abid Ali Ansari. Eutrophication: An ecological vision, dec 2005.

[66] Wlodzimierz Klonowski. Simplifying principles for chemical and enzyme reaction kinetics. *Biophysical Chemistry*, 18(2):73–87, 1983.

[67] Christopher T G Knight, Raymond J Balec, and Stephen D Kinrade. The structure of silicate anions in aqueous alkaline solutions. *Angewandte Chemie*, 119(43):8296–8300, 2007.

[68] CTG Knight, SD Kinrade Studies in Plant Science, and undefined 2001. A primer on the aqueous chemistry of silicon. *Elsevier*.

[69] Alex Krizhevsky, Ilya Sutskever, and Geoffrey E Hinton. Imagenet classification with deep convolutional neural networks. *Communications of the ACM*, 60(6):84–90, 2017.

[70] Utpalendu Kuila and Manika Prasad. Specific surface area and pore-size distribution in clays and shales. *Geophysical Prospecting*, 61(Rock Physics for Reservoir Exploration, Characterisation and Monitoring):341–362, 2013.

[71] Slawomir Kulesza and Miroslaw Bramowicz. A comparative study of correlation methods for determination of fractal parameters in surface characterization. *Applied Surface Science*, 293:196–201, 2014.

[72] R D Kulkarni and P Somasundaran. Mineralogical heterogeneity of ore particles and its effects on their interfacial characteristics. *Powder Technology*, 14(2):279–285, 1976.

[73] C Lai, XM Li, LK Zou, Q Chen, B Xie, YL Li, XL Li Corrosion Science, and undefined 2014. Corrosion of porous silicon in tetramethylammonium hydroxide solution. *Elsevier*.

[74] Keith J Laidler. *Chemical Kinetics.(3rdedn)*. Pearson Education, 2008.

[75] Bin Lian, Jun Chen, P Q Fu, C Liu, and Ye Chen. Weathering of silicate minerals by microorganisms in culture experiments. *Geological Journal of China Universities*, 11(2):181–186, 2005.

[76] S. K. Liu, C. Han, J. M. Liu, and H. Li. Hydrothermal decomposition of potassium feldspar under alkaline conditions. *RSC Adv.*, 5(113):93301–93309, 2015.

[77] Lenis Saweda O. Liverpool-Tasie, Bolarin T. Omonona, Awa Sanou, and Wale Ogunleye. Maize Farming and Fertilizers: Not a Profitable Mix in Nigeria. *Agriculture in Africa: Telling Myths from Facts*, pages 105–114, 2017.

[78] Patricia Macchi and Gaël Raballand. Transport Prices and Costs: The Need to Revisit Donors' Policies in Transport in Africa. *SSRN Electronic Journal*, pages 1–26, 2012.

[79] James M MacDonald, Penni Korb, and Robert A Hoppe. Farm size and the organization of US crop farming. Technical report, 2013.

[80] Nicole Marrone, Christine R Mason, and Gerald Kidd Jr. Evaluating the benefit of hearing aids in solving the cocktail party problem. *Trends in amplification*, 12(4):300–315, 2008.

[81] H. W. Martin and D. L. Sparks. On The Behavior of Nonexchangeable Potassium in Soils. *Communications in Soil Science and Plant Analysis*, 16(2):133–162, feb 1985.

[82] Don McGlinchey. *Characterisation of Bulk Solids*. Blackwell Publishing Ltd., mar 2009.

[83] Alain Meunier and Bruce Velde. Solid solutions in I/S mixed-layer minerals and illite. *American Mineralogist*, 74(9-10):1106–1112, 1989.

[84] P. T. Michaud and D. Babic. A Raman Study of Etching Silicon in Aqueous Tetramethylammonium Hydroxide. *Journal of The Electrochemical Society*, 145(11):4040–4043, nov 1998.

[85] John C Middlebrooks, Jonathan Z Simon, Arthur N Popper, and Richard R Fay. *The auditory system at the cocktail party*, volume 60. Springer, 2017.

[86] Budiman Minasny, Uta Stockmann, Alfred E. Hartemink, and Alex B. McBratney. Measuring and Modelling Soil Depth Functions. pages 225–240. 2016.

[87] M. A. Mojid, A. B.M.Z. Hossain, and G. C.L. Wyseure. Impacts of Municipal Wastewater on Basic Soil Properties as Evaluated by Soil Column Leaching Experiment in Laboratory. *Journal of Soil Science and Plant Nutrition*, 19(2):402–412, jun 2019.

[88] Anibal Montenegro, Yuri Nahmad Molinari, Damiano Sarocchi, Roberto Bartali, and Luis Ángel Rodríguez. Optical granulometry by digital image processing. In *22nd Congress of the International Commission for Optics: Light for the Development of the World*, volume 8011, page 80117G. International Society for Optics and Photonics, 2011.

[89] Fernando J Muzzio, Priscilla Robinson, Carolyn Wightman, and Dean Brone. Sampling practices in powder blending. *International journal of pharmaceutics*, 155(2):153–178, 1997.

[90] W. M. Mwangi. Low use of fertilizers and low productivity in sub-Saharan Africa. *Nutrient Cycling in Agroecosystems*, 47(2):135–147, 1996.

[91] Majid Naderi. Chapter Fourteen - Surface Area: Brunauer–Emmett–Teller (BET). In Steve Tarleton, editor, *Progress in Filtration and Separation*, pages 585–608. Academic Press, Oxford, 2015.

[92] Rajiv Narayan, Virginia Best, Erol Ozmeral, Elizabeth McClaine, Micheal Dent, Barbara Shinn-Cunningham, and Kamal Sen. Cortical interference effects in the cocktail party problem. *Nature neuroscience*, 10(12):1601–1607, 2007.

[93] Usgs National Minerals Information Center. FELDSPAR AND NEPHELINE SYENITE (Data in thousand metric tons unless otherwise noted). Technical report.

[94] Nir I. Nativ, Alvin I. Chen, Gabriel Yarmush, Scot D. Henry, Jay H. Lefkowitch, Kenneth M. Klein, Timothy J. Maguire, Rene Schloss, James V. Guarrera, Francois Berthiaume, and Martin L. Yarmush. Automated image analysis method for detecting and quantifying macrovesicular steatosis in hematoxylin and eosin-stained histology images of human livers. *Liver Transplantation*, 20(2):228–236, feb 2014.

[95] A. D. Noble, M. E. Sumner, and A. K. Alva. The pH Dependency of Aluminum Phytotoxicity Alleviation by Calcium Sulfate. *Soil Science Society of America Journal*, 52(5):1398–1402, sep 1988.

[96] J Oberteuffer. Magnetic separation: A review of principles, devices, and applications. *IEEE Transactions on Magnetics*, 10(2):223–238, jun 1974.

[97] Ivan Odler. The BET-specific surface area of hydrated Portland cement and related materials. *Cement and Concrete Research*, 33(12):2049–2056, 2003.

[98] ONU. *World population prospects 2019*. Number 141. 2019.

[99] Nobuyuki Otsu. A threshold selection method from gray-level histograms. *IEEE transactions on systems, man, and cybernetics*, 9(1):62–66, 1979.

[100] Marc Pansu and Jacques Gautheyrou. *Handbook of soil analysis: mineralogical, organic and inorganic methods*. Springer Science & Business Media, 2007.

[101] Jae Sung Park, Chonhyon Park, and Dinesh Manocha. Efficient probabilistic collision detection for non-convex shapes. In *2017 IEEE International Conference on Robotics and Automation (ICRA)*, pages 1944–1951. IEEE, 2017.

[102] James Pawley. *Handbook of biological confocal microscopy*, volume 236. Springer Science & Business Media, 2006.

[103] Jochen Petersen. Heap leaching as a key technology for recovery of values from low-grade ores–A brief overview. *Hydrometallurgy*, 165:206–212, 2016.

[104] N M Pichugina, A M Kutepov, I G Gorichev, A D Izotov, and B E Zaitsev. Dissolution kinetics of nickel (II) and nickel (III) oxides in acid media. *Theoretical Foundations of Chemical Engineering*, 36(5):485–494, 2002.

[105] Fridrun Podczeck. A shape factor to assess the shape of particles using image analysis. *Powder technology*, 93(1):47–53, 1997.

[106] P. F. Pratt. Potassium. pages 1022–1030. dec 2016.

[107] J Rajagopala Rao, R Nayak, and A Suryanarayana. Feldspar for potassium, fertilisers, catalysts and cement. *Asian Journal of Chemistry*, 10(4):690, 1998.

[108] E Rivlin, M Rudzsky, R Goldenberg, U Bogomolov, and S Lepchev. A real-time system for classification of moving objects. In *Object recognition supported by user interaction for service robots*, volume 3, pages 688–691 vol.3, aug 2002.

[109] R. L. Rudnick. *The crust*. Elsevier, 2005.

[110] R.L. Rudnick and S. Gao. Composition of the Continental Crust. In *Treatise on Geochemistry*, volume 3-9, pages 1–64. Elsevier, dec 2003.

[111] Encarnación Ruiz-Agudo, Christine V. Putnis, Carlos Rodriguez-Navarro, and Andrew Putnis. Mechanism of leached layer formation during chemical weathering of silicate minerals. *Geology*, 40(10):947–950, 2012.

[112] Upendra M Sainju. CARBON AND NITROGEN POOLS IN SOIL AGGREGATES SEPARATED BY DRY AND WET SIEVING METHODS. *journals.lww.com*.

[113] Albert Sasson. Food security for Africa: an urgent global challenge. *Agriculture & Food Security*, 1(1):2, 2012.

[114] M Schöchlin, SE Weissinger, AR Brandes Journal of pathology ..., and undefined 2014. A nuclear circularity-based classifier for diagnostic distinction of desmoplastic from spindle cell melanoma in digitized histological images. *ncbi.nlm.nih.gov*.

[115] Claude E Shannon. A mathematical theory of communication. *The Bell system technical journal*, 27(3):379–423, 1948.

[116] Huiting Shen, E Forssberg, and R J Pugh. Selective flotation separation of plastics by particle control. *Resources, Conservation and Recycling*, 33(1):37–50, 2001.

[117] C J R Sheppard and T Wilson. Depth of field in the scanning microscope. *Opt. Lett.*, 3(3):115–117, sep 1978.

[118] Daisuke Shindo and Tetsuo Oikawa. Energy dispersive x-ray spectroscopy. In *Analytical electron microscopy for materials science*, pages 81–102. Springer, 2002.

[119] William Shotyk and Wayne H. Nesbitt. Incongruent and congruent dissolution of plagioclase feldspar: effect of feldspar composition and ligand complexation. *Geoderma*, 55(1-2):55–78, oct 1992.

[120] Taisiya Skorina and Antoine Allanore. Aqueous alteration of potassium-bearing aluminosilicate minerals: from mechanism to processing. *Green Chem.*, 17(4):2123–2136, 2015.

[121] Jian Guo Song, Xin Zhi Wang, Shao Dan Xiao, and Wei Liu. Study on Extracting Potassium from Potassium Feldspar with Molten Salt Leaching Method. *Advanced Materials Research*, 524-527:1078–1081, may 2012.

[122] George Gabriel Stokes. *On the effect of the internal friction of fluids on the motion of pendulums*, volume 9. Pitt Press Cambridge, 1851.

[123] Ping Sun, John R Grace, C Jim Lim, and Edward J Anthony. Determination of intrinsic rate constants of the CaO–CO2 reaction. *Chemical Engineering Science*, 63(1):47–56, 2008.

[124] Joseph Swift, Jose M Alvarez, Viviana Araus, Rodrigo A Gutiérrez, and Gloria M Coruzzi. Nutrient dose-responsive transcriptome changes driven by Michaelis–Menten kinetics underlie plant growth rates. *Proceedings of the National Academy of Sciences*, 117(23):12531–12540, 2020.

[125] HARRY F.W. TAYLOR. Proposed Structure for Calcium Silicate Hydrate Gel. *Journal of the American Ceramic Society*, 69(6):464–467, 1986.

[126] Oleg N Temkin, Andrew V Zeigarnik, and D G Bonchev. *Chemical reaction networks: a graph-theoretical approach*. CRC Press, 1996.

[127] Firman Thompson. Process of obtaining potash salts from feldspar, 1911.

[128] Lisa Torrey and Jude Shavlik. Transfer learning. In *Handbook of research on machine learning applications and trends: algorithms, methods, and techniques*, pages 242–264. IGI global, 2010.

[129] D S Urch. X-ray spectroscopy and chemical bonding in minerals. In *Chemical Bonding and Spectroscopy in Mineral Chemistry*, pages 31–61. Springer, 1985.

[130] Peter Van Straaten. Farming with rocks and minerals: challenges and opportunities. *Anais da Academia Brasileira de Ciências*, 78(4):731–47, dec 2006.

[131] Eric Vanden-Eijnden and Fabio A Tal. Transition state theory: Variational formulation, dynamical corrections, and error estimates. *The Journal of chemical physics*, 123(18):184103, 2005.

[132] K D Vernon-Parry. Scanning electron microscopy: an introduction. *III-Vs Review*, 13(4):40–44, 2000.

[133] DeLiang Wang. Deep learning reinvents the hearing aid. *IEEE spectrum*, 54(3):32–37, 2017.

[134] Armin Weiss and A Herzog. Isolation and characterization of a silicon-organic complex from plants. In *Biochemistry of silicon and related problems*, pages 109–127. Springer, 1978.

[135] HR Westrich, RT Cygan, WH Casey American Journal of ..., and undefined 1993. The dissolution kinetics of mixed-cation orthosilicate minerals. *earth.geology.yale.edu*.

[136] Justin C Williams Jr. Political redistricting: a review. *Papers in Regional Science*, 74(1):13–40, 1995.

[137] J Wu, Y Liu, and N Xu. Histological characteristics of longissimus dorsi muscle and their correlation with restriction fragment polymorphisms of calpastatin gene in F 2 Jinghua 3 Pié train crossbred pigs. *Animal*, 1(9), 2007.

[138] Y Wu, X Qin, Y Pan, C Yuan 2018 IEEE 3rd International, and undefined 2018. Convolution neural network based transfer learning for classification of flowers. *ieeexplore.ieee.org*.

[139] Die Yang, Melissa Kirke, Rong Fan, and Craig Priest. Investigation of Chalcopyrite Leaching Using an Ore-on-a-Chip. *Analytical Chemistry*, 91(2):1557–1562, jan 2019.

[140] Xiao-e Yang and Hu-lin Hao. Mechanisms and assessment of water eutrophication *. *J Zhejiang Univ Sci B*, 9(3):197–209, mar 2008.

[141] David Yanggen, Valerie A. Kelly, Thomas Reardon, and Anwar Naseem. Incentives for Fertilizer Use in Sub-Saharan Africa: A Review of Empirical Evidence on Fertilizer Response and Profitability. *Food Security International Development Working Papers*, 1998.

[142] CK Yip, GC Lukey, JL Provis Cement . . . , Concrete, and undefined 2008. Effect of calcium silicate sources on geopolymerisation. *Elsevier*.

[143] T Zambelli, J Wintterlin, J Trost, and G Ertl. Identification of the "Active Sites" of a Surface-Catalyzed Reaction. *Science*, 273(5282):1688–1690, 1996.

[144] S J Zheng and J L Yang. Target sites of aluminum phytotoxicity. Technical Report 3, 2005.

[145] JB Zhou, JG Xi, ZJ Chen, SX Li PEDOSPHERE (), and undefined 2006. Leaching and transformation of nitrogen fertilizers in soil after application of N with irrigation: A soil column method. *airitilibrary.com*.

[146] Joviša Žunić and Paul L Rosin. Measuring shapes with desired convex polygons. *IEEE Transactions on Pattern Analysis and Machine Intelligence*, 42(6):1394–1407, 2019.